THE UNIVERSITY OF MICHIGAN

INDUSTRY PROGRAM OF THE COLLEGE OF ENGINEERING

# MEASUREMENT OF DYNAMIC REACTOR PARAMETERS BY PHOTON OBSERVATION

Wayne K. Lehto

A dissertation submitted in partial fulfillment
of the requirements for the degree of
Doctor of Philosophy in the
University of Michigan
Department of Nuclear Engineering
1967

November, 1967

IP-793

ACKNOWLEDGMENTS

The author is grateful for the guidance and assistance received from his doctoral committee. Special thanks go to Professor J. M. Carpenter for his genuine interest in all phases of this work. Without his help and insight into the problems involved, the project would not have reached the present stage in so short a time. The assistance of Professor Kerr in matters not directly related to this thesis is sincerely appreciated.

Special thanks also to Drs. R. W. Albrecht, N. M. Moore, S. H. Hanauer, and C. W. Ricker for their suggestions and critical review of different aspects of this work. Professor R. K. Osborn has also given freely of his time and has helped in the understanding of the theoretical aspects of this problem.

Assistance with the pressure vessel design was given by Bob Martin and help "above and beyond" in the execution of the experiments was given by Jim Miller and the reactor operating staff. Mssrs. Eric Aupperlee, John Balmer, and Richard French made certain of the equipment available for the experiments.

Financial support for the purchase of the tape recorder and for detector fabrication was given by the Michigan Memorial Phoenix Project.

Computations were done on the Ford Motor Company Computer at the Ford Research Center in Dearborn, Michigan through the Time Sharing Terminal in the Nuclear Engineering Computer Laboratory.

All the assistance from these and other sources is greatly appreciated.

Also appreciated is the support received from two Special Fellowships in Nuclear Science and Engineering from the USAEC, from National Science Foundation Traineeships and from a Ford Foundation Faculty Development Loan.

Finally all this would not have been possible without the understanding and sacrifices of my wife Mae and my children Michael, Jaculin, Kelly, and Lisbeth to whom I shall forever be grateful.

TABLE OF CONTENTS


| | | Page |
|---|---|---|
| ACKNOWLEDGMENT | | ii |
| LIST OF TABLES | | vi |
| LIST OF FIGURES | | vii |
| ABSTRACT | | ix |
| CHAPTER | | |
| I | INTRODUCTION | 1 |
| | A. Introductory Remarks | 1 |
| | B. Scope of This Research | 4 |
| II | DETECTOR DESIGN AND OPERATION | 6 |
| | A. Introduction | 6 |
| | B. Cerenkov Light Production and Gamma Detection | 9 |
| | C. Proof of Principle Experiments | 23 |
| | D. Results of Initial Experiments and Discussion | 26 |
| | E. $CO_2$ Cerenkov Detector | 33 |
| | F. The Gaseous Cerenkov Detector as a Power Level Monitor | 36 |
| | G. Experimental Efficiency in Terms of Events/Fission | 39 |
| | H. Initial Behavior of the Detector Near the Reactor Core | 41 |
| | I. Summary of Initial Experiments | 43 |
| III | THEORY AND DETECTOR EFFECTS | 44 |
| | A. Introduction | 44 |
| | B. Spectral Densities | 46 |
| | C. Discussion of Statistical Quantities in Noise Experiments | 57 |
| | D. Effects of a Reactivity Input | 59 |
| IV | DESCRIPTION OF EXPERIMENTS AND INSTRUMENTATION | 61 |
| | A. Experiments | 61 |
| | B. Equipment | 62 |
| | C. Error Analysis | 74 |
| | D. Experimental Procedure | 75 |

TABLE OF CONTENTS (Continued)


| | | Page |
|---|---|---|
| V | RESULTS AND DISCUSSION | 77 |
| | A. Introductory Remarks | 77 |
| | B. Low Frequency PSD and Temperature Measurements | 77 |
| | C. CPSD Measurements | 89 |
| VI | CONCLUSIONS AND RECOMMENDATIONS | 94 |
| | A. Conclusions | 94 |
| | B. Recommendations | 96 |
| APPENDIX A | | 100 |
| APPENDIX B | | 102 |
| REFERENCES | | 103 |

LIST OF TABLES


| Table | | Page |
|---|---|---|
| 2-1 | Intrinsic Efficiencies for an Aluminum Surface ..... | 19 |
| 2-2 | Surface Gamma Source Strengths for the FNR ..... | 23 |
| 2-3 | Effect of Fill Gas on Detector Output ..... | 33 |
| 3-1 | Statistical Quantities in Noise Measurements ..... | 58 |

LIST OF FIGURES


| Figure | | Page |
|---|---|---|
| 2-1 | Schematic of the Cerenkov Detection Principle | 7 |
| 2-2 | Prompt and Delayed Gamma Ray Line Spectra | 8 |
| 2-3 | Number of Cerenkov Photons Produced by Electrons of Energy E in Freon-22 | 14 |
| 2-4 | Number of Cerenkov Photons Produced by Electrons of Energy E in $CO_2$ | 15 |
| 2-5 | Electron Source Geometry | 17 |
| 2-6 | Relative Number of Cerenkov Photons Produced per Incident Gamma Ray of Energy E | 21 |
| 2-7 | Gaseous Cerenkov Detector | 25 |
| 2-8 | Variation of Count Rate with Pressure | 27 |
| 2-9 | Cerenkov Pulse Height Distribution | 31 |
| 2-10 | Schematic of $CO_2$ Cerenkov Detector | 35 |
| 2-11 | Response of the Gaseous Cerenkov Detector to Changes in Reactor Power | 37 |
| 2-12 | Slope of Detector Output and Background versus Photomultiplier Tube Voltage | 40 |
| 3-1 | Event Sequence for Detecting Prompt Fission Gammas | 47 |
| 4-1 | Reactor Core Configurations | 63 |
| 4-2 | One and Two Detector Schematics | 65 |
| 4-3 | Gamma and Temperature Power Spectral Density Data Collection Schemes | 66 |
| 4-4 | Equipment for Power Spectral Density Calculations | 69 |
| 4-5 | Two Detector Data Collection and Processing Equipment | 72 |

LIST OF FIGURES (Continued)


| Figures | | Page |
|---|---|---|
| 5-1 | Power Spectral Densities with Forced and Free Convection | 78 |
| 5-2 | Power Spectral Densities of Gamma Ray and Temperature Fluctuations | 79 |
| 5-3 | Power Spectral Densities of Gamma Ray Fluctuations at Several Power Levels | 80 |
| 5-4 | Power Spectral Densities of Temperature Fluctuations at Several Power Levels | 81 |
| 5-5 | Mean Value of the Gamma Ray PSD versus Reactor Power | 83 |
| 5-6 | Gamma-Temperature Cross Correlation Function | 84 |
| 5-7 | Cross Power Spectral Density-Core Loading 1 | 90 |
| 5-8 | Cross Power Spectral Density-Core Loading 2 | 91 |

MEASUREMENT OF DYNAMIC REACTOR PARAMETERS
BY PHOTON OBSERVATION

Wayne K. Lehto

ABSTRACT

Fission rate fluctuations at low power in a reactor with a large fission product inventory have been observed in the pool-type Ford Nuclear Reactor. A gaseous Cerenkov detector was used to sense the high energy prompt fission gamma rays in the presence of a fission product gamma field of $10^5$ to $10^6$ R/hr. The ratio $\beta/\ell$ is determined from the cross power spectral density of the fluctuations in the signals from two of these detectors. Both this spectrum and the power spectral density in the output of a single detector show a large low frequency component. This is attributed to moderator temperature fluctuations present when the fission product decay heat is removed by natural circulation of the coolant. The temperature fluctuations as measured with a short time constant thermocouple are shown to be correlated to those in the fission rate.

A basis for calculating the performance of the detector is developed and a theory of the experiment is presented. Results of tests to prove the operating principles of the detector and to investigate its response to changes in reactor power level are reported. The detector is described and improvements to the present model are outlined with suggestions for desirable future experiments.

# CHAPTER I

# INTRODUCTION

## A. Introductory Remarks

The discrete nature of the capture, fission and leakage processes in reactor systems give rise to fluctuations in the neutron level. As was pointed out very early, the observations of these fluctuations will yield information about the system kinetic parameters.[1,2] Following this initial work, numerous experiments have been performed in various ways to obtain information regarding the dynamic behavior[3,4,5,6] and to measure dynamic reactor parameters.[3,5,7,8,9] Measurements of dynamic behavior have been done to determine among other things the shape of the reactor transfer function and to search for abnormal reactor behavior, such as resonances, when power, coolant flow, etc. are varied. The principle objective of the experiments done to measure reactor parameters has been to determine the ratio of the effective delayed neutron fraction to prompt neutron lifetime, $\beta/\ell$, from the spectral shape. However other reactor parameters such as subcritical reactivity[5,9] and reactor power[3] can be determined depending on the model used to analyze the data and the condition of the reactor.

The latter experiments are restricted to clean, cold reactors and have been performed using conventional methods of neutron detection. The former type experiments are generally done at substantial power levels on power reactors or reactors with high fission product inventory and the attendant fission product gamma rays. Because of the pile-up problems and inability to effectively discriminate against these low energy gammas, reactor parameter measurements and like experiments have not been done

on reactors with any significant amount of fission product gamma ray flux. Reactors with high fission product inventories are frequently termed "dirty".

Hanauer and co-workers[45] have investigated the use of pulse type detectors employing pulse height discrimination to reduce the contribution from the gamma rays. Kryter et al.[10] used the two detector cross correlation techniques[11,12,13,23] to achieve improvement in the signal to noise ratios and eliminate the gamma induced background. Efforts have also been made to devise new detectors[14] and optimize existing ones.[15] In spite of the above, the present methods appear to be limited to use with gamma fields of less than $10^5$ R/hr, well below the anticipated maximum of $\sim 10^7$ R/hr. It is about at this gamma level, $10^5$ R/hr, that even the best neutron detectors become unusable.[15,16] The work done here is an attempt to alleviate the problems of the low energy gammas in "dirty" systems and to verify the predictions[17] concerning the conduct of noise experiments in which the observable is the prompt fission gamma ray distribution.

For this purpose, a detector has been developed in which the high energy gamma rays are detected through the Cerenkov light produced by the secondary electrons in a gaseous radiator. The Cerenkov threshold, and hence the detected gamma ray energy, is controlled by adjusting the refractive index through pressure changes.

The gamma experiment has been suggested by Gelinas and Osborn[17] and as was pointed out by them, the prompt gamma ray distribution above 4 to 5 Mev conveys the same information as the neutron distribution. A detector sensitive to only the gamma rays above 4 to 5 Mev could in

principle do parameter experiments on "dirty" reactor systems because of its insensitivity to the lower energy fission product gamma rays which convey no information about the instantaneous power level.

A previous experiment observing the Cerenkov light produced by secondary electrons in a water radiator has been done by Kenney.[18] His experiments were done on a relatively "dirty" core. This required operation at power levels $\sim$200 kW to achieve adequate signal to noise ratios because the water radiator with a refractive index of 1.33 produces Cerenkov light from electrons down to about 0.17 Mev and hence is sensitive to the majority of the delayed fission product gammas. Reactors operated at such high power levels are subject to important feedback effects, and consequently fluctuation measurements are not as readily interpretable to yield such parameters as $\beta/\ell$ as are measurements at low powers.

The ability of the gaseous Cerenkov detector to measure $\beta/\ell$ by observing the gamma distribution at low powers has been tested experimentally on the Ford Nuclear Reactor (FNR) which by nature of its operation qualifies as a "dirty" reactor. Surface gamma ray fields at shutdown are between $10^5$ and $10^6$ R/hr.

A number of experimental investigations of the FNR have been carried out previously. Since the autocorrelation function measurements of Velez,[19] Albrecht[20] and Pluta[21] have made measurements of the time distribution of the pulses from an in-core neutron detector to determine $\beta/\ell$. Boennighausen[22] measured the power spectral density directly with a current type chamber and inferred $\beta/\ell$ from the spectral shape. With the exception of Velez's work, the measurements have been done on

clean, cold fuel in the FNR. Velez's experiments were done on a core which operated at 1 MW and was then shut down. The high background necessitated operation of the detectors at large distances from the core, thereby reducing the efficiency, which helps in part to explain his inability to measure a meaningful autocorrelation function.

All of these measurements were done on small graphite reflected systems as opposed to the slightly larger water reflected and more contaminated cores used here. Also, since these prior measurements, a $D_2O$ tank has been added to the reactor which covers the north face of the core. Its purpose is to enhance the thermal neutron flux at the beam ports. Because of the differences in the core configurations studied previously and the cores used in these studies, exact agreement between previous results and the results to be presented is not necessarily anticipated, although the present measurement gives a value for $\beta/\ell$ in close agreement with that of Albrecht.[20]

B. Scope of this Research

The initial work was to design a Gaseous Cerenkov Detector (GCD) and verify its predicted behavior, such as the threshold properties and detection efficiency for high energy gamma rays. Subsequent work involved the redesign of the instrument to accommodate a higher pressure $CO_2$ radiator and experiments to determine its behavior near the reactor core and its response to changes in reactor power level. The preliminary and final designs, the experiments, and discussion of the operating behavior are presented in Chapter II.

Chapter III outlines the development of a theory of the gamma noise experiment, including the statistics of the detection process, using the Langevin technique. A discussion of the relative efficiency requirements in a gamma ray or neutron experiment is presented taking into account the detector statistics. Also the effect of a power independent reactivity driving function on the measured spectrum is discussed.

Chapter IV presents a discussion of the experiments and the experimental arrangements.

Chapter V presents and discusses the results of a series of measurements of the output of the GCD and a thermocouple placed in the reactor core and the results of a series of two detector cross power spectral density measurements from which the ratio $\beta/\ell$ was inferred. The connection between fission product gamma ray heating and the measured spectra is made.

Finally, Chapter VI concludes with a summary of the results and conclusions along with a section in which desirable future work is outlined.

# CHAPTER II

# DETECTOR DESIGN AND OPERATION

## A. Introduction

The detector developed for the experiments to be reported later is a gaseous Cerenkov detector capable of detecting high energy gamma rays in the presence of a very significant low energy flux, i.e., fission product gamma rays from a highly contaminated reactor. The high energy gamma rays incident on the detector eject electrons from the walls of the device and directly in the Cerenkov radiator. The electrons in turn produce Cerenkov photons which are directed to a photomultiplier tube (Figure 2-1). The Cerenkov radiator is a gas whose refractive index (and thus the Cerenkov threshold energy) can be adjusted by changing the pressure. Only those electrons with energies above the threshold will produce photons to be detected by the photomultiplier and since these electrons are the result of collisions with still higher energy gamma rays, the device operates as a threshold gamma detector.

The association of gamma rays having $E > 4$ Mev with fission events has been made previously.[17] The fact that the delayed fission product gamma spectrum contains insignificant numbers of high energy gammas is illustrated in Figure 2-2, in which the prompt and delayed spectra from Reference 2 are plotted as a histogram. Therefore, by restricting the detection process to only those gammas above $\sim 4$ Mev, fission events are monitored while the effects of delayed gammas are eliminated.

The concept of a gaseous Cerenkov detector is not new as numerous detectors have been constructed for the detection, separation, or

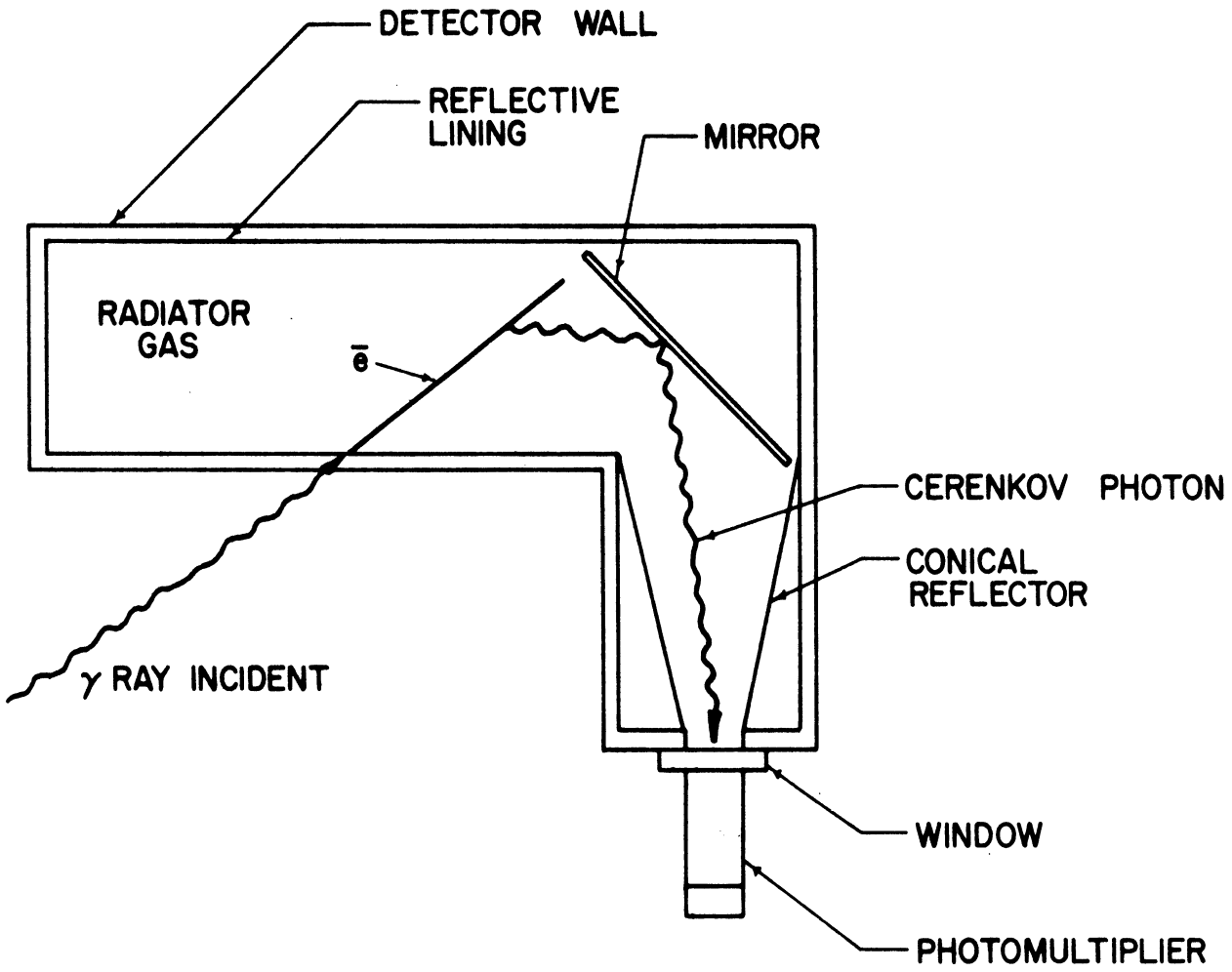


Figure 2-1. Schematic of the Cerenkov Detection Principle.

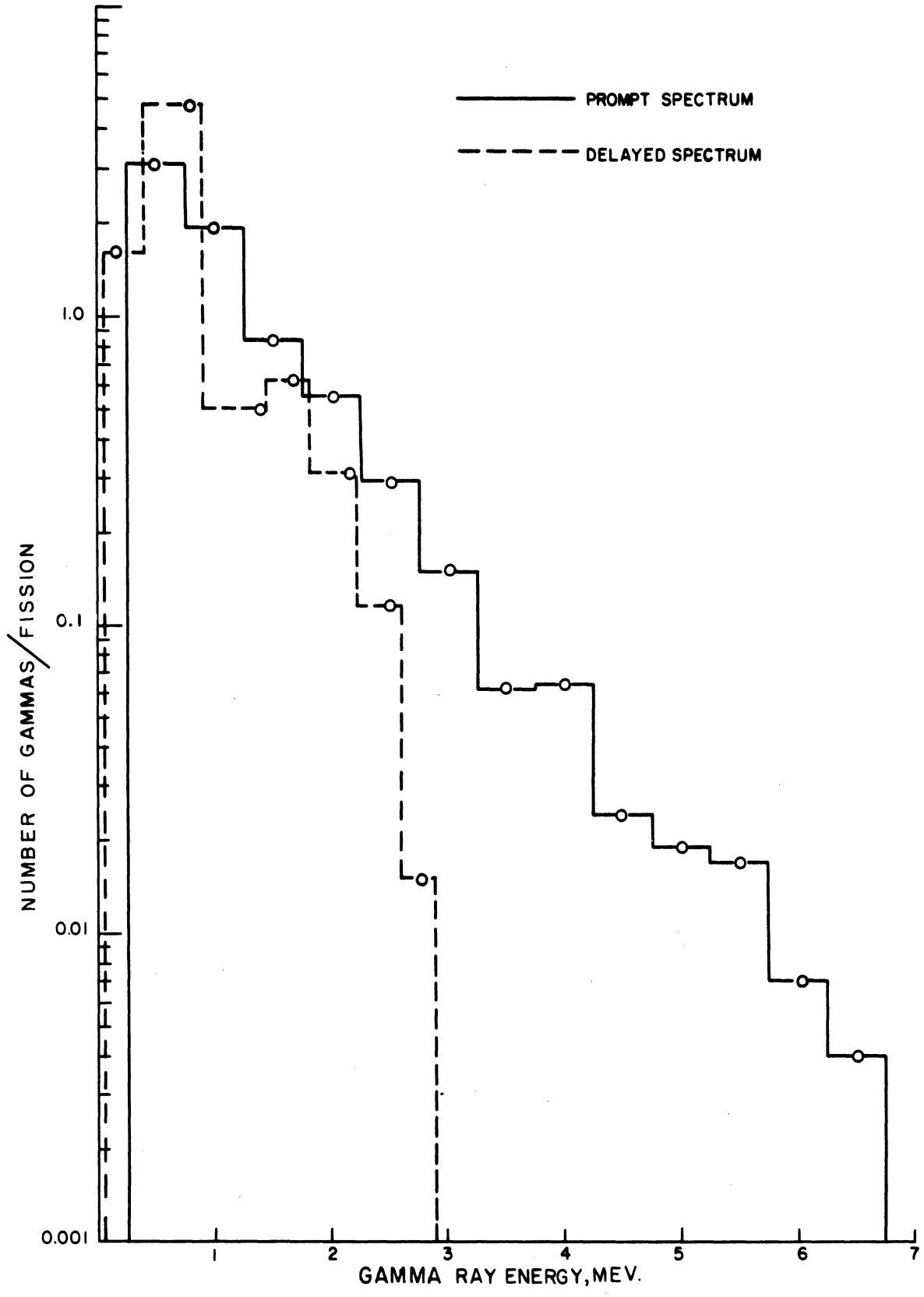


Figure 2-2. Prompt and Delayed Gamma Ray Line Spectra.

energy determination of high energy charged particles produced directly or indirectly by accelerators[24,25,26] or found as components of cosmic radiation.[27] Extremely high energy gamma rays have been detected by the so-called total absorption Cerenkov counter.[28] Only a few applications have been made to the detection of particles in the low Mev range. Among these are the experiments of Jennings and Kalmus[29] and Doyle and Dickinson.[30] In the first of these, a small nitrogen-loaded Cerenkov counter was used for the accurate determination of the energy of 3.5 Mev electrons produced in a cyclotron. In the second experiment, a determination was made of the Cerenkov light output of lucite and quartz due to neutrons and gammas in the energy range around 6 Mev. Their purpose was to monitor nuclear explosions through the emitted gammas.

In addition, effort has been made to utilize the Cerenkov light produced by charged particles in the water surrounding swimming pool reactors[31] and to apply Cerenkov detection techniques to monitor the soluble, beta-emitting fission products in water moderated reactors.[32]

This work is believed to be the first use of a gaseous Cerenkov detector in a reactor application although Cerenkov detectors utilizing water radiators have been used.[33,34,35] However, as noted previously, water radiators because of their high refractive index are sensitive to the delayed as well as prompt gammas.

## B. Cerenkov Light Production and Gamma Detection

In order that an incident gamma ray result in a detectable event at the output of the photomultiplier, it is necessary that the gamma ray eject an electron, from the detector wall or in the radiator,

with energy above the Cerenkov threshold. Secondly, this electron must travel far enough in the radiator to produce a sufficient number of photons, so that when the collection efficiency and quantum efficiency are taken into account enough photoelectrons are liberated from the photocathode to be detected. Estimates of the number of detectable photons as a function of initial gamma ray energy are made in this section along with calculations of the intrinsic efficiency for electron production from plane surfaces of aluminum, i.e., detector walls.

This efficiency is then used along with the calculated prompt fission gamma ray flux at the core surface to arrive at an overall efficiency in terms of events per fission.

The intrinsic efficiency calculated here is analogous to the efficiency for gamma ray detection by wall effects with GM tubes.[36] It is defined as the flux of electrons with energies above the Cerenkov threshold entering the radiator per unit incident gamma ray flux. The efficiency depends on the fraction of gammas producing electrons of appropriate energy and on the probability that these electrons reach the Cerenkov radiator. Only those electrons which are scattered from a point in the wall which is no greater than their range to the Cerenkov threshold energy can produce Cerenkov photons.

Photon Production by Electrons

Cerenkov radiation is the electromagnetic shock wave produced by a charged particle which travels faster than the speed of light in the medium through which it is traveling. The cosine of the angle between the direction of the emitted radiation and the particle path is given by

$$\cos\theta = \frac{1}{\beta n} \tag{2-1}$$

where $\beta = \frac{v}{c}$ is the ratio of the electron speed to the speed of light in vacuum and n is the refractive index.

For any photons to be produced at all, $\beta$ must be $> \frac{1}{n}$. In terms of the kinetic energy, the threshold is[28]

$$E_T = m_0 c^2 \left[\frac{1}{\sqrt{2\eta}} - 1\right] \tag{2-2}$$

where $\eta = n - 1$.

The number of photons produced by an electron in the wavelength interval $d\lambda$ about $\lambda$, emitted per unit path is[36]

$$\frac{\partial^2 N}{\partial x \partial \lambda} d\lambda = \frac{2\pi}{137\lambda^2}\left(1 - \frac{1}{\beta^2 n^2}\right) d\lambda \tag{2-3}$$

A continuous wavelength distribution of light photons is produced, of which only the fraction which have wavelengths in the response region of the phototube will be detected. If $\epsilon_q(\lambda)$ is the quantum efficiency of a photomultiplier for photons of wavelength $\lambda$, the number of photons emitted per unit path length which are equivalent to photons of wavelength $\bar{\lambda}$ for producing photoelectrons is given by

$$\frac{dN}{dx} = \frac{1}{\epsilon_q(\bar{\lambda})} \int \frac{\partial^2 N}{\partial x \partial \lambda} \epsilon_q(\lambda)\, d\lambda \tag{2-4}$$

where $\epsilon_q(\bar{\lambda})$ is the peak value of the phototube quantum efficiency over the response region.

The above integral was evaluated numerically over the response region of both the RCA8575 which has a bialkali photocathode and a conventional S-11 phototube. The results are

S-11 $$\frac{dN}{dx} = 450\left(1 - \frac{1}{\beta^2 m^2}\right) \text{ Photons/cm} \qquad (2\text{-}5)$$

RCA 8575 $$\frac{dN}{dx} = 660\left(1 - \frac{1}{\beta^2 m^2}\right) \text{ Photons/cm} \qquad (2\text{-}6)$$

The 8575 tube is thus seen to be better for the present purposes than the S-11 tube.

The ratio v/c is not constant over the electron path length and depends on distance through the following[37]

$$\left.\frac{dE}{dx}\right|_{ion} = \frac{4\pi r_0^2 m_0 c^2 N B}{\beta^2} \qquad (2\text{-}7)$$

where

$$B = Z\left\{\ln\left[\beta\left(\frac{m_0c^2+E}{\bar{I}}\right)\left(\frac{E}{m_0c^2}\right)^{1/2} - 1/2\,\beta^2\right]\right\}$$

and is called the atomic stopping number.[36]

The average ionization potential is given by[37]

$$\bar{I} = 13.5\,Z \times 10^{-6} \text{ Mev}$$

and the kinetic energy E and $\beta$ are related by the familiar expression

$$E = m_0c^2\left[\frac{1}{(1-\beta^2)^{1/2}} - 1\right] \qquad (2\text{-}8)$$

In using the above expression for the energy loss per unit path, we have neglected Bremstrahlung and Cerenkov losses as energy degradation mechanisms.

Following Doyle and Dickinson[30] we argue that the atomic stopping number is a slowly varying function of energy and therefore can be treated as a constant with its value at 6.0 Mev being $Z \times 11.0$. Then

$$\frac{dE}{d\nu} = \frac{A}{\beta^2} \quad \text{Mev/cm} \tag{2-9}$$

The constant A depends on the radiator material through N and Z .

Combining Equations (2-9, 2-8 and 2-6) and integrating between the limits of $\beta = \frac{v}{c}$ and $\beta_{min} = \frac{1}{n}$, we get the result for , the number of Cerenkov photons generated by an electron of initial energy $E_\beta$. (30)

$$N(E_\beta) = \frac{m_0 c^2 660}{A}\left[\frac{2-\beta^2-\frac{1}{n^2}}{(1-\beta^2)^{\frac{1}{2}}} - \frac{2}{n}(n^2-1)^{\frac{1}{2}}\right] \tag{2-10}$$

Figure 2-3 shows this equation plotted for a Freon-22 ($CHClF_2$) radiator and Figure 2-4 for a $CO_2$ radiator. The number of photons, detectable with the RCA8575 phototube, produced by electrons in slowing down from an energy E to the threshold energy is plotted versus E for several different values of refractive index. Data are taken from Reference 38.

The curves show that sufficient photons are generated at higher electron energies, so that with reasonable collection efficiencies enough photons will be formed in the phototube response region to generate detectable output pulses.

Intrinsic Efficiency

The intrinsic efficiency defined above is derived by considering the flux of electrons ejected from the detector wall into the radiator, assuming an isotropic incident gamma flux. The resultant electron angular distribution is also isotropic due to the incident isotropic gamma ray flux.

Cerenkov Medium - $CHClF_2$ (Freon-22)

Temperature 26°C

| Curve | Pressure-psia | $E_{th}$-Mev | n |
|---|---|---|---|
| 1 | 80 | 4.23 | 1.0053 |
| 2 | 90 | 4.14 | 1.0060 |
| 3 | 100 | 3.90 | 1.0067 |
| 4 | 110 | 3.70 | 1.0073 |
| 5 | 120 | 3.52 | 1.0080 |
| 6 | 130 | 3.36 | 1.0086 |

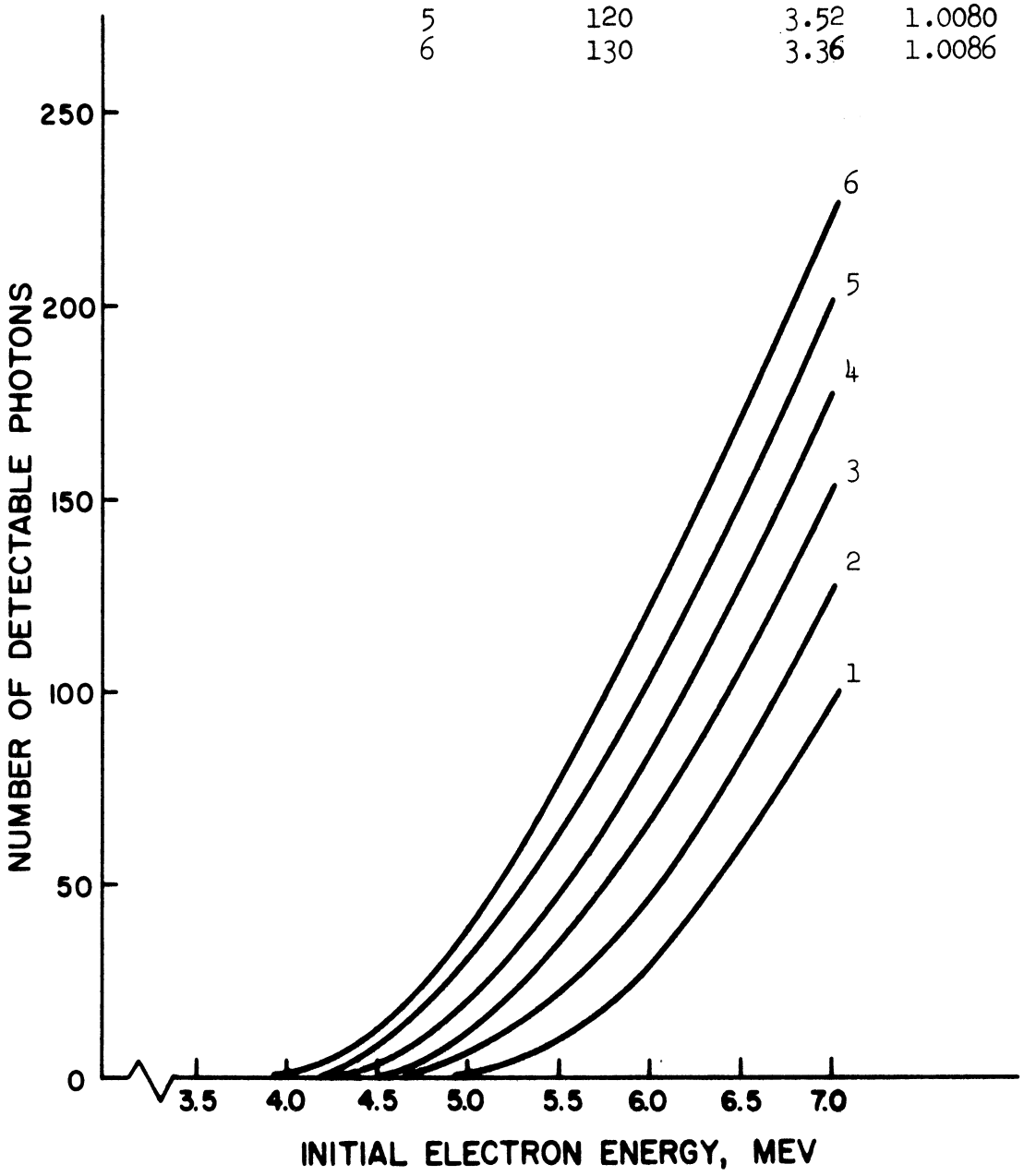


Figure 2-3. Number of Cerenkov Photons Produced by Electrons of Energy E in Freon-22.

Cerenkov Medium--$CO_2$

Temperature 30°C

| Curve | Pressure-psia | $E_{th}$-Mev | n |
|---|---|---|---|
| 1 | 200 | 3.80 | 1.0070 |
| 2 | 250 | 3.34 | 1.0087 |
| 3 | 300 | 3.00 | 1.0105 |
| 4 | 350 | 2.75 | 1.0122 |
| 5 | 400 | 2.54 | 1.0140 |
| 6 | 450 | 2.36 | 1.0157 |

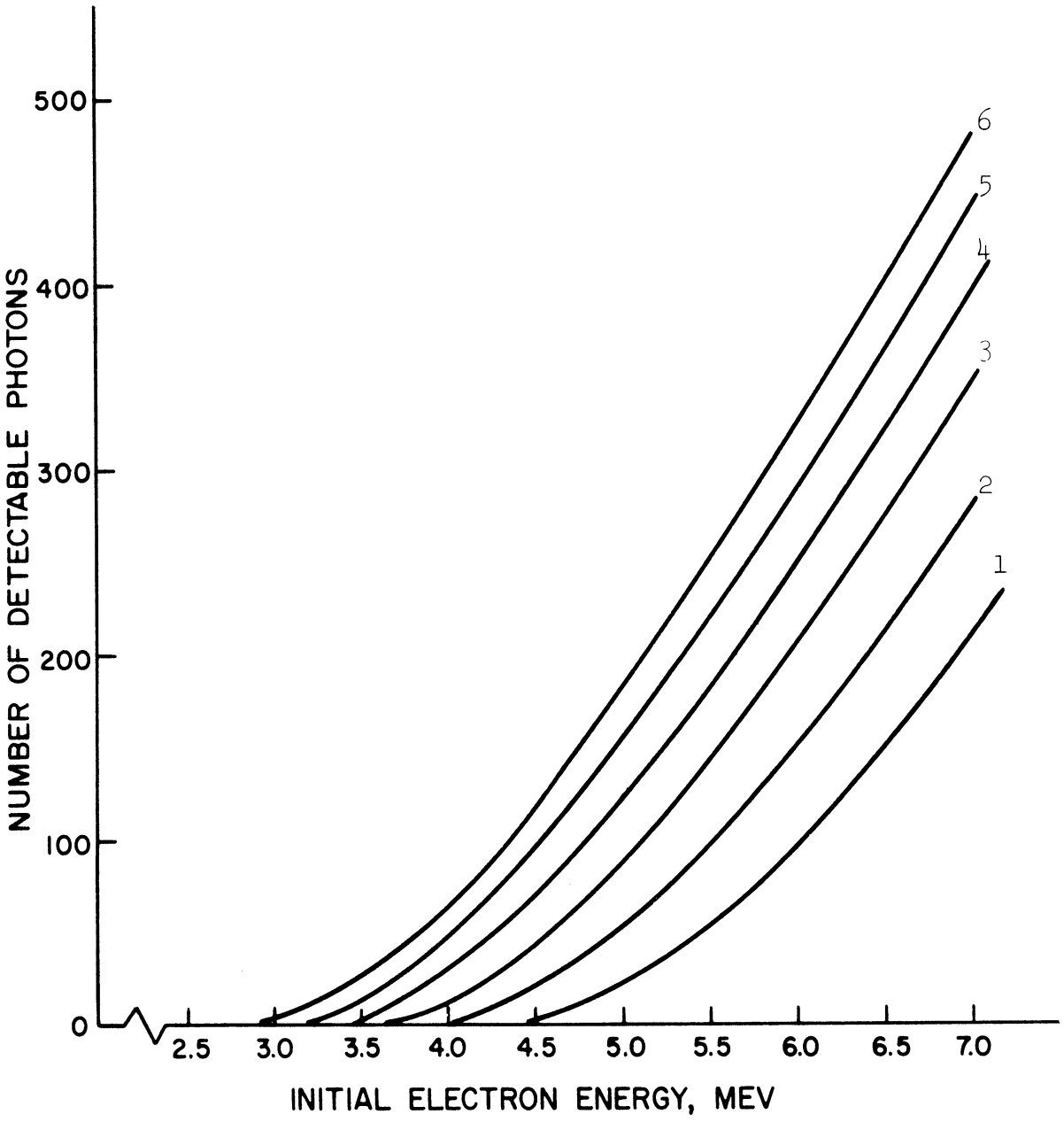


Figure 2-4. Number of Cerenkov Photons Produced by Electrons of Energy E in $CO_2$ .

Consider a small area 1 $cm^2$ lying in the x-y plane as shown in Figure 2-5.

The number of electrons per unit electron energy formed in the volume element $d^3r$ by the isotropic gamma flux, $\phi(E_\gamma)$ gammas/$cm^2$-sec., which pass through the area at the origin is

$$\phi_e(T, E_\gamma) = \phi_\gamma(E_\gamma) N_e \int_{T'} \int_{r} \frac{d\sigma}{dT}(T, E_\gamma) \cos\theta / 4\pi r^2 \times \delta\left(T - T' - \frac{r}{\bar{r}}\right) d^3r\, dT \tag{2-11}$$

where $\frac{d\sigma}{dT}(T, E_\gamma)$ is the differential cross section per unit energy interval for producing an electron with energy T. $\delta\left(T - T' - \frac{r}{\bar{r}}\right)$ is a Dirac delta function relating energy loss to path length and $\cos\theta/4\pi r^2$ is the element of solid angle subtended by the unit area at the origin.

Integrating in spherical coordinates we have

$$\phi_e(T, E_\gamma) = \phi_\gamma(E_\gamma) N_e \int_{T=T'}^{\infty} \int_{r=0}^{\infty} \int_{0}^{\pi/2} \frac{d\sigma}{dT}(T, E_\gamma) \times \frac{\cos\theta}{4\pi r^2} r^2 \sin\theta\, d\theta\, dr\, dT \tag{2-12}$$

Since $\delta\left(T - T' - \frac{r}{\bar{r}}\right) = \bar{r}\,\delta[\bar{r}(T - T') - r]$, the result after the $\theta$ and $r$ integrations is

$$\phi_e(T, E_\gamma) = \frac{\pi}{4} N_e \phi_\gamma(E_\gamma) \int_{T=T}^{T_{max}} \frac{d\sigma}{dT}(T, E_\gamma)\, dT \tag{2-13}$$

The intrinsic efficiency is then

$$\eta(T, E_\gamma) = \frac{\phi_e(T, E_\gamma)}{\phi_\gamma(E_\gamma)} = \frac{\pi}{4} N_e \int_{T=T}^{T_{max}} \frac{d\sigma}{dT}(T, E_\gamma)\, dT \tag{2-14}$$

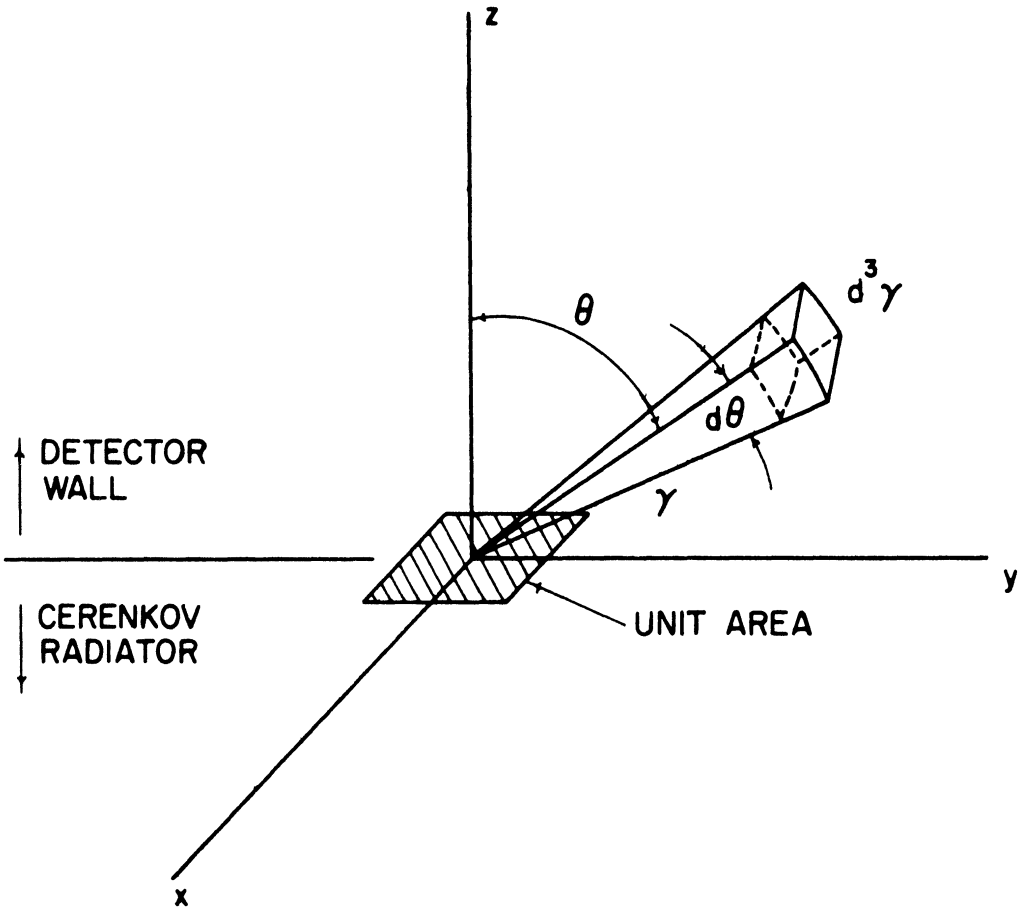


Figure 2-5. Electron Source Geometry.

The lower limit on the electron energy is determined by the refractive index of the radiator and the upper limit by the incident gamma ray energy.

The differential cross section is given by[37]

$$\frac{d\sigma}{dT} = \frac{d\sigma}{d\Omega}\frac{2\pi}{\alpha^2 m_0c^2}\left[\frac{(1+\alpha)^2-\alpha^2\cos^2\phi}{(1+\alpha)^2-\alpha(\alpha+2)\cos^2\phi}\right] \qquad (2\text{-}15)$$

where $\alpha = \frac{h\nu_0}{m_0c^2}$, $h\nu_0$ being the initial gamma energy.

$$\frac{d\sigma}{d\Omega} = \frac{r_0^2}{2}\left[\left(\frac{\alpha-\nu}{\alpha}\right)^2\left(\frac{\alpha}{\alpha-\nu}+\frac{\alpha-\nu}{\alpha}-\sin^2\theta\right)\right] \qquad (2\text{-}16)$$

where $\nu = \frac{T}{m_0c^2}$, T being the scattered electron kinetic energy.

$\alpha, \nu, \phi$ and $\theta$ are related by the familiar expressions describing the mechanics of the Compton collision[37]

$$\nu = \frac{2\alpha^2\cos^2\phi}{(1+\alpha^2-\alpha^2\cos^2\phi)} \qquad (2\text{-}17)$$

$$\cos^2\theta = \left[1 - \frac{\nu}{\alpha(\alpha-\nu)}\right]^2 \qquad (2\text{-}18)$$

The rate of energy loss is assumed to be linear, i.e.

$$\frac{dT}{dr} = \frac{1}{\gamma} \qquad (2\text{-}19)$$

where $\gamma$ is obtained from Equation (2-7) with B, the atomic stopping number, being treated as a constant evaluated at 6.0 Mev for Al.

Solving for $\cos^2\phi$ and $\sin^2\theta$ and substituting into Equation (2-14) along with Equation (2-15) we obtain

$$\eta(T,E_\gamma) = \frac{T}{4}\frac{N_e\pi r_0^2}{\alpha^2}\Bigg/\int_{\nu_{min}}^{\nu_{max}}\left[\frac{\alpha}{\alpha-\nu}+\frac{\alpha-\nu}{\alpha}+\frac{\nu^2}{(\alpha^2-\alpha\nu)^2}-\frac{2\nu}{(\alpha^2-\alpha\nu)}\right]d\nu \qquad (2\text{-}20)$$

The result of the integration is

$$\eta(T, E_\gamma) = \frac{\tau}{4} \frac{N_e \pi r_0^2}{\alpha^2} \left[ \frac{1}{(\alpha^2 + \frac{2}{\alpha} + 1)} \left( \sqrt{\tau}_{max} - \sqrt{\tau}_{min} \right) \right.$$
$$- \frac{1}{2\alpha} \left( \sqrt{\tau}_{max}^2 - \sqrt{\tau}_{min}^2 \right) + \frac{1}{\alpha - \sqrt{\tau}_{max}} - \frac{1}{\alpha - \sqrt{\tau}_{min}}$$
$$\left. + (2 - \alpha) \log \left( \frac{\alpha - \sqrt{\tau}_{max}}{\alpha - \sqrt{\tau}_{min}} \right) + \frac{1}{\alpha} \log \left[ \left( \frac{\alpha^2 - \alpha \sqrt{\tau}_{max}}{\alpha^2 - \alpha \sqrt{\tau}_{min}} \right)^2 \right] \right] \qquad (2\text{-}21)$$

where $\sqrt{\tau}_{max} = \frac{2\alpha^2}{1 + 2\alpha}$ and $\sqrt{\tau}_{min} = \frac{1}{\sqrt{2\eta}} - 1$

Except for a slow variation of B/Z with Z, the product $\tau N_e$ is independent of material and consequently all materials are equally effective for ejecting electrons into the radiator by Compton events.

The above expression was evaluated for several initial energies, ejecting electrons into a radiator having a Cerenkov threshold at 4.0 Mev.

TABLE 2-1

INTRINSIC EFFICIENCIES FOR AN ALUMINUM SURFACE

| Initial Gamma Energy-Mev | Efficiency- $\eta(T, E_\gamma)$ |
|---|---|
| 6.5 | $1.70 \times 10^{-3}$ |
| 6.0 | $1.64 \times 10^{-3}$ |
| 5.5 | $1.54 \times 10^{-3}$ |
| 5.0 | $1.31 \times 10^{-3}$ |
| 4.5 | $0.76 \times 10^{-3}$ |

The above calculation gives reasonable values of the intrinsic efficiency comparable to those attained in GM tubes at energies from 0.5 to 1.5 Mev, which also depend primarily on wall effects for electron production.[36]

The calculations assume each Cerenkov producing electron ejected from the wall into the radiator produces enough photons to be detected. Obviously this is not so and as a result, the calculated efficiencies are overestimates. The exact problem taking into account the energy and angular distribution of the electrons and the subsequent photon production and collection is more difficult and is beyond the scope of this work. Similarly the Cerenkov photon production calculations are slight overestimates in that not all electrons slow down to threshold in the radiator.

In any event, the above calculations serve as an indication of the efficiencies and photon production available in a device of this type and also indicates that large volume Cerenkov radiators are desirable in view of the small number of photons produced per unit path length, the large path lengths available in large radiators, and the increased interaction rate due to the larger surface area.

Effect of Threshold Energy on Cerenkov Photon Production per Incident Gamma

As the Cerenkov threshold is lowered, the photon production per electron increases and path length decreases. The net result is increased efficiency for event detection because of the increased photon production. Smaller radiators are permitted due to the decreased path length of electrons in the radiator. This is illustrated by reference to Figure 2-6 in which the relative number of Cerenkov photons produced per incident gamma of energy $E$ is plotted versus gamma energy.

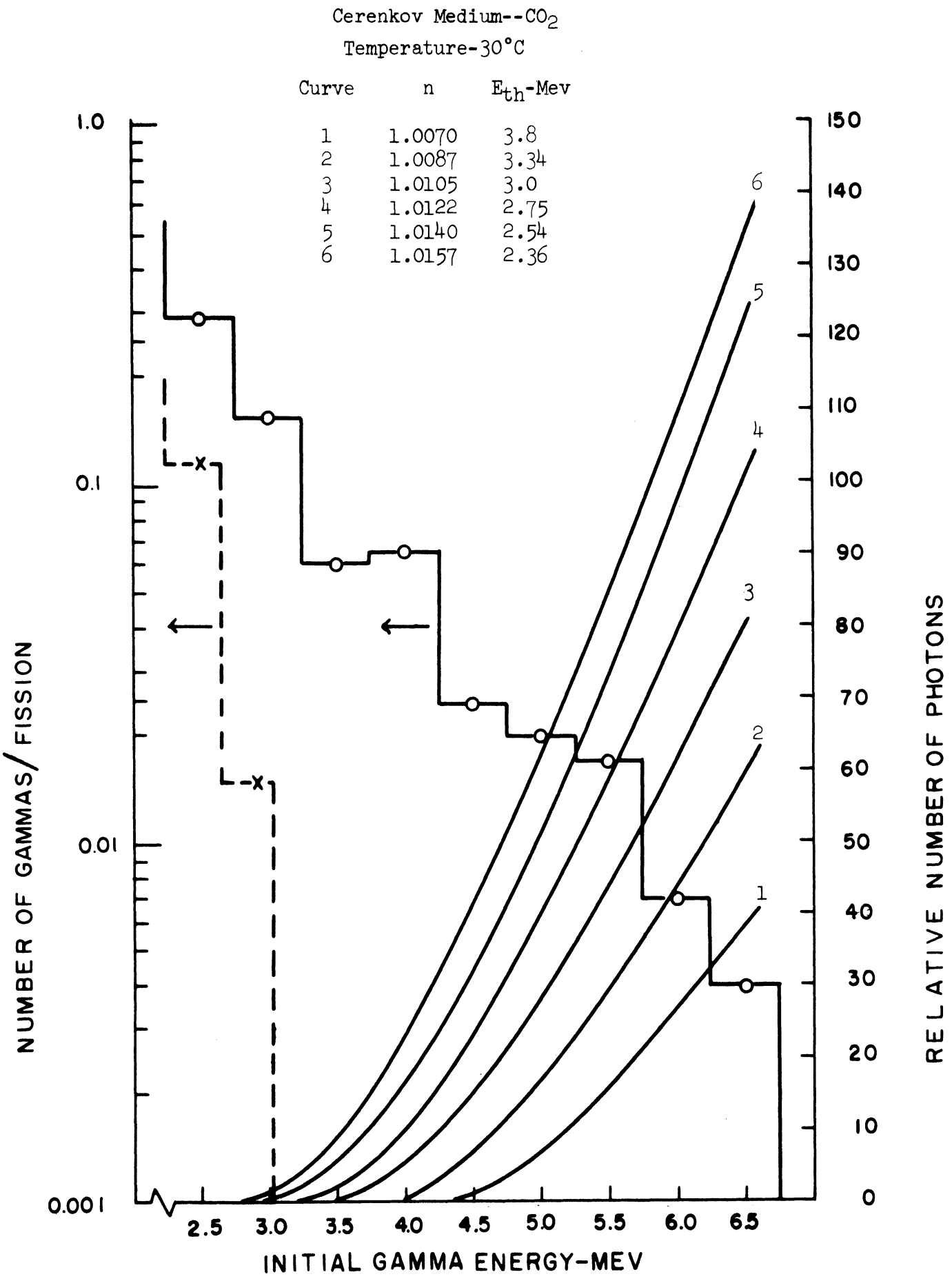


Figure 2-6. Relative Number of Cerenkov Photons Produced per Incident Gamma Ray of Energy E .

The relative number of Cerenkov photons per gamma is calculated from

$$N_\gamma(E_\gamma) = \int \eta(T, E_\gamma)\, N(E_\beta)\, dT \qquad (2\text{-}22)$$

and is the product of the probability an incident gamma of energy $E_\gamma$ ejects an electron of energy T into the radiator and the number of Cerenkov photons produced by the electron integrated over all possible electron energies. The above integral was done numerically on the Ford computer, access being through the teletype terminal in the Nuclear Engineering Computer Laboratory.

Also shown in Figure 2-6 are the prompt and delayed gamma ray spectra from fission for comparison. The calculation shows that as the refractive index increases (threshold decreases), the number of photons detected from higher energy gammas becomes increasingly significant while the lower energy gammas are not as important because of the small effective gamma interaction length in the detector wall. Detection efficiency is increased by about a factor of 4 from curve 1 to 6 with no increase in the contribution from delayed gammas. In fact, the Cerenkov threshold can be lowered to well below 3 Mev before a small contribution from delayed gammas becomes evident.

The above calculation considers only Compton events in the wall as being responsible for producing electrons. At lower energies electrons produced through photoelectric interactions will have to be considered, if materials having higher electron number densities than aluminum are to be used in contact with the Cerenkov radiator.

Calculated Efficiency in Terms of Events per Fission

Using the prompt leakage gamma ray flux at the core surface and the above intrinsic efficiencies, the number of detections per fission is calculated for the FNR.

The surface source strength based on a uniform power distribution, the previously mentioned prompt gamma ray spectra[39] and a simple shielding model[40] are shown in Table 2-2.

TABLE 2-2

SURFACE GAMMA SOURCE STRENGTHS FOR THE FNR

| Gamma Energy - Mev | Gammas/Fission | Gammas/Fission-$cm^2$ |
|---|---|---|
| 6.5 | 0.004 | $4.33 \times 10^{-7}$ |
| 6.0 | 0.007 | $7.35 \times 10^{-7}$ |
| 5.5 | 0.017 | $1.73 \times 10^{-6}$ |
| 5.0 | 0.019 | $1.83 \times 10^{-6}$ |
| 4.5 | 0.024 | $2.17 \times 10^{-6}$ |

Multiplying each of the surface source strengths by the previously calculated conversion efficiencies at each energy and adding the results, a value of $8.66 \times 10^{-9}$ events/fission-$cm^2$ is obtained. This value multiplied by the surface area of the end of the 10" diameter detector used in the noise measurements gives an efficiency

$$\epsilon = 4.25 \times 10^{-6} \text{ events/fission} \qquad (2\text{-}23)$$

C. Proof of Principle Experiments

Initial experiments were done at the Ford Nuclear Reactor (FNR) to verify the predictions from theory and specifically to measure the

pulse height distribution, to show the existence of the Cerenkov threshold and to uncover any problems which might be present in a more severe radiation environment, such as near a reactor core.

The detector schematic is shown in Figure 2-7. The reflectors are highly polished aluminum (0.02" Alzak processed sheet) while the 45° mirror is a front surface aluminized mirror. The entire construction is of aluminum except the endwindow which is a Corning 7740, UV transmitting, tempered glass, 3.5 inches in diameter and 0.5 inch thick. The phototube, mentioned previously, is a RCA8575 chosen for its high quantum efficiency for Cerenkov photons and low dark current which is desirable for detecting low level pulses from Cerenkov events.

The high energy gamma source was provided by pumping water drawn from the reactor pool through 5/16 inch aluminum tubing which extended into the reactor core. The $O^{16}$ in the water is activated through the $O^{16}(n,p)N^{16}$ reaction and then directed to the experiment area through a flat circular coil at the end of the detector. $N^{16}$ decays primarily with a 6.13 Mev gamma ray which initiates the Cerenkov radiation indirectly. In 28 percent of the decays, a beta of maximum energy of 10 Mev is emitted. This mode of decay does not contribute to the Cerenkov output as only those few electrons above 9 Mev would be able to penetrate the detector wall and still be above the threshold. The number above 9 Mev is insignificant.

The output of the photomultiplier was recorded with a Nuclear Data Model ND120 multichannel pulse height analyzer. Data at various pressures were taken with the source on and the background was subtracted with the source off. Experiments were also done with $Co^{60}$ and $Sr^{90}$

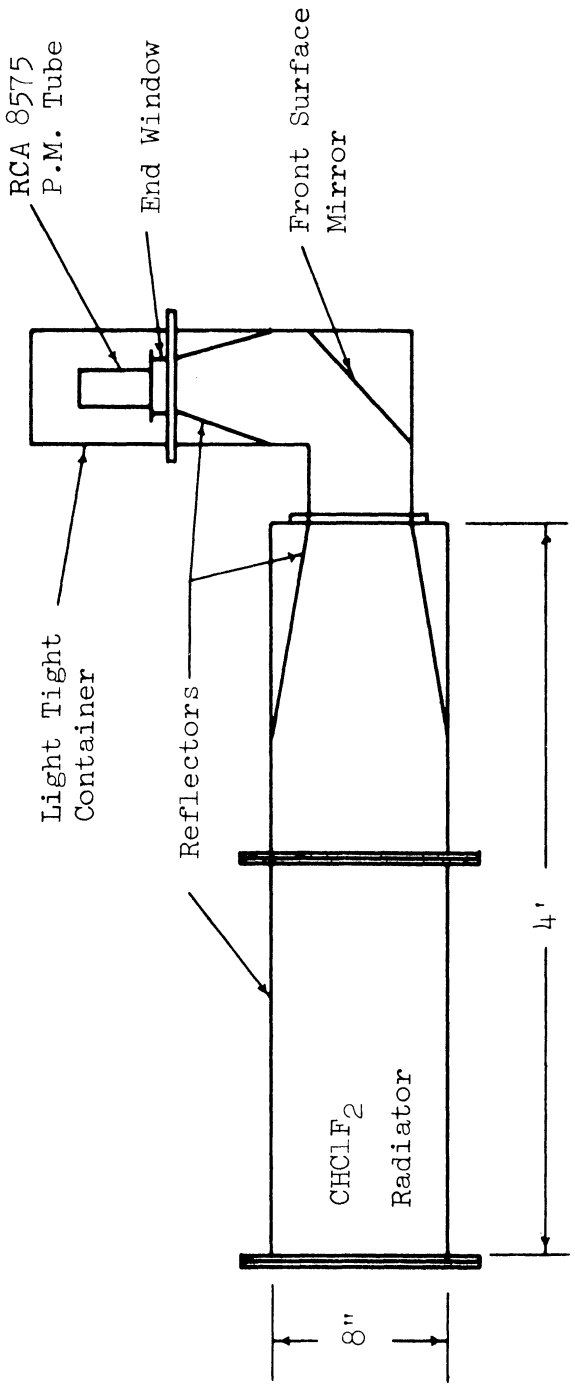


Figure 2-7. Gaseous Cerenkov Detector.

in place of the $N^{16}$ source to determine whether any of the signal was due to scintillations. The $Sr^{90}$ source (a beta source of maximum energy 2.26 Mev) was placed inside the pressure vessel.

D. Results of Initial Experiments and Discussion

Shown in Figure 2-8 is the net count rate (background subtracted) versus the absolute pressure obtained with the source arrangement at the FNR. Data were recorded at 10 psia intervals from 135 psia to 65 psia. A broad threshold exists due to the continuous energy spectrum of beta particles produced by $N^{16}$ gamma rays. The count rate appears to be reaching a maximum at higher pressures while at lower pressures the number of counts is insignificant. The relatively few events that were recorded below 65 psia are due to particle interactions in the phototube and end-window. Pressures above 135 psia could not be attained without heating the radiator.

The solid line drawn through the data points in Figure 2-8 is the theoretical pressure dependence of the count rate normalized to the experimental point at 135 psia.

We postulate that the number of counts recorded is

$$N_0 = \phi(E_\gamma) \int \eta(T, E_\beta) P(N) dT \qquad (2\text{-}24)$$

where $\eta(T, E_\beta)$ is the efficiency defined by Equation 2-21. P(N) is the probability that an output pulse is generated when N Cerenkov photons are produced in the radiator.

P(N) is given in terms of the probability $P(r|N)$, that if N photons are produced $r$ will be collected, as

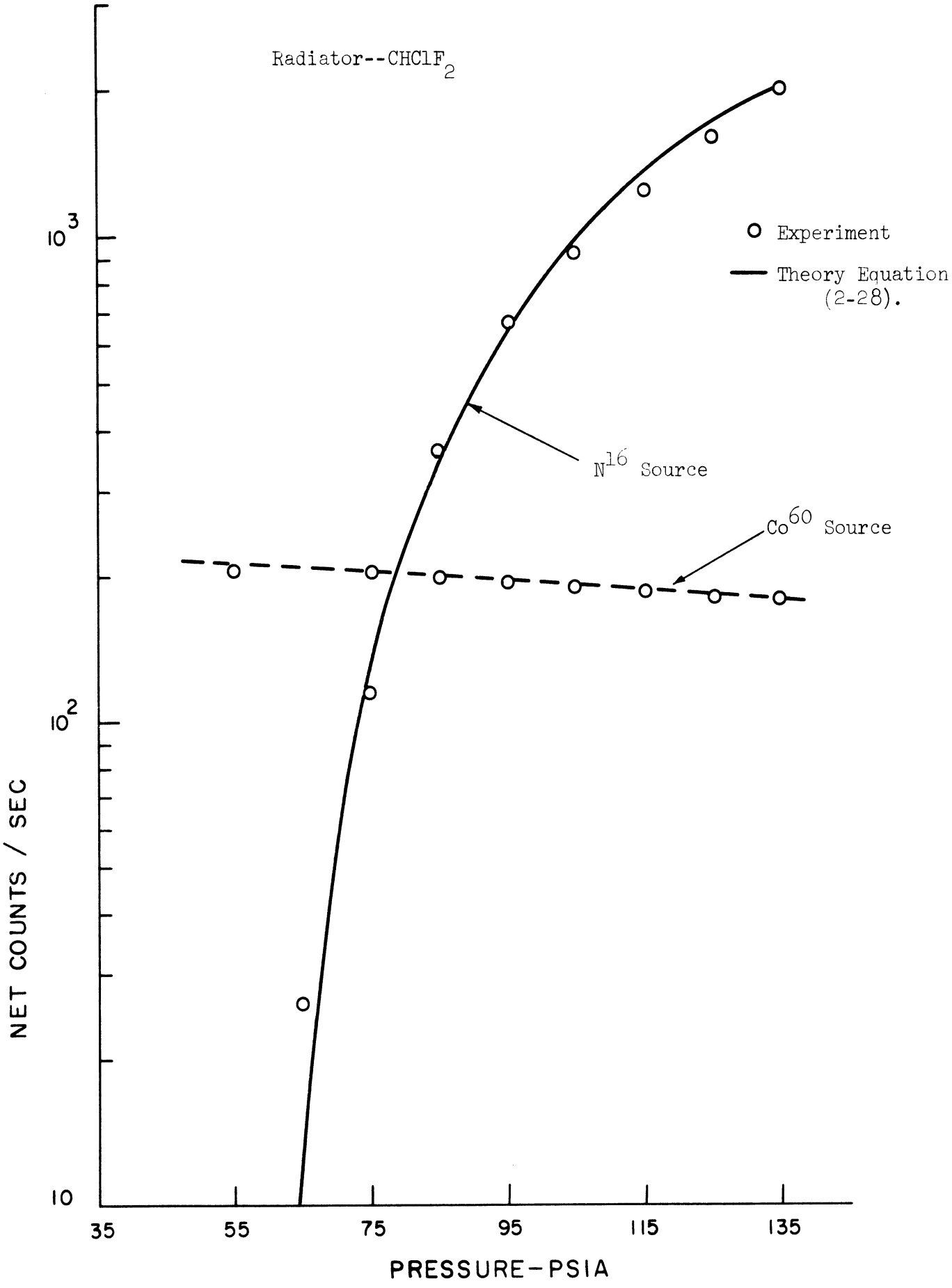


Figure 2-8. Variation of Count Rate With Pressure.

$$P(N) = \sum_{r=r_{min}}^{N} P(r/N) = 1 - \sum_{0}^{r=r_{min}-1} P(r/N) \qquad (2\text{-}25)$$

where $r_{min}$ is the minimum number of photons which must be collected to produce a pulse.

P(r/N) is given rigorously by the binomial distribution.

$$P(r/N) = \frac{N!}{(N-r)!\,r!}\, p^r (1-p)^{N-r} \qquad (2\text{-}26)$$

where p is the probability that any photon be collected at the photomultiplier cathode and N is the total number of photons generated by an electron of energy T .

If it is assumed that only one photon need be collected to produce a pulse ($r_{min} = 1$) then

$$P(N) = 1 - P(0/N) = 1 - (1-p)^N$$

which for small Np is just

$$P(N) \sim Np \qquad (2\text{-}27)$$

Similarly if $r_{min} = 2$ , P(N) is approximately $\frac{N^2 p^2}{2}$ .

The collection probability, p , is the product of the photon collection efficiency and the phototube quantum efficiency and is justifiably considered to be small.

With this the number of counts is

$$N_0 = \phi(E_\gamma)\, p \int \eta(T, E_\gamma)\, N(E_\beta)\, dT \qquad (2\text{-}28)$$

where $N(E_\beta)$ is given by Equation 2-10.

This expression was evaluated numerically for $N^{16}$ gammas ejecting electrons into the Freon-22 radiator. This is the solid line

in Figure 2-8. The agreement of the experiment with the above model is excellent. It may be concluded that Np is small and that in the counting experiment, the counts accepted correspond to the collection of single photons.

During the course of these initial experiments, it was noted that events (scintillations and Cerenkov) were initiated in the endwindow and phototube envelope by the source gamma rays. To eliminate this effect, the phototube and endwindow were shielded with lead bricks between the source and endwindow. All the data were taken with this lead shielding in position.

Because of the relatively small pulse height of the Cerenkov events, the Cerenkov spectrum was superimposed on the phototube dark pulse spectrum. This required operation of the internal amplifier in the analyzer at a high gain and required discriminator settings to remove the peak of the dark pulse spectrum to negative channels so that these events would not be counted along with the Cerenkov events.

Replacing the $N^{16}$ source with the $Co^{60}$ and $Sr^{90}$ sources showed no such response as with the $N^{16}$ source. Figure 2-8 shows the results of the tests with the $N^{16}$ source replaced by the $Co^{60}$ source. The rise in the response curve with decreasing pressure appears to be due to the removal of gas which has a shielding effect.

A simple shielding calculation tends to support the last observation. We consider

$$N_{135} = N_0 e^{-\rho_{135} \frac{A_0}{M} \sigma L} \qquad (2\text{-}29)$$

and

$$N_{55} = N_0 e^{-\rho_{55} \frac{A_0}{M} \sigma L}$$

where $N_{135}$ and $N_{55}$ are the observed total counts at 135 and 55 psia respectively and the exponential represents the attenuation due to the gas. For $Co^{60}$ gamma rays(39)

$$\frac{\mu}{\rho} = \frac{A_0 \sigma}{M} \sim .043 \text{ cm}^2/\text{gm} \qquad (2\text{-}30)$$

and L is the length through the gas from the source end to the photomultiplier tube (120cm). $\rho$ is the gas density.

Dividing and taking the logarithm of each side we have

$$\ln\left(\frac{N_{135}}{N_{55}}\right) = \left(\rho_{55} - \rho_{135}\right)\frac{\mu}{\rho} L \qquad (2\text{-}31)$$

The right hand side calculated from the data in Figure 2-8 is equal to 0.104 and the left hand side is evaluated to be 0.119. The agreement lends considerable support to the above observation.

The important thing to note in the $Co^{60}$ results is the relative flatness of the curve. $Sr^{90}$ showed the same behavior, only the rise was slightly higher at lower pressures. This discounted the possibility of scintillations being responsible for the observed counts. In addition, if scintillations were responsible for the output, the response would be expected to be linear down to 0 psia, and obviously, this is not the case.

It is also notable that the number of counts is insignificant at about one atmosphere above the pressure corresponding to the 6.13 Mev threshold. This is approximately 50 psia in Freon-22.

The reasons for this are readily explained by reference to the pulse height distribution curves shown in Figure 2-9. As is evident,

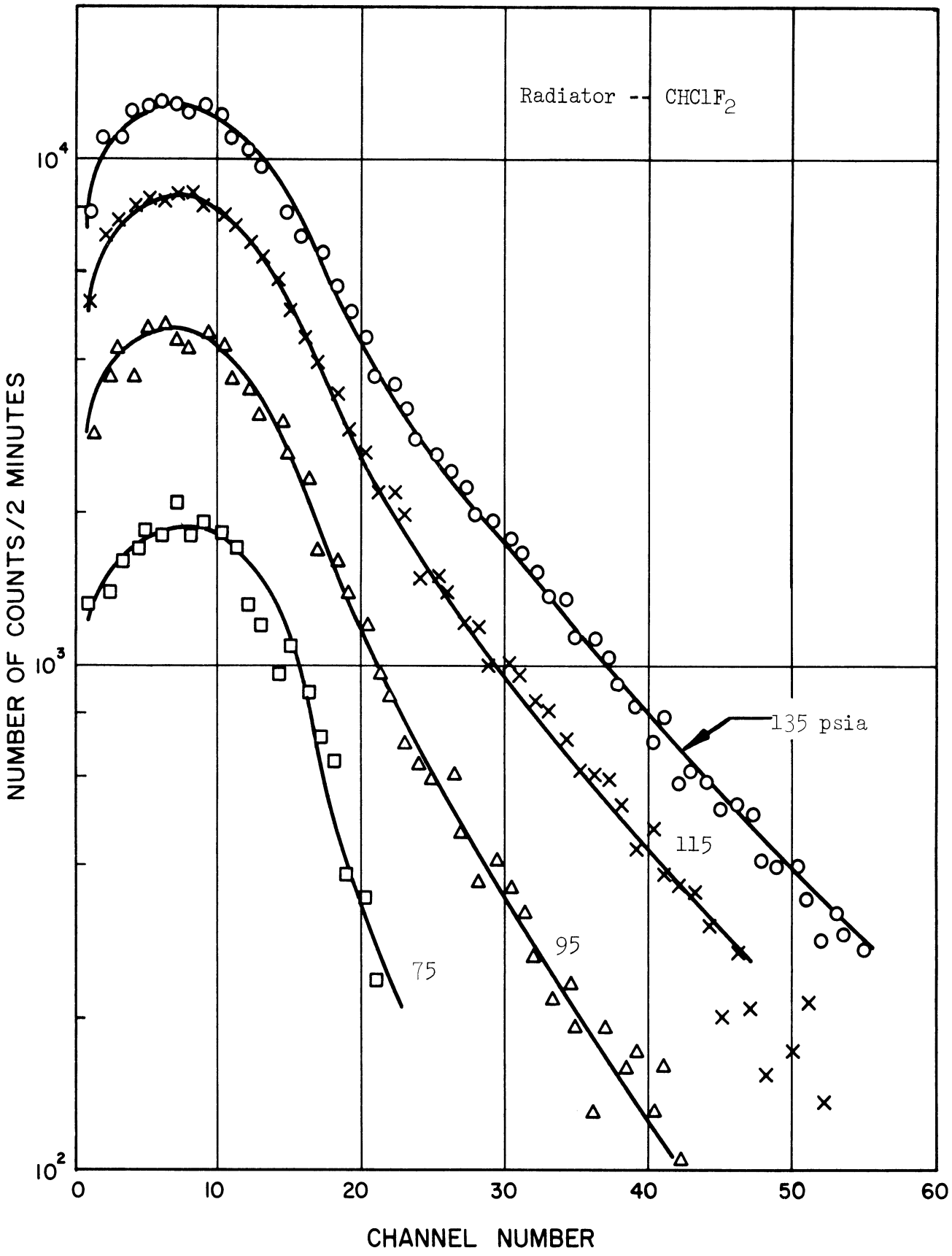


Figure 2-9. Cerenkov Pulse Height Distribution.

the pulse height and number of events both decrease as the pressure is lowered. At higher pressures, an electron forms more Cerenkov photons due to the larger refractive index, which results in larger pulse heights and more pulses than at lower pressures. Eventually, the refractive index is decreased so that no events are recorded. This occurs slightly above the 6.13 Mev threshold as mentioned previously. Again this behavior is consistent with the theory and operation of gaseous Cerenkov counters.

The results of these initial experiments verified the predictions from the theory and pointed up several important results which influenced the design of a detector to be used near the reactor. Foremost was the fact that unwanted events were initiated in the phototube envelope and pressure vessel endwindow as evidenced by the $Co^{60}$ and $Sr^{90}$ tests.

In order to test the capabilities of the device for fission gamma detection, a six foot section was added to the detector shown in Figure 2-7 and the assembly was lowered to within 6 inches from the south face of the reactor core. The detector output increased 45% when the reactor power was raised to 5 Kw. No change was observed over the same power increment with the detector unpressurized.

These results are shown in Table 2-3. Case 1, detector unpressurized, end $\sim$ 6" from core. Case 2, detector pressurized, end approximately same place as in Case 1.

TABLE 2-3

EFFECT OF FILL GAS ON DETECTOR OUTPUT

| Reactor Power | Case 1 Output at 1500 v | Case 2 Output at 1500 v |
|---|---|---|
| Shutdown | $1.0 \times 10^{-6}$ amps | $7.0 \times 10^{-7}$ amps |
| 0.5 Kw | $1.0 \times 10^{-6}$ | $7.2 \times 10^{-7}$ |
| 5 Kw | $1.0 \times 10^{-6}$ | $1.1 \times 10^{-6}$ |

In Case 2, the detector position of Case 1 was not exactly duplicated; the detector was within 1" of Case 1 position and farther from the core. The lower output at shutdown observed in Case 2 is due to the inaccurate positioning and the following two reasons: (1) the pressure vessel endwindow became slightly etched during these experiments, which would reduce light collection efficiency and (2) the introduction of radiator gas must necessarily reduce the background producing gamma flux at the endwindow. The response with the unit pressurized is indicative of the detector's selectivity for prompt fission gamma rays.

Disassembly of the detector after these tests revealed that the $CHClF_2$ radiator suffered severe radiolysis in the high gamma field surrounding the reactor. Breakdown of the Freon-22 produced, among other things, HCl, $F_2$ and HF which attacked the aluminum mirror surfaces and endwindow, seriously degrading their performance.

## E. $CO_2$ Cerenkov Detector

In view of the experience gained with the previous model, a new detector was designed to accommodate $CO_2$ as the Cerenkov radiator.

$CO_2$ (99.5% pure) was chosen because of its relative insensitivity to breakdown, ready recombination in radiation fields and the fact that radiolysis products of $CO_2$ will not affect mirror surfaces. However, because of the lower electron number densities, $CO_2$ requires much higher pressures to attain the same refractive indices as with Freon-22. It was decided, in view of the observations above, to make the new detector larger and longer than the previous model. The diameter was increased for the following reasons: increased electron paths, increased conversion efficiency due to larger surface area and the increased geometrical efficiency for detecting gammas from the reactor core.

The pressure vessel was designed for 200 psig service according to the ASME Code for Unfired Pressure Vessels. A schematic showing the detector and its relation to the reactor core is shown in Figure 2-10. The new design incorporated several improvements over the old in that it contained more lead in the form of collimators and a beam catcher was incorporated in the redesigned elbow. These improvements, along with the increased length of the main tube and vertical section, reduced the background to manageable proportions.

The main pressure vessel was constructed of 10" diameter, schedule 40, T6061 alloy aluminum pipe. The reflectors as mentioned previously were constructed of Alzak processed, 0.02" aluminum lighting sheet. The 45° mirror is an aluminized front surface, 1/4" thick flat glass plate.

The lead collimators are annuli 4" thick, 10" O.D. and 5" I.D. with the exception of the collimator near the end window which has a 3" I.D. The placement and size of the collimators were chosen such that

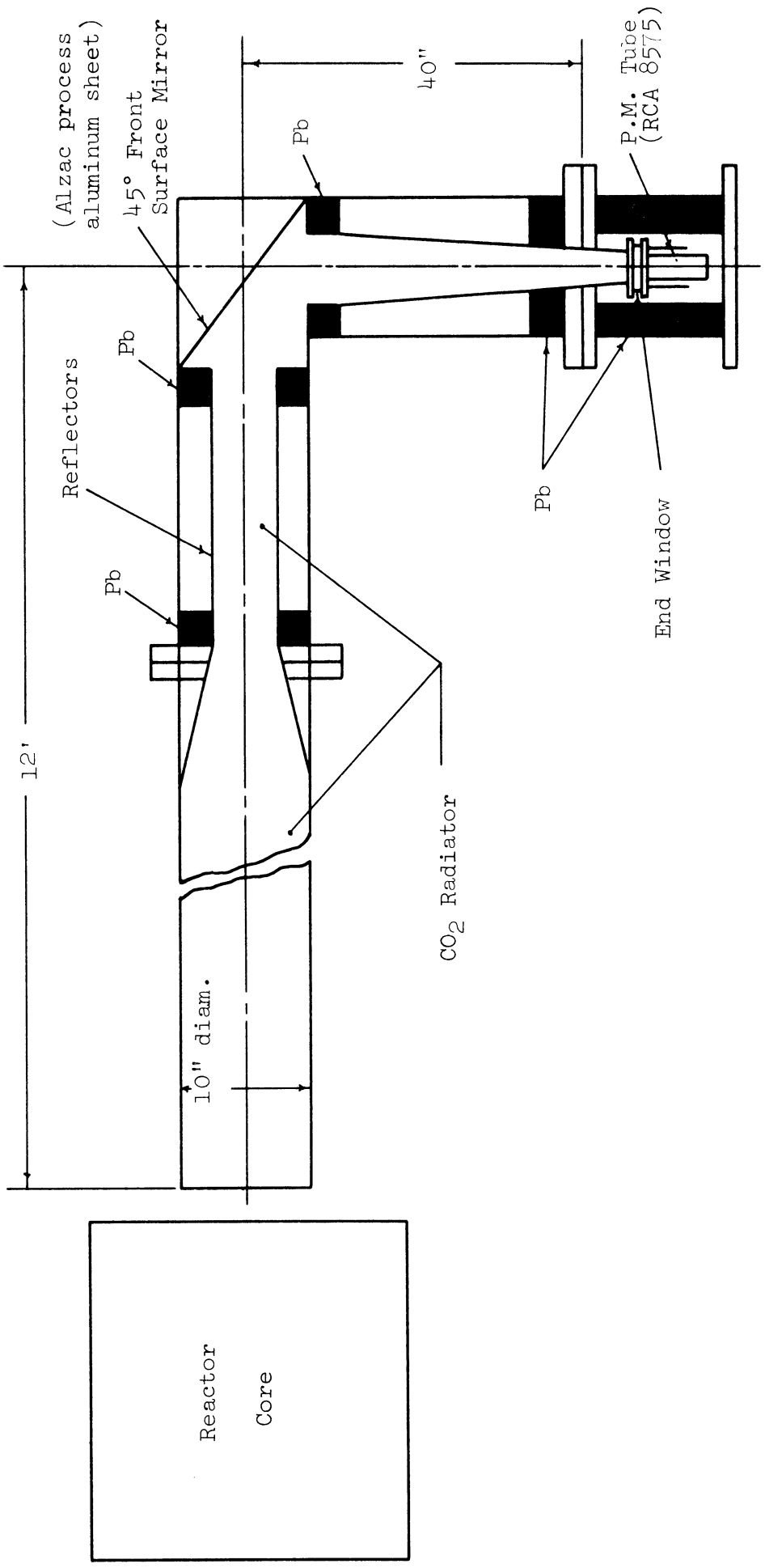


Figure 2-10. Schematic of $CO_2$ Cerenkov Detector.

any gamma ray streaming down the tube will have to scatter at least twice to enter the endwindow without passing through a considerable thickness of lead.

An extension was provided on the end flange of the pressure vessel to extend the phototube and pressure vessel endwindow into a lead annulus to provide additional shielding and reduce the solid angle subtended by the horizontal surfaces in the elbow.

The pressure was monitored by a guage connected to the main pressure vessel with high pressure rubber tubing.

Prior to operation the device was hydraulically pressure tested to $\sim$ 295 psia.

F. The Gaseous Cerenkov Detector as a Power Level Monitor

The modified Gaseous Cerenkov Detector was tested as a power level monitor at the FNR. The experiments were done two days after shutdown from operation at a level of 2 Mw for 600 hours. Surface gamma dose rates were of the order of $10^5$ to $10^6$ R/hr, consequently the FNR can properly be termed a "dirty" reactor. The photomultiplier output current* was observed as the power level and phototube high voltage were varied. The results are presented in Figure 2-11 for a radiator pressure of 195 psia and temperature of 100°F. Shown are the total and net detector current, I (background subtracted) versus the power level, P , along with an arbitrary reference curve which indicates ideal behavior, i.e., $I = \text{const.} \times P$ . The background was measured immediately prior

* In the experiments described previously in section D, the phototubes were operated in the pulse mode. In all reactor experiments, the observable was the current output of the phototubes.

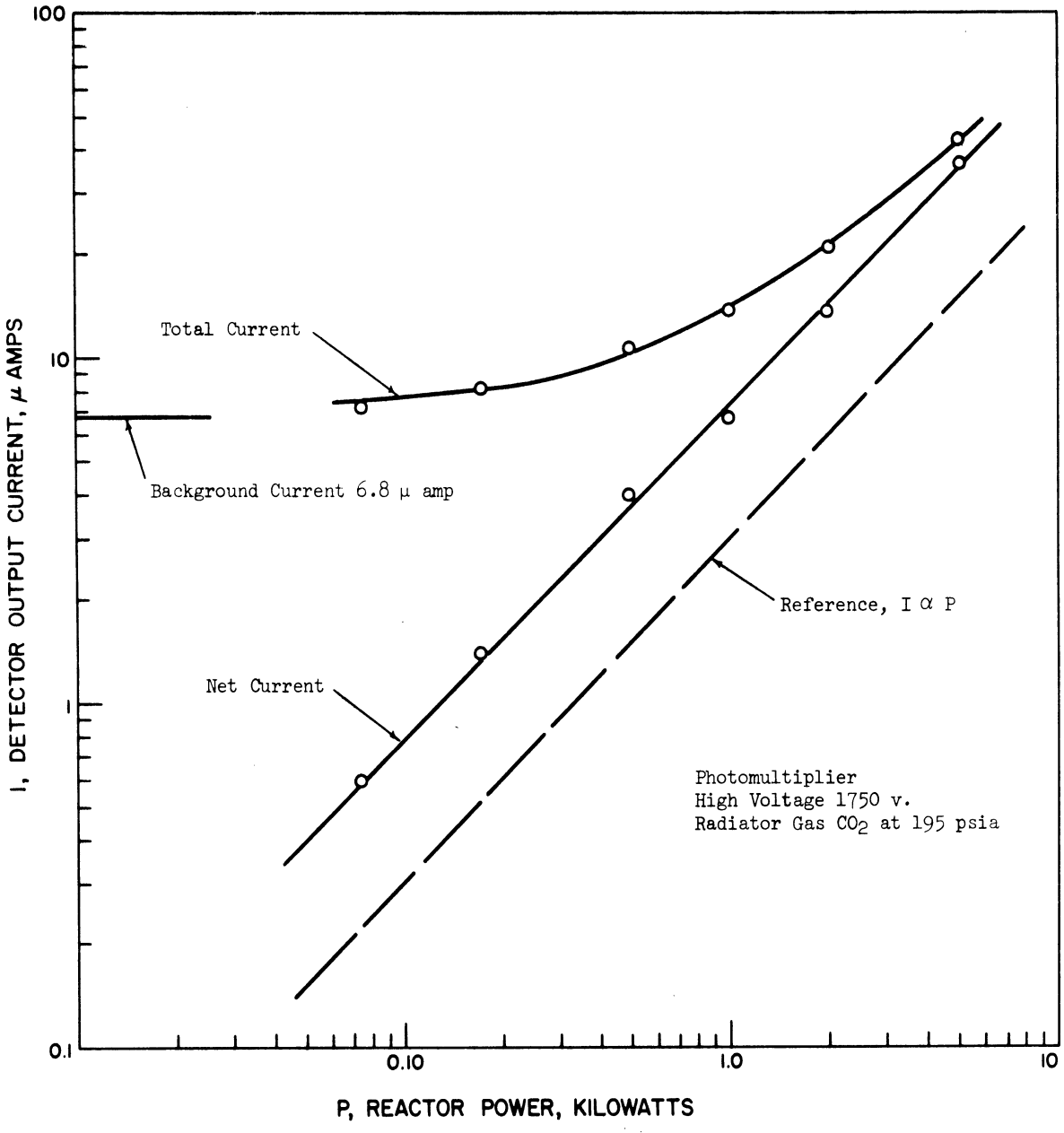


Figure 2-11. Response of the Gaseous Cerenkov Detector to Changes in Reactor Power.

to these measurements with the reactor shutdown. It is observed that the net current is directly proportional to reactor power. The total current is seen to be twice the background current at a power level of 1 kW, so that discrimination is effective above this power level. Measurements at different phototube voltages gave similar results except for a change of a constant factor, as did measurements with different reactor-detector separations and a slightly higher radiator pressure (230 psia). The reactor power was determined by averaging the counting rates in two fission chambers which were calibrated against existing reactor instrumentation. The total fission chamber count in each case exceeded 10,000 so that relative power was indicated to within 1%. The greatest uncertainty in these measurements is the calibration of the fission chamber counting rates in terms of absolute power level. Detector output was able to be read to within 2% from the picoammeter.

An experiment was also done with the unit pressurized to 85 psia. The reactor was raised in one step from shutdown to 800 watts and a change of $< 1\%$ was observed versus $\sim 160\%$ with unit at 200 psia. This small change is attributed to the few gamma rays with energies above the 6.5 Mev threshold at 85 psia. The results of the tests of the previous model detector, both with the $N^{16}$ source and the reactor source, and these observations indicate that the output of the pressurized detector is due to Cerenkov photons caused indirectly by high energy gamma rays from fission. The qualitative behavior as a function of radiator pressure is easily inferred by reference to Figure 2-8.

These results demonstrate the applicability of the detector as a reactor power level monitor. Although this particular model is not

superior to existing reactor instrumentation in discriminating against fission product gamma radiation, it is clearly better than Cerenkov detectors that use water or other high refractive index materials as radiators.[33,34] Other advantages are its virtually instant time response, simplicity of construction, freedom from major radiation damage, and the facts that detector efficiency can be varied by changing the gas pressure while the instrument range may be varied by simply changing the phototube voltage for multidecade response.

This last point is illustrated in Figure 2-12 in which the slope of the net output current $dI/dP = K$ is shown versus the phototube voltage, $V$. By varying the voltage, the instrument can be made suitable for use over many decades.

Also shown in Figure 2-12 is the background, $B$, as a function of phototube voltage, along with the manufacturer's published cathode sensitivity. It is observed that the output current and the background current both vary as the phototube voltage to the tenth power as does the manufacturer's cathode sensitivity curve. Comparison strongly suggests that the background is due to light (Cerenkov radiation and scintillations) caused by gammas incident on the pressure vessel end-window and phototube envelope.

G. Experimental Efficiency in Terms of Events/Fission

An estimate of the efficiency can be obtained by considering the detector output as a function of reactor power. The output current is related to power by

$$I = \epsilon \alpha \varphi P \qquad (2\text{-}32)$$

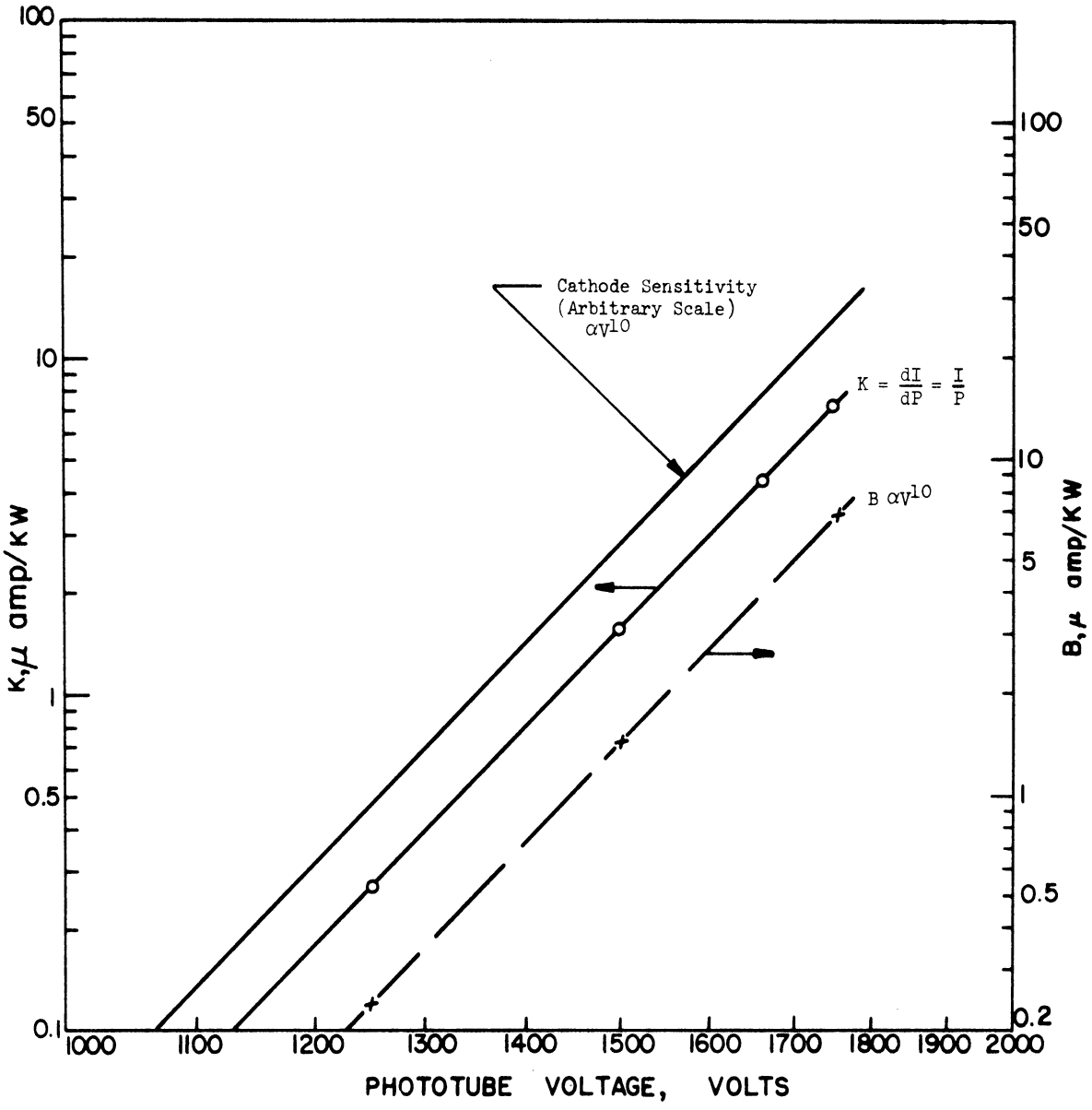


Figure 2-12. Slope of Detector Output and Background Versus Photomultiplier Tube Voltage.

and the derivative of the current with respect to reactor power is

$$\frac{dI}{dP} = \epsilon \alpha Q \qquad (2\text{-}33)$$

where $\epsilon$ = Number of events/fission

$\alpha$ = $3.2 \times 10^{10}$ fissions/watt sec.

Q = Charge collected per event

P = Reactor power in kW.

Q is more properly defined as the product of the number of photoelectrons liberated from the photocathode, the phototube gain and the charge per electron. From prior measurements with the first detector, the average number of photoelectrons per event was estimated to be between one and two. $\frac{dI}{dP}$ is obtained from Figure 2-10 with its value at 1750 volts being 7.5 $\mu$amps/kW. At 1750 volts, the tube gain is approximately $10^6$ (manufacturer's specs.). Combining these values, an efficiency of approximately $1.4 \times 10^{-6}$ events/fission is obtained. In spite of the approximate nature of the previous calculation, Equation (2-23), and the uncertainties in the tube gain etc., the agreement between the calculated and experimental values of efficiency is very good.

In any case, the above value of efficiency is considered adequate to do a cross power spectral density measurement,[23] while it is not adequate to do a power spectral density measurement[7] to determine $\beta/\ell$.

H. Initial Behavior of the Detector Near the Reactor Core

In the time immediately following placement of the detector near the reactor core prior to data recording, it was observed that the

output of the detector immediately after positioning near the core was erratic (sharp up and down fluctuations) and decreased by as much as a factor of 200 over a period of $\sim$ two hours. For two data runs, the detector was evacuated and then filled with $CO_2$ prior to positioning near the core.

Following this procedure, the output was down almost the factor of 200 without the two hour waiting time and it decreased approximately 16.5% over the first hour near the core. In the second run, a 19.5% decrease in 20 minutes was observed after evacuation, flushing with one atmosphere of $CO_2$ , evacuation, and then filling to the desired pressure. All subsequent data runs were made with the detector filled according to the last procedure above and the output was observed to stabalize in 15 to 20 minutes. The above observations cannot be accounted for by the normal 0.5 to 1.0% initial gain shift inherent in the phototube.[53]

Considering the above observations, it is reasoned that air as an impurity contributes to the high initial background, the speculation being that nitrogen, which constitutes 78% of atmospheric air, is responsible for the high initial detector current.[41] Nitrogen, being a good scintillator,[42] causes initial light output while at the same time is ionized by the intense gamma and electron flux inside the pressure vessel. The ionized nitrogen then slowly combines with other radiolysis products, such as oxygen, to form compounds which are not luminescent. Eventually, all the free nitrogen is removed in this manner accounting for the eventual attainment of a steady state output.

As stated in Reference 42, 60 percent of the nitrogen emission is in the wave length region from 3200 to 3900°A. The phototube quantum efficiency is maximum at 3850°A.

Another possible mechanism for light production is that the nitrogen could act as an energy transfer agent to absorb U.V. radiation from the excitation of carbon atoms and re-emit this absorbed radiation in the response region of the phototube. In this manner, nitrogen would act as a wavelength shifter.

In any event, the output does stabalize within a reasonable length of time and after the required waiting period, no interference from changing background was observed.

## I. Summary of Initial Experiments

The basic conclusions of these initial experiments were that the GCD operates as predicted both with a $N^{16}$ source and with reactor gammas. The detector concept should prove useful as a power level monitoring device and in certain applications it should prove superior to existing reactor instrumentation. Adequate signal to noise ratios were attained which justified continuing the work to measure reactor parameters. The results of the efficiency estimates seem reasonable in view of the results of the PSD and CPSD experiments to be reported later.

Certain disadvantages are noted, primary ones being the relatively high background and the large size. The first of these can be overcome by incorporating another 90° bend to reduce the scattering into the pressure vessel endwindow and the diameter could be decreased substantially. The decreased Cerenkov light production due to restricted electron path lengths could be more than offset by increasing the pressure without seriously affecting the discrimination properties of the device.

# CHAPTER III

# THEORY AND DETECTOR EFFECTS

## A. Introduction

In this section the power spectral density (PSD) and cross power spectral density (CPSD) of the gamma noise measurement as done by observing the output current of the GCD are derived. The detection scheme here is a more complicated chain of events than occurs in the conventional neutron experiment using $BF_3$ or similar type detectors. Due to the complexity, the problem has been formulated following the Langevin technique [43,44] rather than the more complicated doublet theory.[17,45] The results obtained are identical to those of Gelinas and Osborn[17] with the very important exception, that the effect of the detector statistics on the measured PSD is derived in terms of a quantity obtained from experiment, i.e. the variance and mean of the number of Cerenkov photons per event.

In the following derivation certain assumptions are made concerning the statistics of Cerenkov photon production and prompt fission gamma ray production. It is assumed that the statistics of the above two events are the same as the production of neutrons in the fission event. In addition loss of electrons, gamma rays and Cerenkov photons will be treated as being statistically similar to neutron absorption. The statistics of events borrowed from the neutron problem are,[44] (1) the events are statistically independent, (2) similar events in non overlapping time intervals are also independent and (3) the probability of an event per unit time is given by the product of the appropriate average number density and interaction rate. Also we assume the production of

an electron above the Cerenkov threshold is in a one to one correspondence with the loss of a gamma ray by an appropriate Compton event in the detector walls, as it is unlikely that gammas in the energy range of interest produce more than one Cerenkov producing electron.

The point reactor kinetic equations are also used as space effects are assumed to be negligible in the small FNR core. Natelson[45] has shown for the neutron fluctuation experiment that if the ratio of the migration length of neutrons to the greatest reactor dimension is large enough, a space independent theory is adequate. Such is the case for the FNR when the neutron distribution is observed. In the present case, the correlation length between fissions is still the neutron migration length, but the gamma detector sees events within a region characterized by the gamma ray mean free path which is greater than the neutron migration length. Since the migration length (5-7 cm) is nearly equal to the gamma ray mean free path (8-10 cm), it is expected that conditions similar to those for the neutron experiment apply, and the spatial effects are negligible as in the case discussed by Natelson.

This chapter includes a discussion of the various statistical quantities which enter into the experiment due to the detector and source, i.e. fluctuations in the number of ions and neutrons in the neutron experiment or Cerenkov photons, prompt gamma rays and neutrons in the gamma experiment.

The last section concludes with a discussion of the effects on the measured spectrum of the power level fluctuations induced by an independent reactivity input, in this case a temperature dependent reactivity driving function not coupled to reactor power.

B. Spectral Densities

The detection process employed here involves the observation of power level changes by monitoring the output current of a photomultiplier tube. The output is caused indirectly by prompt gamma rays emitted in fission events.

The process is shown schematically in Figure 3-1. The prompt fission gamma rays eject Cerenkov photon producing electrons from the detector wall. The photons in turn eject photoelectrons from the photocathode of the photomultiplier to form a continuous output current.

Using the notation of Osborn and Nieto[43] we form the spectral density in terms of the observable, the output current

$$\Phi_{xy}(\omega) = \frac{1}{2\pi} \langle \bar{i}(x,\omega)\, \bar{i}(y,-\omega) \rangle \qquad (3\text{-}1)$$

where $\bar{i}(x,\omega)$ and $\bar{i}(y,-\omega)$ are the Fourier transforms of the time dependent output current of detector x and y respectively.

These time dependent currents are to be related to the neutron distribution. For this purpose we postulate the following Langevin's equations for the stochastic variables and assume that the only stochastic processes are those of neutron, prompt fission gamma ray, Cerenkov photon-producing electron, and Cerenkov photon creation and annihilation. The instantaneous output current is assumed to be directly proportional to the instantaneous Cerenkov photon number density, hence the statistics of the phototube are neglected. It should be recognized that the variance in the number of photoelectrons from the photocathode is a source of uncorrelated events, but will be neglected as being small compared to contributions from other processes.

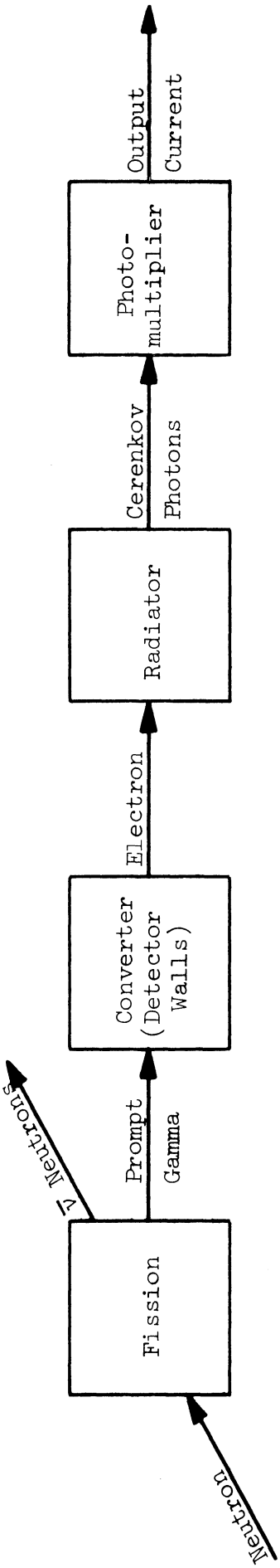


Figure 3-1. Event Sequence for Detecting Prompt Fission Gammas.

The following Langevin system equations are postulated.

$$i(t) = g G j(t) \tag{3-2}$$

$$j(t) = \epsilon r_p n_p(t) \tag{3-3}$$

$$\frac{dn_p(t)}{dt} = \langle \eta \rangle r_{pe} n_e(t) - r_p n_p(t) + S_p(t) \tag{3-4}$$

$$\frac{dn_e(t)}{dt} = r_{af} n_f(t) - r_{pe} n_e(t) + S_e(t) \tag{3-5}$$

$$\frac{dn_f(t)}{dt} = \langle \xi \rangle r_f n_m(t) - r_{af} n_f(t) + S_f(t) \tag{3-6}$$

$$\frac{dn_m(t)}{dt} = \langle J \rangle r_f n_m(t) - r_a n_m(t) + S_m(t) \tag{3-7}$$

where $g$ = Charge/electron

$G$ = Phototube gain $\left(\frac{\text{electrons out}}{\text{electrons in}}\right)$.

$\epsilon = \epsilon_q(\bar{\lambda})\epsilon_c$ the product of the quantum efficiency and the collection efficiency

$\langle \xi \rangle$ = Average number of prompt gamma rays per fission.

$\langle J \rangle$ = Average number of neutrons per fission.

$\langle \eta \rangle$ = Average number of Cerenkov photons produced per electron lost in the Cerenkov radiator.

$j(t)$ = Rate of photoelectron production at the photocathode

The small n's are the instantaneous number densities denoted by

$n_p(t)$ = Cerenkov photons

$n_e(t)$ = Cerenkov photon producing electrons

$n_\gamma(t)$ = Prompt fission gamma rays

$n_n(t)$ = Neutrons

The r's are the appropriate reaction rates defined as the probability per unit time per particle that an event of the type denoted by subscript will occur. Thus

$r_{pe}$ = Reaction rate of electrons for all loss processes

$r_{p}$ = Reaction rate of Cerenkov photons for all loss processes.

$r_{c\gamma}$ = Reaction rate of fission gammas producing Compton electrons of appropriate energy.

$r_f$ = Reaction rate of neutrons producing fissions

$r_a$ = Reaction rate of neutrons for all loss processes

$r_{a\gamma}$ = Reaction rate of gammas for all loss processes.

$S_n(t)$ , $S_\gamma(t)$ , $S_e(t)$ and $S_p(t)$ are the noise equivalent sources for neutrons, gammas, electrons and Cerenkov photons respectively, each having ensemble averages equal to zero.

A set of equations identical to Equations (3-2) through (3-5) apply to each detector, thus identical detectors are assumed in the two detector experiment.

For the moment we consider only Equations (3-4) and (3-5) and write

$S_e(t) = S_e^G(t) + S_e^L(t)$ , the sum of a gain and loss term

and define

$$Z(t) \equiv r_{c\gamma}\, n_\gamma(t) + S_e^G(t) \qquad (3\text{-}8)$$

It will be shown later that the transform of the correlation function $\langle Z(t)\, Z(t+\tau)\rangle$ will yield the spectral density derived by Gelinas and Osborn[17] for the gamma noise experiment.

Taking the Fourier transforms of Equations (3-2) through (3-5) and solving for the detector current we arrive at the Fourier transform of the instantaneous detector output current.

$$i(\omega) = qG\epsilon\tau_p \left\{ \frac{\langle n \rangle \tau_{pe}}{(\tau_{pe}+i\omega)(\tau_p+i\omega)} \left[ \bar{Z}(\omega) + \bar{S}_e^L(\omega) \right] + \frac{\bar{S}_p(\omega)}{(\tau_p+i\omega)} \right\} \tag{3-9}$$

The spectral density from Equation (3-1) is then

$$\phi_{iy}(\omega) = \frac{(q\tau_p G\epsilon)^2}{2\pi} \left\{ \frac{\langle n \rangle^2 \tau_{pe}^2}{(\tau_{pe}+\omega^2)(\tau_p^2+\omega^2)} \right.$$

$$\times \left\langle \left[ \bar{Z}(x,\omega) + \bar{S}_e^L(x,\omega) \right] \left[ \bar{Z}(y,-\omega) + \bar{S}_e^L(y,-\omega) \right] \right\rangle$$

$$+ \frac{\langle n \rangle \tau_{pe}}{(\tau_p^2+\omega^2)(\tau_{pe}-i\omega)} \left\langle \left[ \bar{Z}(x,\omega) + \bar{S}_e^L(x,\omega) \right] \bar{S}_p(y,-\omega) \right\rangle$$

$$+ \frac{\langle n \rangle \tau_{pe}}{(\tau_p^2+\omega^2)(\tau_{pe}+i\omega)} \left\langle \bar{S}_p(x,\omega) \left[ \bar{Z}(y,-\omega) + \bar{S}_e^L(y,-\omega) \right] \right\rangle$$

$$\left. + \frac{\langle \bar{S}_p(x,\omega)\, \bar{S}_p(y,-\omega) \rangle}{(\tau_p^2+\omega^2)} \right\} \tag{3-10}$$

Using the definition of $Z(\omega)$ and the fact that the correlation among $Z$, the electron gain noise source and the Cerenkov photon source is zero, the spectral density becomes

$$\phi_{xy}(\omega) = \frac{(qG\epsilon\tau_p)^2}{2\pi} \left\{ \frac{\langle n \rangle^2 \tau_{pe}^2}{(\tau_{pe}^2+\omega^2)(\tau_p^2+\omega^2)} \left[ G_{xy}(\omega) \right.\right.$$

$$\left.\left. + \left\langle \bar{S}_e^L(x,\omega)\, \bar{S}_e^L(y,-\omega) \right\rangle \right] + \frac{\langle n \rangle \tau_{pe}}{(\tau_p^2+\omega^2)} \left[ \frac{\langle \bar{S}_e^L(x,\omega)\, \bar{S}_p(y,-\omega) \rangle}{(\tau_{pe}-i\omega)} \right. \right. \tag{3-11}$$

$$+\frac{\langle \bar{S}_p(x,\omega)\,\bar{S}_e^{L}(y,-\omega)\rangle}{(\tau_{pe}+i\omega)}\Big] + \frac{\langle \bar{S}_p(x,\omega)\,\bar{S}_p(y,-\omega)\rangle}{(\tau_p^2+\omega^2)}\Big\} \quad \text{(3-11 Continued)}$$

where $G_{xy}(\omega) = \frac{1}{2\pi}\langle \bar{Z}(x,\omega)\,\bar{Z}(y,-\omega)\rangle$

Taking the statistics of production and losses of all particles to be analogous to those for neutrons (fission and absorption) and applying the results of the Langevin's technique,[43,44] the following transformed correlation functions are

$$\langle \bar{S}_e^{L}(x,\omega)\,\bar{S}_p(y,-\omega)\rangle = -2\pi\langle n\rangle \tau_{pe} N_e^{o} \delta_{xy} \qquad (3\text{-}12)$$

$$\langle \bar{S}_e^{L}(x,\omega)\,\bar{S}_e^{L}(y,-\omega)\rangle = 2\pi \tau_{pe} N_e^{o} \delta_{xy} \qquad (3\text{-}17)$$

$$\langle \bar{S}_p(x,\omega)\,\bar{S}_p(y,-\omega)\rangle = \langle \bar{S}_p^{G}(x,\omega)\,\bar{S}_p^{G}(y,-\omega)\rangle$$

$$+\langle \bar{S}_p^{L}(x,\omega)\,\bar{S}_p^{L}(y,-\omega)\rangle = 2\pi\left[\langle n^2\rangle \tau_{pe} N_e^{o} + \tau_p N_p^{o}\right]\delta_{xy} \qquad (3\text{-}18)$$

where $\delta_{xy}$ is the Kronecker delta. The large N's with a superscript o denote average values as obtained from the steady state equations

$$\tau_{pe} N_e^{o} = \tau_c N_t^{o} \qquad (3\text{-}19)$$

$$\tau_p N_p^{o} = \tau_{pe} N_e^{o} \langle n\rangle \qquad (3\text{-}20)$$

Using the steady state equations and the transformed correlation functions evaluated above, the spectral density becomes

$$\phi_{xy}(\omega) = \frac{(g G \epsilon \tau_p)^2}{(\tau_p^2+\omega^2)} \langle n \rangle^2 \left\{ \frac{\tau_{pe}^2}{(\tau_{pe}^2+\omega^2)} G_{xy}(\omega) + \tau_c N_y^0 \left[ \frac{\langle n^2 \rangle - \langle n \rangle^2 + \langle n \rangle}{\langle n \rangle^2} \right] \delta_{xy} \right\} \tag{3-21}$$

When x=y the result is the single detector power spectral density and if x≠y the result is the cross power spectral density.

For frequencies of interest in a reactor noise experiment $\omega << \tau_p$ & $\tau_e$ , therefore (3-21) becomes

$$\phi_{xy}(\omega) = (g G \epsilon)^2 \langle n \rangle^2 \left\{ G_{xy}(\omega) + \tau_c N_y^0 \left[ \frac{\langle n^2 \rangle - \langle n \rangle^2 + \langle n \rangle}{\langle n \rangle^2} \right] \delta_{xy} \right\} \tag{3-22}$$

$G_{xy}(\omega)$ can now be calculated by use of the Langevin's technique. Fourier transforming Equation (3-6) and (3-7) we get

$$(\alpha + i\omega) \bar{n}_n(\omega) = \bar{S}_n(\omega) \tag{3-23}$$

$$(\tau_{af} + i\omega) \bar{n}_f(\omega) = \langle g^0 \rangle \tau_f \bar{n}_n(\omega) + \bar{S}_f(\omega) \tag{3-24}$$

where $\alpha = \langle J \rangle \tau_f - \tau_a$ .

$Z(\omega)$ is formed

$$Z(\omega) = \tau_c \bar{n}_f(\omega) + \bar{S}_e^G$$

$$= \frac{\tau_c \langle g \rangle \tau_f \bar{S}_n(\omega)}{(\alpha + i\omega)(\tau_{af} + i\omega)} + \frac{\tau_c \bar{S}_f(\omega)}{(\tau_{af} + i\omega)} + \bar{S}_e^G(\omega) \tag{3-25}$$

The spectral density is then

$$G_{xy}(\omega) = \frac{1}{2\pi}\left\{\frac{\bar{\nu}_c^2\langle\rho\rangle\bar{\nu}_f^2}{(\alpha^2+\omega^2)(\bar{\nu}_{ag}+\omega^2)}\langle\bar{S}_m(x,\omega)\,\bar{S}_m(y,-\omega)\rangle\right.$$

$$+\frac{\bar{\nu}_c^2\langle\rho\rangle\bar{\nu}_f}{(\bar{\nu}_{ag}^2+\omega^2)}\left[\frac{\langle\bar{S}_m(x,\omega)\,\bar{S}_f(y,-\omega)\rangle}{(\alpha-i\omega)}+\frac{\langle\bar{S}_f(x,\omega)\,\bar{S}_m(y,-\omega)\rangle}{(\alpha+i\omega)}\right]$$

$$+\frac{\bar{\nu}_c^2}{(\bar{\nu}_{ag}^2+\omega^2)}\langle\bar{S}_f(x,\omega)\bar{S}_f(y,-\omega)\rangle+\frac{\bar{\nu}_c}{(\bar{\nu}_{ag}-i\omega)}\langle\bar{S}_f(x,\omega)\,\bar{S}_e^G(y,-\omega)\rangle$$

$$\left.+\frac{\bar{\nu}_c^2}{(\bar{\nu}_{ag}+i\omega)}\langle\bar{S}_e^G(x,\omega)\,\bar{S}_f(y,-\omega)\rangle+\langle\bar{S}_e^G(x,\omega)\,\bar{S}_e^G(y,-\omega)\rangle\right. \quad (3\text{-}26)$$

The transforms of the correlation functions are evaluated as before.

At this point we made an assumption concerning the gamma distribution. We assume that the gamma distribution as viewed by each detector is the same as in the neutron experiment. That is, that the gamma level rises and falls at each detector location simultaneously. This is tantamount to saying that the gammas diffuse as neutrons do and whenever more than one gamma is formed per fission the spatial distribution is isotropic. This results in a correlated component in the outputs of the separate detectors due to the fluctuations in the number of gammas per fission.

$$\langle\bar{S}_m(x,\omega)\,\bar{S}_m(y,-\omega)\rangle = 2\pi\left[\bar{\nu}_a N_m^0+\langle J^2\rangle\bar{\nu}_f N_m^0\right] \quad (3\text{-}27)$$

$$\langle\bar{S}_m(x,\omega)\,\bar{S}_f(y,-\omega)\rangle = -2\pi\langle\xi\rangle\bar{\nu}_f N_m^0 \quad (3\text{-}28)$$

$$\langle\bar{S}_f(x,\omega)\,\bar{S}_f(y,-\omega)\rangle = 2\pi\left[\langle\xi\rangle\bar{\nu}_f N_m+\langle\xi^2\rangle\bar{\nu}_f N_m^0\right] \quad (3\text{-}29)$$

$$\langle \bar{S}_\gamma(x,\omega)\bar{S}_e^{\sigma}(y,-\omega)\rangle = -2\pi\langle\varphi\rangle\frac{\bar{\nu}_f}{\bar{\nu}_{a\gamma}}N_m^0\bar{\nu}_{c\gamma}\delta_{xy} \qquad (3\text{-}30)$$

$$\langle \bar{S}_e^{\sigma}(x,\omega)\bar{S}_e^{\sigma}(y,-\omega)\rangle = \bar{\nu}_c\langle\varphi\rangle\frac{\bar{\nu}_f}{\bar{\nu}_{a\gamma}}N_m^0\delta_{xy} \qquad (3\text{-}31)$$

The steady state equations for neutrons and gammas have been used in the above to put the results in terms of the neutron steady state values.

Substituting the above results into Equation (3-26) and simplifying we get

$$G_{xy}(\omega) = \frac{\bar{\nu}_c\langle\varphi\rangle\bar{\nu}_f N_m^0}{\bar{\nu}_{a\gamma}}\left\{\delta_{xy} + \frac{\bar{\nu}_c\langle\varphi\rangle}{\bar{\nu}_{a\gamma}}\right.$$
$$\times\left[\frac{k^2}{(1-k)^2}\,\frac{\langle J^2\rangle-\langle J\rangle}{\langle J\rangle^2}\,\frac{\alpha^2}{(\alpha^2+\omega^2)}\right.$$
$$\left.\left.+\frac{\bar{\nu}_{a\gamma}^2}{(\bar{\nu}_{a\gamma}^2+\omega^2)}\,\frac{\langle\varphi^2\rangle-\langle\varphi\rangle}{\langle\varphi\rangle^2}\right]\right\} \qquad (3\text{-}32)$$

In arriving at the above result it has been assumed that $\omega \ll \bar{\nu}_{a\gamma}$ in the denominator of the multiplier of the term in the square brackets.

For x=y , the single detector, this result is identical to that obtained by Gelinas and Osborn[17] using the doublet theory. This is to be expected as it was shown by Akcasu and Osborn[44] that both approaches yield identical results.

For $x \neq y$ , Equation (3-32)describes the two detector gamma experiment and is strikingly different than the result for the same experiment conducted observing neutrons. In the conventional two detector neutron experiment, the usual uncorrelated term does not enter in, i.e.

a term analogous to the first one in Equation (3-32). This term is also zero in the two detector gamma experiment but according to the above theory, another term $\frac{\langle \rho^2 \rangle - \langle \rho \rangle}{\langle \rho \rangle^2}$, plays a role and should have the same effect on the measured cross power spectral density as the uncorrelated term has on the power spectral density.

The origin of this term is the fluctuation in the number of gamma rays per fission. In the experiments to be reported later the effects of this term on the measured spectrum was not observed. The reason being that the second term in Equation (3-32) is much larger than the last. Compare

$$\frac{k^2}{(1-k)^2} \frac{\langle J^2 \rangle - \langle J \rangle}{\langle J \rangle^2} \frac{\alpha^2}{(\alpha^2+\omega^2)}$$

$$\simeq \frac{k^2}{(1-k)^2} (.795) \frac{1}{2} \qquad @ \alpha = \omega$$

and $$\frac{\bar{\nu}_{\alpha\gamma}^2}{(\bar{\nu}_{\alpha\gamma}^2+\omega^2)} \frac{\langle \rho^2 \rangle - \langle \rho \rangle}{\langle \rho \rangle^2} \simeq 0.25 \qquad @ \omega << \bar{\nu}_{\alpha\gamma}$$

k is the prompt multiplication factor, $k = k_{eff} (1 - \beta_{eff})$, and at critical is approximately equal to $1 - \beta_{eff}$. As a consequence

$$(.397) \frac{k^2}{(1-k)^2} >> 0.25$$

and the effect of the additional term is hardly observable in an experiment where the detection efficiency is low, i.e., small ratio of correlated to uncorrelated signal as was the case in the experiments to be discussed later. Since the observed $\rho$ depends on the detector threshold, an experiment in which the threshold is low (large observable $\rho$) and detector efficiency high, should be able to measure the gamma-gamma correlations.

Combining Equation (3-22) and (3-32) we arrive at the spectral density as determined from the output of the GCD.

$$\phi_{xy}(w) = (g\,G\,\epsilon)^2 \langle n \rangle^2 \left\{ \frac{\tau_c \langle \rho \rangle \tau_f N_m^0}{\tau_{ax}} \left\{ \delta_{xy} \right.\right.$$

$$+ \frac{\tau_c \langle \rho \rangle}{\tau_{ax}} \left[ \frac{k^2}{(1-k)^2} \; \frac{\langle J^2 \rangle - \langle J \rangle}{\langle J \rangle^2} \; \frac{\alpha^2}{(\alpha^2 + w^2)} \right.$$

$$\left.\left. + \frac{\tau_{ax}^2}{(\tau_{af}^2 + w^2)} \; \frac{\langle \rho^2 \rangle - \langle \rho \rangle}{\langle \rho \rangle^2} \right] \right\}$$

$$+ \tau_f \langle \rho \rangle N_m^0 \left[ \frac{\langle n^2 \rangle - \langle n \rangle^2 + \langle n \rangle}{\langle n \rangle^2} \right] \delta_{xy} \Bigg\} \qquad (3\text{-}33)$$

The term amenable to measurement in a fluctuation experiment is the second term in Equation (3-33). Specifically the quantity of interest is $\alpha$ and it is inferred from the spectral shape of the Lorentzian $\frac{\alpha^2}{\alpha^2+w^2}$. When delayed neutrons are taken into account (single delay group) this term becomes, for a critical reactor[46]

$$\frac{(\ell/\beta)^2}{\left(\frac{w^2}{w^2+\lambda^2}\right)^2 + w^2\left(\frac{\ell}{\beta} + \frac{\lambda}{w^2+\lambda^2}\right)^2}$$

and for a subcritical reactor

$$\frac{(\ell/\beta)^2}{\left(-\rho + \frac{w^2}{w^2+\lambda^2}\right)^2 + w^2\left(\frac{\ell}{\beta} + \frac{\lambda}{\lambda^2+w^2}\right)^2}$$

At midfrequencies such that $w^2 \gg \lambda^2$ the expression for the critical reactor reduces to

$$\frac{1}{\left(\frac{\ell}{\beta}\right)^2 + w^2}$$

As noted previously the results of a spectral density measurement observing the gamma rays yields the same information as obtained from a neutron experiment at low frequencies around $\omega = \beta/\ell$ . At very high frequencies one might derive information about the additional spectral term in Equation (3-32), i.e., the term involving the statistics of the number of Cerenkov photons per event.

The advantages in doing the gamma noise experiment arise not from any additional information gained but from the fact that the detector used in the experiment may be a threshold type device which is insensitive to fission product gamma rays because of their lower energy. It is this aspect of the experiment that enables the measurements to be done on "dirty" reactors where present neutron detectors fail.

C. Discussion of Statistical Quantities in Noise Experiments

In the frequency range of interest $\omega << \sqrt{\lambda_\gamma}$ , the total uncorrelated term becomes

$$1 + \frac{\langle n^2 \rangle - \langle n \rangle^2 + \langle n \rangle}{\langle n \rangle^2} + \frac{\langle \xi(\xi - 1) \rangle}{\langle \xi \rangle^2} \qquad (3\text{-}34)$$

The contribution from the detector is the second term above

$$\frac{\langle n^2 \rangle - \langle n \rangle^2 + \langle n \rangle}{\langle n \rangle^2} = \frac{V}{M^2} + \frac{1}{M} \qquad (3\text{-}35)$$

where $V$ is the variance and $M$ is the mean.

This term has been estimated to be approximately two from a pulse height distribution obtained with a similar type detector using an $N^{16}$ source. With a prompt fission gamma spectrum this term would be

expected to be slightly larger due to the variance in the energy distribution of the fission gammas.

In any case this term added to the constant term in $G(\omega)$ would dictate an efficiency requirement of approximately two times the previously estimated minimum of $5 \times 10^{-5}$.[47] An analogous term involving the distribution in charge per event was derived by Osborn and Nieto[43] for a $BF_3$ detector. In this case the variance in the number of charges collected per event is considerably less than in the case of the GCD, hence the problem is not as serious in these type detectors. Similar problems exist with fission chambers when operated in the current mode.[48]

The overall difficulty in the conduct of noise experiments using neutron or gamma ray detectors can be qualitatively evaluated by reference to the data in Table 3-1.

TABLE 3-1

STATISTICAL QUANTITIES IN NOISE MEASUREMENTS

| Quantity | Term | Value | Reference |
|---|---|---|---|
| Neutrons / Fission | $\frac{\langle J(J-1)\rangle}{\langle J\rangle^2}$ | 0.785 | 8 |
| Gammas / Fission | $\frac{\langle \xi(\xi-1)\rangle}{\langle \xi\rangle^2}$ | 0.25 | 17 |
| Cerenkov Photons / Event | $\frac{\langle n^2\rangle - \langle n\rangle^2 + \langle n\rangle}{\langle n\rangle^2}$ | 2.0 | This work |
| $BF_3$ - Charge / Event | $\frac{\langle q^2\rangle - \langle q\rangle^2 + \langle q\rangle}{\langle q\rangle^2}$ | $\ll 1$ | 36 |

Comparing the different quantities which enter into each experiment it is immediately noted that regardless of the detector used the uncorrelated term in the gamma noise experiment is larger than in the neutron experiment due to the term $\frac{\langle q(q-1)\rangle}{\langle q\rangle^2}$ which is inherent in the gamma noise experiment. Also considering the statistics the Cerenkov detector it is worse off than the $BF_3$ detector. The effect of these statistical quantities is to contribute to the uncorrelated term in the PSD. The particular advantage of the two detector CPSD experiment is that these uncorrelated components do not enter in because of the data processing procedure, rather they contribute only to the statistical error in the result.

The above discussion helps in part to explain the inability of the present model of the GCD to isolate the $\beta/\ell$ breakpoint in a single detector experiment. This is not meant to say that the experiment is impossible but that it requires a slightly higher efficiency to obtain the same information with comparable accuracy as in the neutron experiment using conventional detectors.

D. Effects of a Reactivity Input

The theory developed in Section B of this chapter predicts the spectral shape of the PSD and CPSD in a zero power experiment with the only noise sources being due to variations in the fission, capture and leakage rates. In this section the effect of an external reactivity input, specifically reactivity fluctuations induced by heating is qualitatively revealed, to show the power dependence of the amplitudes and effect on the zero power spectrums.

Since contributions to the PSD from independent noise sources add as squares in the output,[47] the resultant spectral densities are the sums of products of the input spectral densities and the square modulus of the transfer function.[49] Thus

$$\phi_{oo}(\omega) = \sum_{j} \phi_{ii}^{j} \left| G_j(\omega) \right|^2 \qquad (3\text{-}35)$$

where $\phi_{oo}(\omega)$ is the output spectral density, $\phi_{ii}^{j}(\omega)$ is the input spectral density and $G_j(\omega)$ is the transfer function for inputs of type $j$.

The type of reactivity fluctuations encountered in the experiments to be discussed later are due to temperature variations in the coolant, induced by steady fission product gamma ray heating. Heat is formed directly in the coolant and fuel elements and is removed by natural circulation. This mode of cooling introduces large unsteady variations in the coolant density which affect the moderating and absorbing properties and hence the neutron level. Fluctuations are also introduced by uneven cooling and subsequent heating of the water in the core. Reactivity fluctuations induced in this way through the temperature coefficient of reactivity are independent of reactor power and are reflected in the spectral densities as a component which varies as the square of the reactor power.[3,4]

# CHAPTER IV

## DESCRIPTION OF THE EXPERIMENTS AND INSTRUMENTATION

### A. Experiments

The object of the initial experiments was to measure the PSD of the FNR. A determination of $\beta/\ell$ from the spectral shape would serve to accomplish the overall goals of this study, that is to prove the detection concept applied to reactor measurements and to verify the predictions of the theory, i.e., the feasibility of the gamma noise experiment.

During the course of these early experiments a sharp rise in the PSD below 2.5 cps was observed which was totally unexpected. The preliminary results as presented in Figure 5-1 show a change in amplitude from natural to forced convection. The different nature of the known flow patterns in the two cases suggested that the observed fluctuations were caused indirectly by temperature variations in the coolant water. This further suggested fluctuation experiments observing the output of a thermocouple placed above the core. In order to better understand the relationship between the temperature and gamma ray PSD's, fluctuation experiments were done as a function of power level with forced and natural convection. The cross correlation function between the two signals was measured from data records taken simultaneously.

Because the efficiency of this model of the GCD was rather low, a series of CPSD measurements were made to isolate the $\beta/\ell$ breakpoint. Also an experiment was done to determine the effect of the fission product gamma level in the reactor. For this, the center six elements were

replaced by new fuel and the rest of the core was made up of fuel that had cooled at least sixty days.

In addition to the reactor experiments, a series of experiments were done to test equipment response and determine correction factors to be applied to the measured spectra. These were the analysis of white noise records obtained by placing a $Co^{60}$ source against the pressure vessel endwindow and measurements of the output of a test oscillator into various detecting circuits.

B. Equipment

1. Reactor.

The experiments were done on the Ford Nuclear Reactor at the University of Michigan. The FNR is a swimming pool type reactor having fully enriched BSR type fuel elements. A $D_2O$ tank covers the north face of the reactor core. Its purpose is to enhance the thermal neutron flux at the beam ports. Prior to the experiments the reactor was operated for 25 days at 2MW. The experiments were done on the second day after shutdown. The majority of the fuel had a longer operating history than 25 days. Surface gamma dose rates were between $10^5$ and $10^6$ R/hr., as measured with a Victoreen Roentgen-Rate Meter.

Most of the experiments were performed with the core configuration shown in Figure 4-1a, the fuel in which had an operating history described above. Shown in Figure 4-1b is the core configuration used in one series of CPSD measurements. The center six elements were new fuel, previously unirradiated and the remainder of the core consisted of elements which had decayed at least 60 days. The background for this latter core was $\sim$ 1/4 that measured on Core loading I.

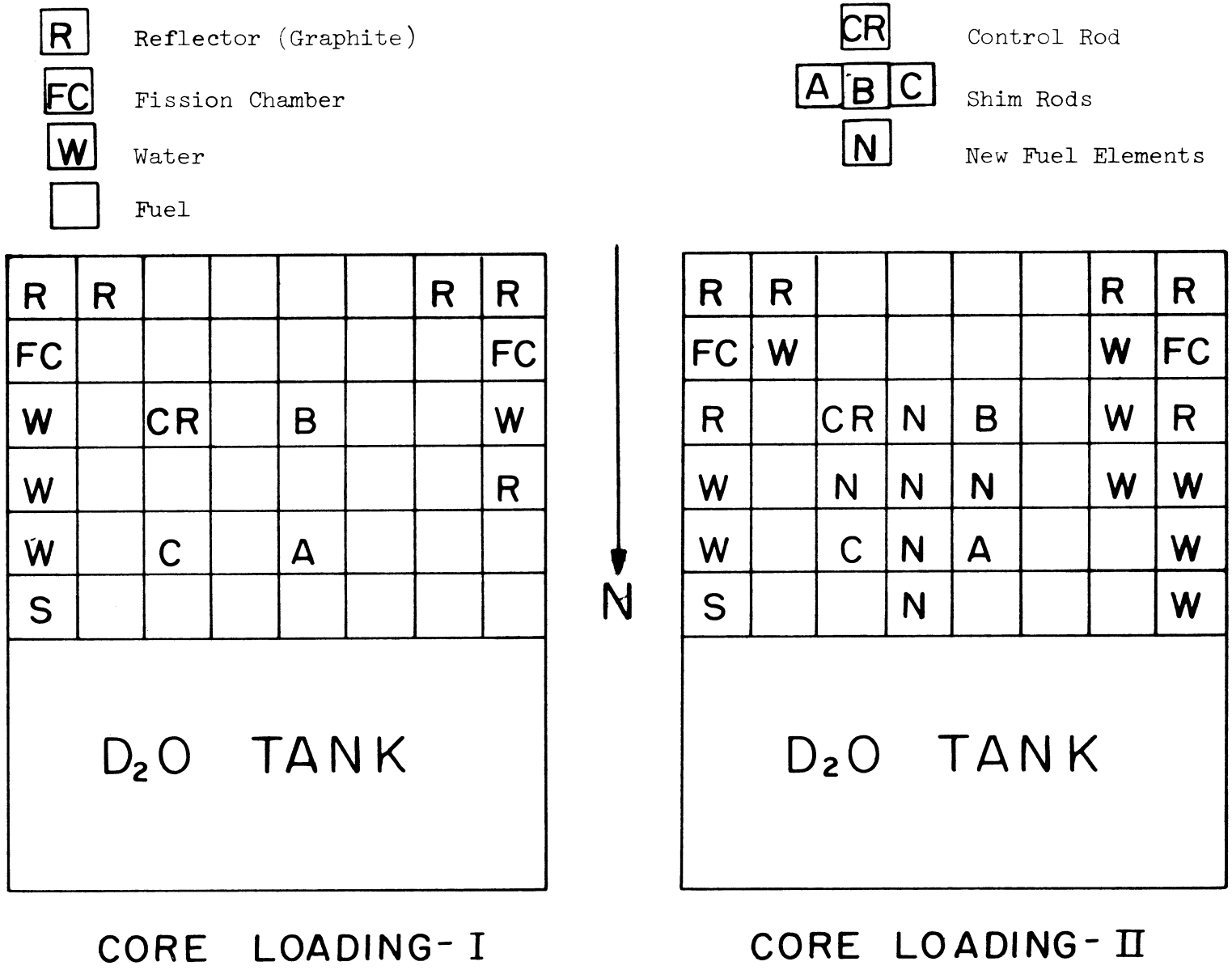


Figure 4-1. Reactor Core Configurations.

The reactor-detector configuration is shown in Figure 4-2. Refer also to Figure 2-8. Shown in a plan view is the arrangement for the single-detector and two-detector experiments. The actual distance between the fuel and detector was $\sim$ 1 inch. This, added to the 1-1/4 inch end plate, places the Cerenkov radiator at 2-1/4 inches from the fuel. The reactivity worth of the detector was negligible.

2. PSD Data Collection.

A block diagram of the data collection equipment for the gamma ray noise experiments and the temperature experiments is shown in Figure 4-3. Data for all the experiments were recorded on tape for subsequent data processing.

Tape Recorder

The FM tape recorder, a Hewlett Packard Model 3907, was operated at 1-7/8 ips for data collection. The quoted noise is 39 db down from a nominal input of $\pm$ 2.5 volts p-p. This value was verified by a measurement. The bandwidth at this speed is dc to 312 cps.

Pico-ammeter

The Keithly Model 417 pico-ammeter has a range from $10^{-13}$ to $3 \times 10^{-5}$ and rise times, on the scales used, of less than 0.001 seconds. Dc drift is less than one percent for eight hours. The instrument has provisions for suppressing the dc level of the input signals so that only the ac component appears in the output which is $\pm$ 3 volts full scale. The ac component was amplified sufficiently for direct recording on tape.

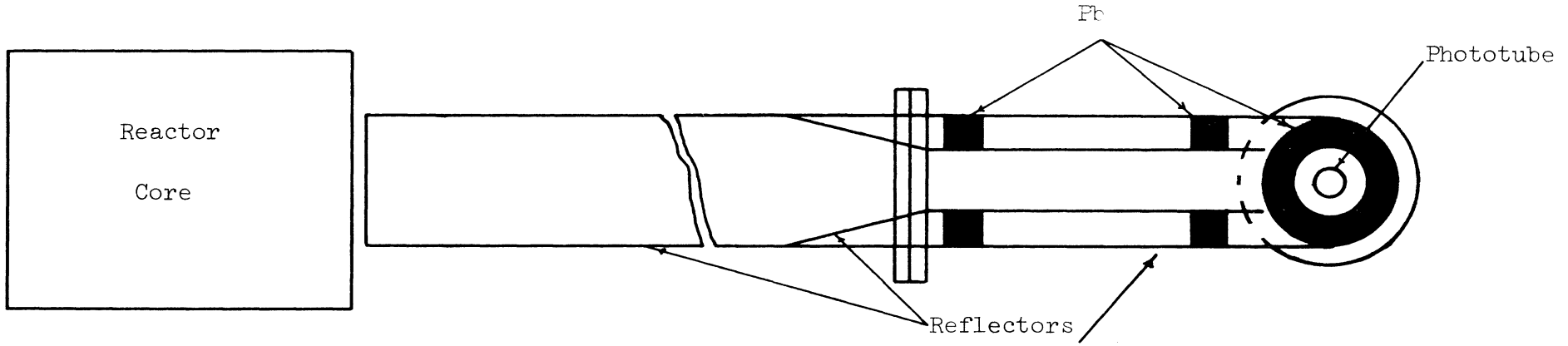


SINGLE DECTECTOR ARRANGEMENT

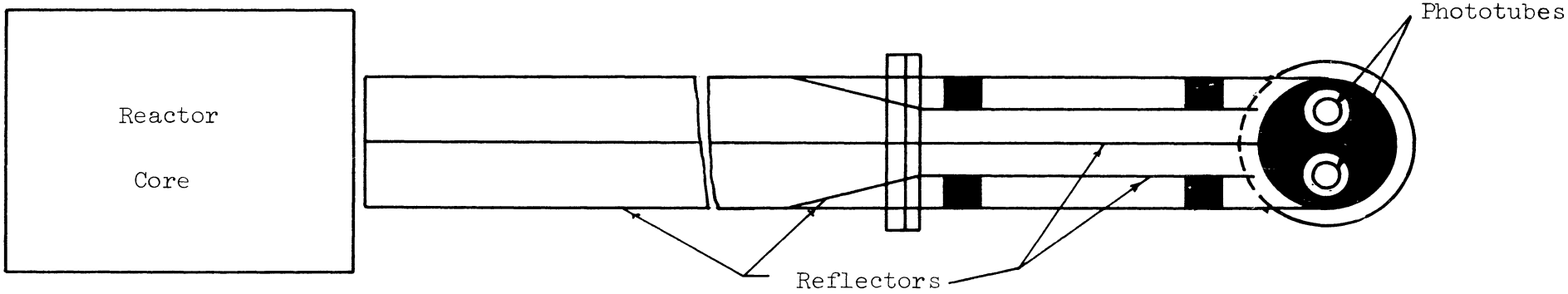


TWO DETECTOR ARRANGEMEMENT

Figure 4-2. One and Two Detector Schematics.

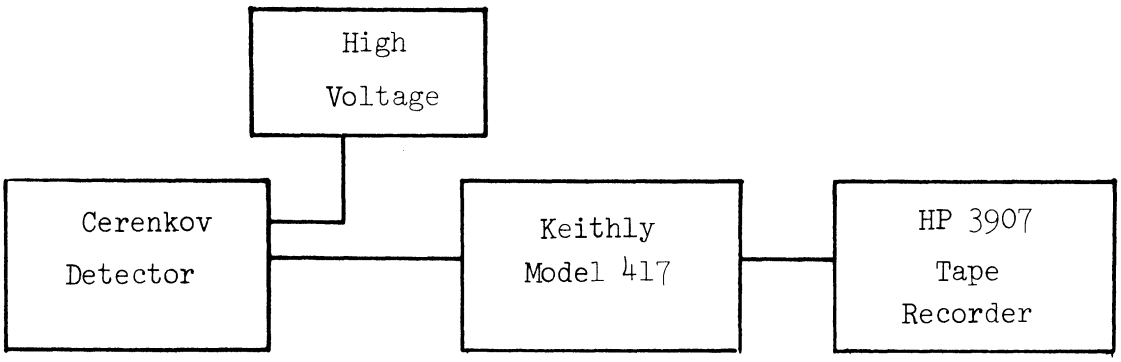


GAMMA NOISE DATA

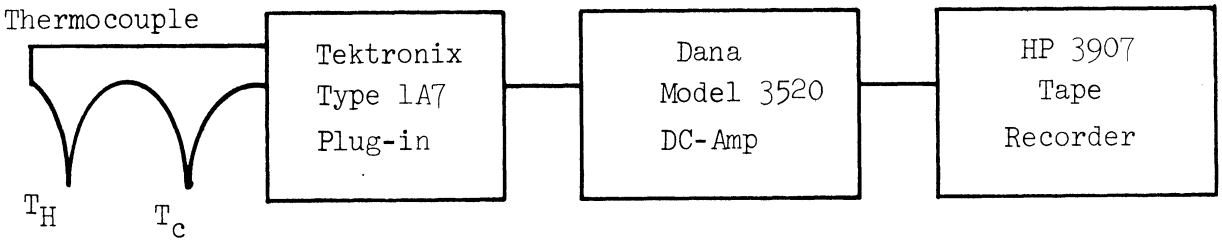


TEMPERATURE DATA

Figure 4-3. Gamma and Temperature Power Spectral Density Data Collection Schemes.

Thermocouple

A copper-constantan thermocouple was used which had a time constant of less than 10 msec (upper frequency cutoff $\sim$ 17 cps). The hot junction was formed from 20 mil wire which was flattened and trimmed into a very thin ribbon. The time constant was determined from photographs of the oscilloscope trace obtained by rapidly inserting the hot junction into warm water. The time required for the couple output to relax by approximately a factor of e was taken as the time constant. The thermocouple hot junction was placed beneath the bail of the center fuel element in the second row of elements from the south face of the core, while the cold junction was held at a constant temperature in an ice bath.

Tektronix Type 1A7 Plug-in Unit

The temperature fluctuations were separated from dc level with a Type 1A7 plug-in used in conjunction with a Tektronix 531A oscilloscope. The unit has a dc offset control to suppress the dc component and has an output of 34 mv/cm of deflection. Input sensitivities range from 10 microvolts/cm to 20 volts/cm.

DC Amplifier

The output of the 1A7 unit was amplified with a Dana Model 3520 dc Amplifier. The upper cutoff frequency is variable from 0.01 to 10 kc; 0.1 kc was used here. The frequency response is flat to within ± 1 percent from dc to upper cutoff frequency.

3. PSD Data Reduction Equipment

To obtain the PSD of both the GCD and thermocouple outputs,

the signals were processed with the equipment shown in Figure 4-4. The amplifiers marked P are those contained in the Pace Model 16-31R-4 Analog Computer in the Computer Laboratory of the Nuclear Engineering Department. Because of the limited frequency response of the Pace equipment, a Hewlett Packard 3400A True RMS Voltmeter was used to obtain the instantaneous power in the bandwidth defined by the band pass filters. For the lower frequencies below 10 cps, the HP3400A was removed because of the adequacy of the amplifiers in this range. All PSD measurements were done with a tape speedup factor of 32. This extended the lower frequency range of all the equipment and reduced the time required for data processing. The Krohn-Hite filter was used over the whole frequency range and the HP302A Wave Analyzer was used only to supplement and verify the results of the Krohn-Hite filter. It has the disadvantage of having a fixed bandwidth of 3.5 cps.

Krohn-Hite Filter

The K. H. Model 330M is an adjustable band pass filter useful over the frequency range from 0.02 to 2000 cps. The gain in the pass band is unity, 0 db. The lower frequency limit was extended by a factor of 32 by using tape speedup as mentioned previously.

RMS Voltmeter

The voltmeter used in the high frequency PSD measurements was a Hewlett Packard 3400A. The meter measures the true root mean square value of the input by the heat produced in a thermocouple. The sensitivity can be varied from 0.0001 to 300 volts, full scale. The output is -1.0 volt dc at full scale deflection and its frequency range is 10 to 10 Mc, flat to within $\pm$ 1 percent.

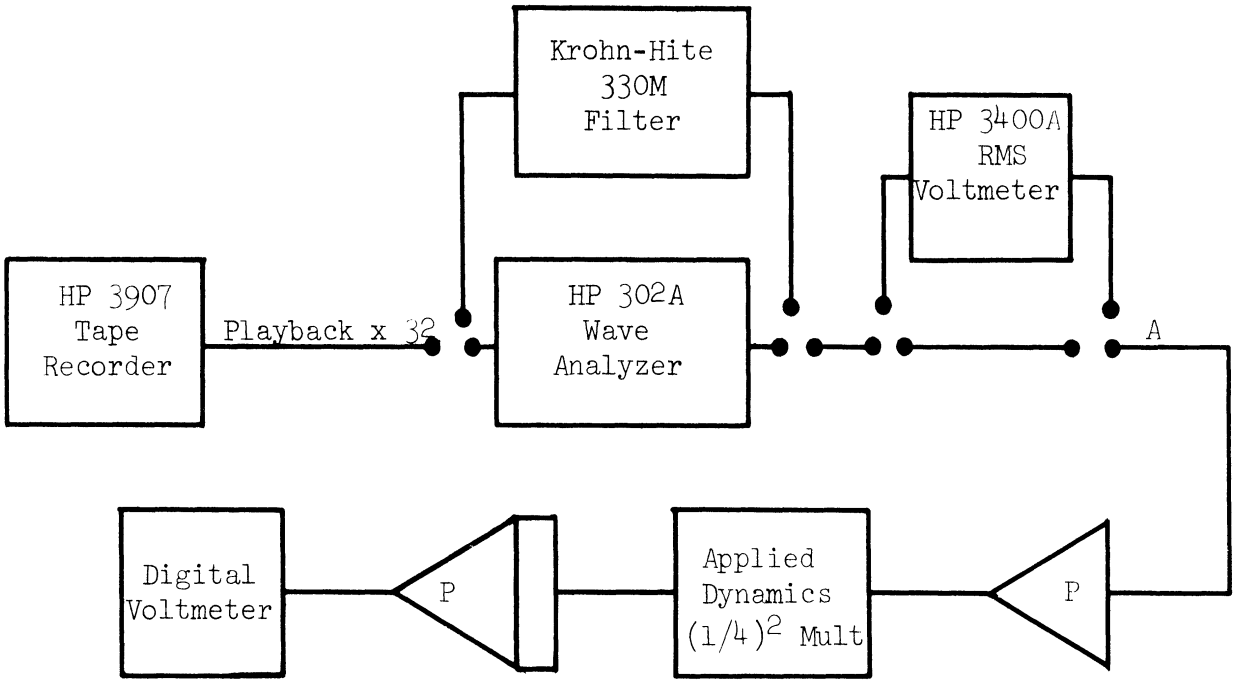


Computation Circuit--

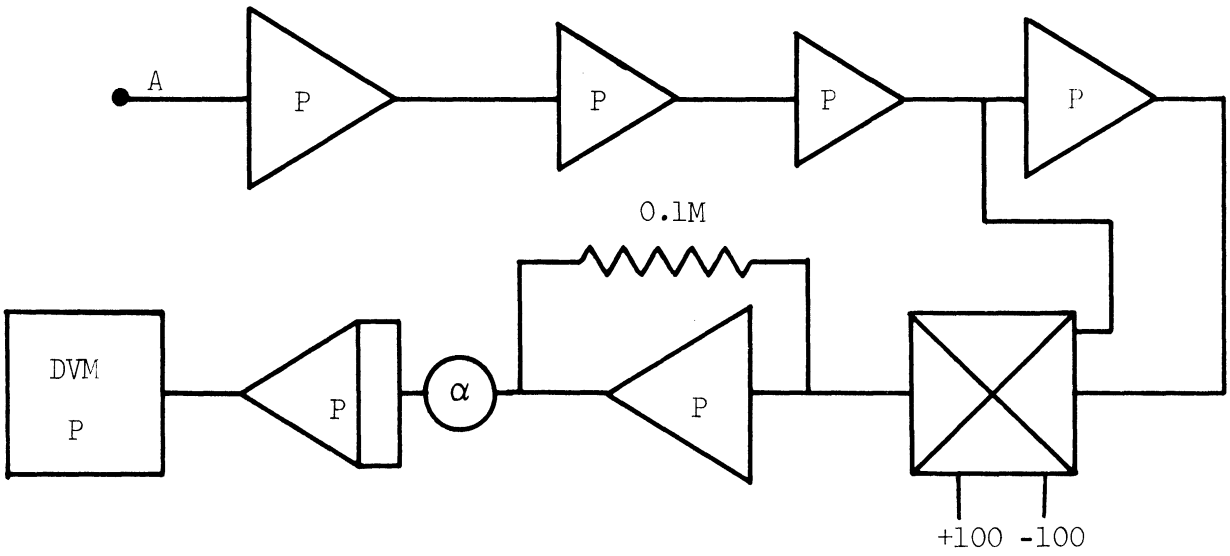


P - Pace Analog Computer Component

Figure 4-4. Equipment for Power Spectral Density Calculations.

Multiplier

The multiplier is an Applied Dynamics Model 166-2 solid state multiplier operating on the quarter square principle. The maximum input is $|x| + |y| = 200$ volts and the output is proportional to $xy$. The output applied to the summing junction of an operational amplifier with a 0.1 megohm feedback resistor is $-XY/100$. The unit was powered using the ± 100 volt supplies on the patchboard of the Pace Analog Computer. The frequency response of unit is governed by the frequency characteristics of the output amplifier which was flat, ± 1% to 800 cps.

4. Cross Correlator.

The cross correlation function and correlation coefficients were measured using an Instrument for Statistical Analogue Computation (ISAC). The ISAC was first designed and built by the Automatic Control Laboratory, Norwegian Institute of Technology, Trondheim and was made available for this work by Dr. C. W. Ricker.* The device is a multispeed tape recorder equipped with a tape loop. The signals to be correlated are multiplied and integrated over the length of the loop. The delay time is achieved by a movable head which reads one track. Results are printed on an x-y recorder. A clear, compute, printout, and head advance sequence are initiated and resequenced by relays activated by photocells, which sense the beginning and end of the loop by light shining through appropriately placed holes. The head can be moved in increments of 0.25 or 1 mm up to 100 mm. Recording times are varied from 5 seconds to 85 minutes for the short tape loop and from 15 seconds to 4 hours and

* Manufacturer's representative in U.S. is the Sterling Instrument Co., Southfield, Michigan.

56 minutes for the long loop in 10 steps. The instrument will also calculate the PSD over bandwidths which can be varied from essentially dc to 0.2 cps and dc to 200 cps in 10 steps.

5. CPSD Experimental Arrangement.

Data for the CPSD experiments were collected with equipment shown in Figure 4-5. In these experiments the fluctuations were isolated from the dc level with the use of high pass filters having time constants of 0.3 $sec^{-1}$ . This was necessary because the large amplitude fluctuations at the lower frequencies used most of the dynamic range of the tape recorder and the higher frequency fluctuations were very close to tape recorder noise. This "prewhitening" operation was corrected for in the data processing procedure. This system was also more stable in that the dc level was continuously eliminated.

Shown also in Figure 4-5 is the schematic diagram of the equipment used for data processing. The outputs of the tuned bandpass filters are amplified and multiplied to yield the CPSD.

All the equipment used for these experiments has been described previously with the exception of the Tektronix Type O Operational Amplifiers.

These amplifiers used in conjunction with a Tektronix Type 531 oscilloscope have bandwidths from dc to 14 Mc with rise time of 25 ms. The maximum output is ± 50 volts and noise is typically less than 0.5 mv p-p.

6. Equipment Response.

Corrections to the measured PSD were made for irregularities in filter response. The response curves were determined in the conventional

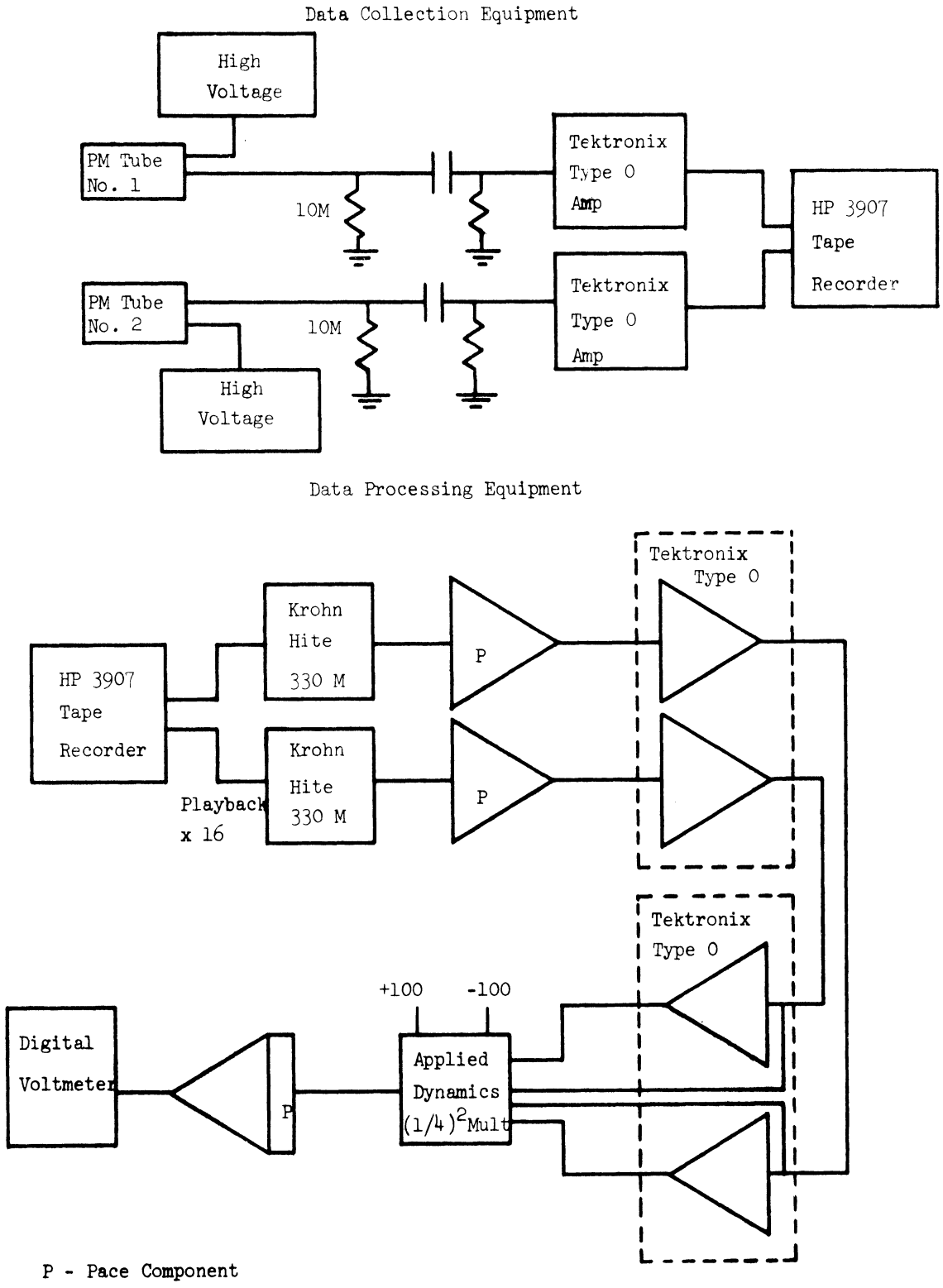


Figure 4-5. Two Detector Data Collection and Processing Equipment.

manner[9] using a sinusoidal oscillator and the detection circuits described above. Overall system response was determined by recording the output of the detector with a $Co^{60}$ source placed near the endwindow. The Cerenkov light induced by the $Co^{60}$ gammas in the endwindow (n = 1.5) is a white noise source whose frequency dependence is flat. The source was not quite strong enough to duplicate the detector output at all power levels used in the experiments. However it did approximate the output equivalent to a reactor power of 100 watts. The PSD of this signal was flat above 1 cps using the HP 302A Wave analyzer and indicated only minor corrections in the frequency response of the Krohn-Hite Filter in this range. In the range below 2.5 cps. the combined oscillator and $Co^{60}$ source tests showed a falling off of the Krohn-Hite filter response below 0.025 cps which necessitated correction. Again the correction was not excessive. The flat response obtained with the HP 302A Wave Analyzer showed no corrections were necessary due to the picoammeter, tape recorder and other equipment in the data collection and processing system.

Two-detector experiments of the type done here require finely tuned filters to eliminate phase shifts introduced by them. The filters were tuned over the frequency range 0.5 to 50 cps by applying the output of the test oscillator to both filters and observing their outputs on a dual trace oscilloscope. At each frequency one of the filters was adjusted by dial changes so that both outputs were in phase. This procedure was facilitated by choosing the upper and lower cutoff frequencies of each filter to be the same. After the tuning procedure, the filter response was determined with the oscillator and the CPSD detection circuit. Overall corrections for the "prewhitening" mentioned previously were determined

using $Co^{60}$ white noise sources recorded with identical equipment settings as used in the actual experiments. Again the filter corrections in the higher frequency ranges showed that only minor corrections were necessary.

C. Error Analysis

The error in the measured PSD can be obtained from(11)

$$\frac{\Delta\phi}{\phi} = \frac{K}{\sqrt{\Delta f T}} \qquad (4\text{-}1)$$

where $\Delta f$ is the filter bandwidth and $T$ is the record length. The factor $\frac{1}{\sqrt{\Delta f T}}$ is the statistical error(50) and $K$ is a constant to account for any associated frequency independent errors due to equipment. The constant $K$ was determined by first calculating the standard deviation from a series of PSD measurements from adjacent sections of a tape record at several frequencies. After calculating the error (variance)$^{1/2}$/ mean $K$ was taken as the average of $\frac{\sigma}{M}\sqrt{\Delta f T}$ at the several different frequencies used and was found to be 1.18 for the data shown in Figure 5-2 to be presented later.

The error in the CPSD density can be calculated from the formula(23)

$$\frac{\Delta\phi}{\phi} = \left[\frac{K + Q_1^{-1} + Q_2^{-1} + (Q_1 Q_2)^{-1}}{\pi \Delta f T}\right]^{1/2}$$

This result has been verified independently by Kryter et al.(10)

The difficulty in this procedure is the need to know the ratio denoted by $Q$, the quotient of the correlated and uncorrelated components in the PSD. Since no indication of this ratio was available from the PSD experiments, the CPSD experiment was repeated and the error bars shown are

determined from the variance and mean as calculated from six independent experiments.

D. Experimental Procedure.

All the data for the experiments were taken at the FNR and recorded on tape. The detector was placed in position near the core and after the initial background had stabalized, the reactor was brought critical, as indicated by the existing reactor instruments. The power level was then raised in increments and the output current of the detector was recorded. Relative power levels were determined from fission chamber counts and from the compensated ion chamber output. In the later CPSD experiments both the output current and the peak to peak value of the fluctuations were noted. For core loading I the signal to noise ratio was 2.5/1 to 3/1 and for core loading II at the same power the ratio was 10. After determination of the "optimum" power level the equipment was adjusted to separate and amplify the fluctuations and the data were recorded. Optimum power level in these experiments was defined as the power which gave a signal to noise ratio of at least 2.5/1. Continuous monitoring of the tape recorded signal was done with a dual beam oscilloscope.

All data were taken with the reactor operating manually. This method afforded the greatest degree of stability against drift and large reactivity changes.

After data recording, the tape recorder was moved to the Computer Laboratory, where the data were reduced. The time averaged data were then plotted and compared after the appropriate corrections were applied.

Consistent with the theory discussed in Chapter III a function of the form

$$\phi(\omega) = \phi^{T}(\omega)\left|G_p(\omega)\right|^2 + \phi^{N}(\omega)\left|G_s(\omega)\right|^2$$

was fitted to the CPSD data by a least squares method outlined in Appendix A. The analysis was done on the Ford Computer in Dearborn, access being through a teletype terminal in the Nuclear Engineering Department's Computer Laboratory.

In order to obtain optimum signal level (2 to 2.5 volts p-p) for recording, the high voltage was varied, particularly in those experiments in which the power level was varied. Corrections were made to the measured PSD so that meaningful comparisons could be made. Data were normalized to one phototube voltage Vo , by a factor $(Vo/V)^{20}$ . The justification for this is the observation made previously in Chapter II that the output current varies as $V^{10}$ . This enters into the PSD as the square, hence the exponent is 20.

# CHAPTER V

# RESULTS AND DISCUSSION

## A. Introductory Remarks

In this chapter the results of the measurements will be presented along with a discussion of them. The results of the single detector, temperature PSD and cross correlation function measurements will be presented and discussed first and then the results of the two detector measurements.

Since this particular model of the GCD was not able to isolate the $\beta/\ell$ breakpoint, using a single detector, the discussion of these single detector experiments will be restricted to the low frequency region where the temperature effects predominate. PSD measurements on the outputs of two detectors in parallel in the frequency range around the breakpoint will be presented and discussed with the results of the CPSD.

## B. Low Frequency PSD and Temperature Measurements

Figure 5-1 shows the results of the PSD measurements on the output of the GCD with the primary coolant pump off and on. Figure 5-2 shows the relationship between the gamma ray PSD and the PSD of the temperature fluctuations. Figure 5-3 is a plot of the measured gamma ray PSD's at several power levels, while Figure 5-4 presents the temperature PSD's at these same powers. The temperature and gamma data were taken simultaneously at each power level as were the data shown in Figure 5-2.

The following observations are made from the data thus far presented. The PSD of the power level fluctuations is larger with the coolant pump off than with the pump on; there is a strong similarity in the spectral shape at lower frequencies between the gamma and temperature fluctuations; and the amplitudes of the temperature fluctuations are independent of power level.

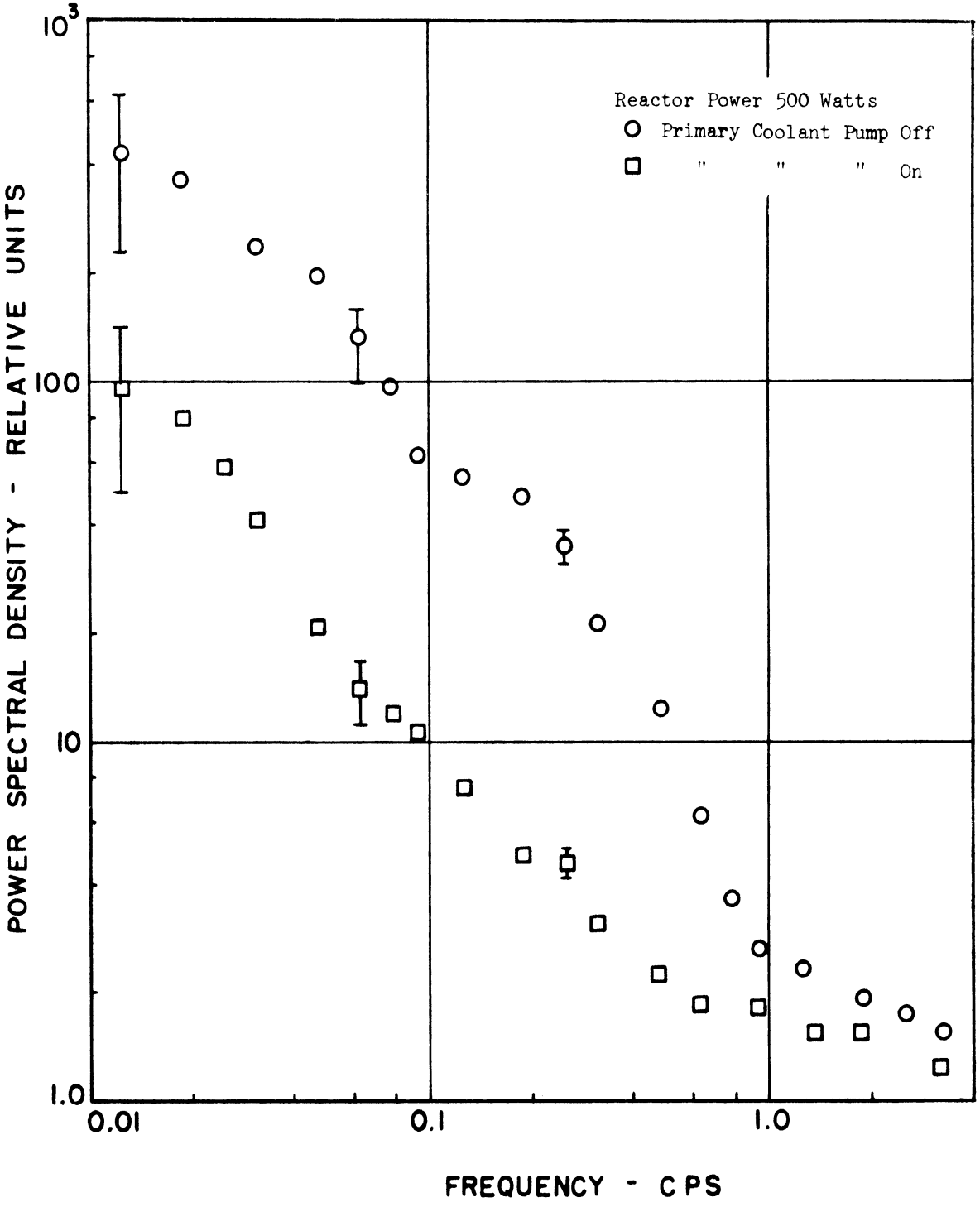


Figure 5-1. Power Spectral Densities with Forced and Free Convection.

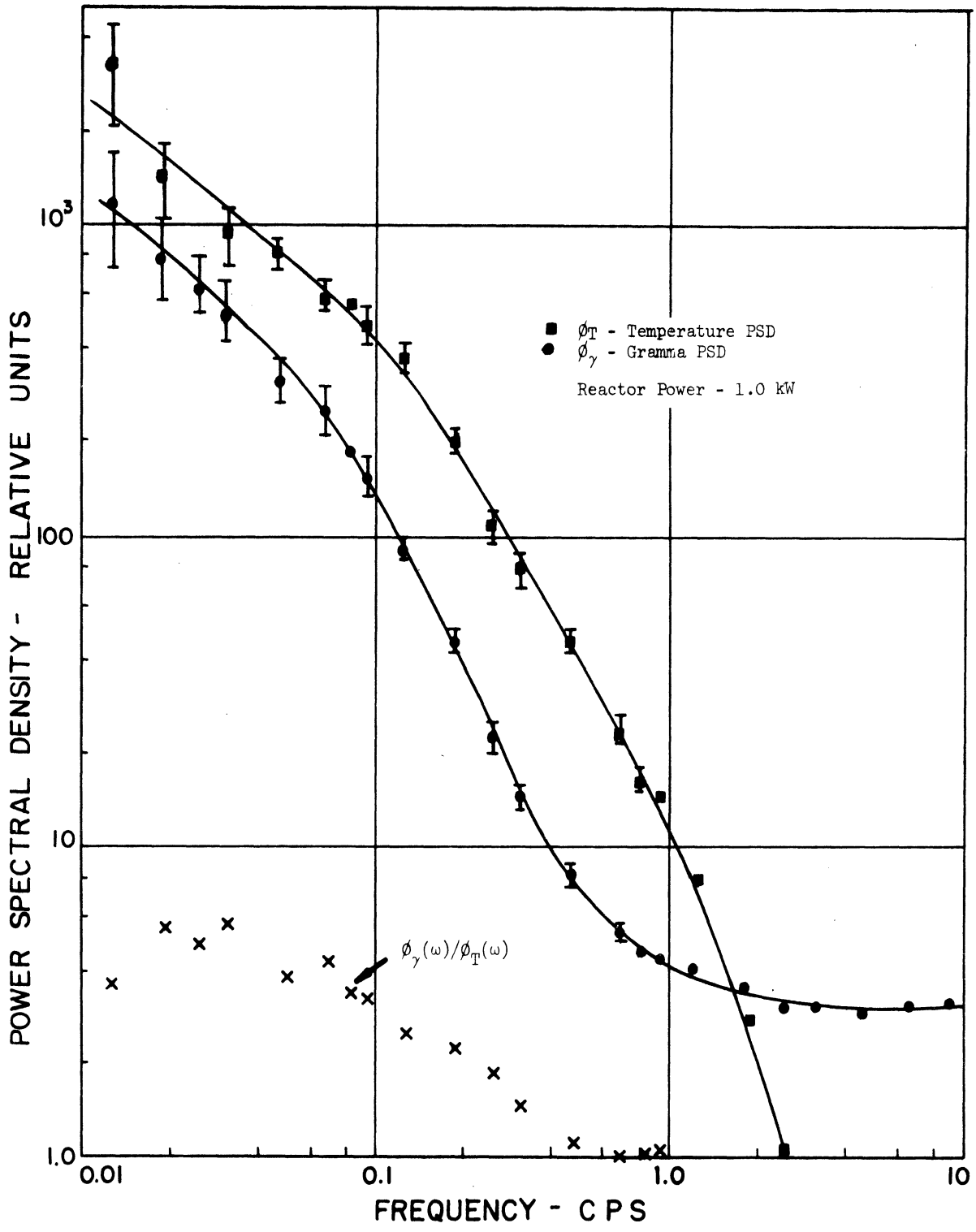


Figure 5-2. Power Spectral Densities of Gamma Ray and Temperature Fluctuations.

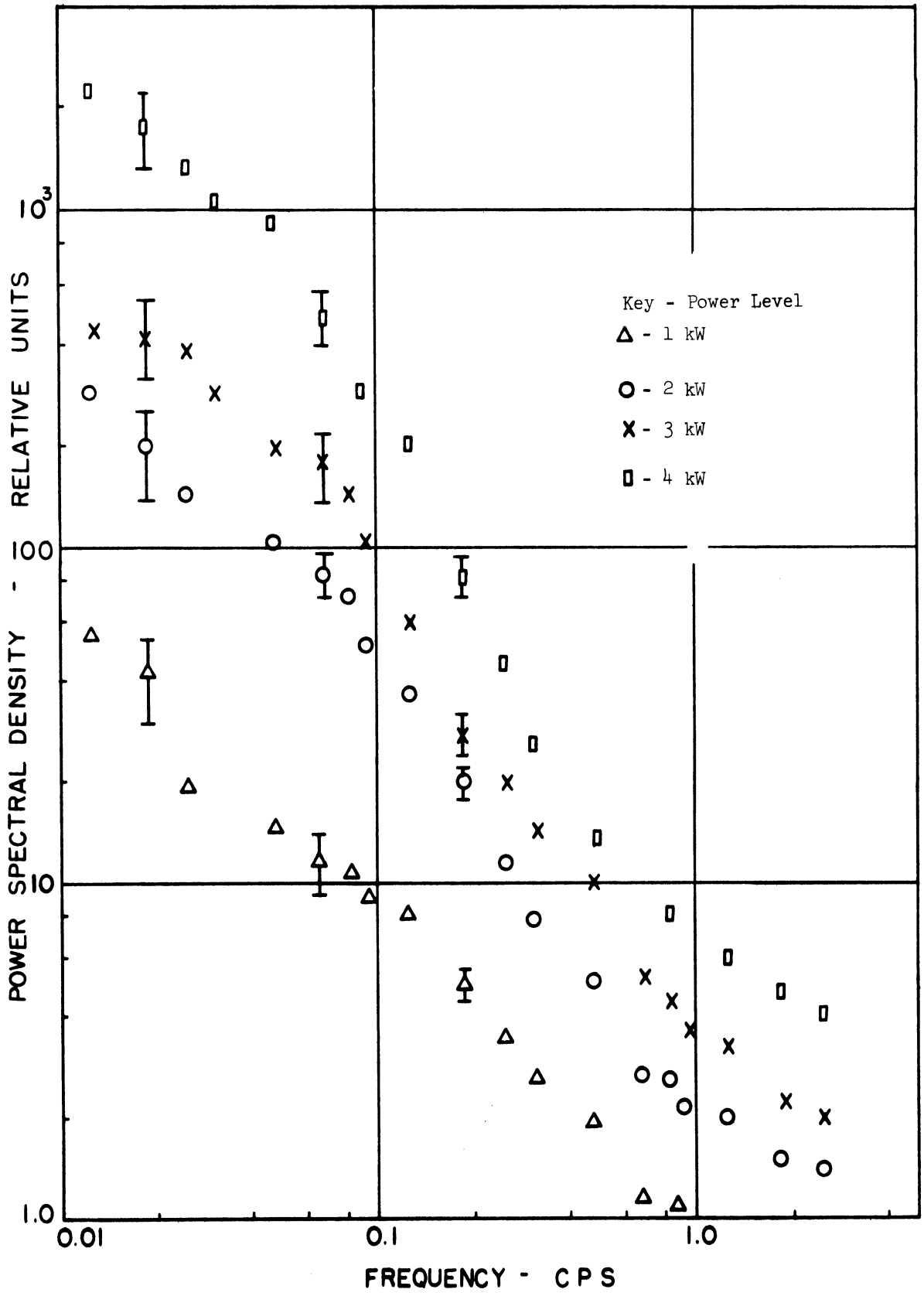


Figure 5-3. Power Spectral Densities of Gamma Ray Fluctuations at Several Power Levels.

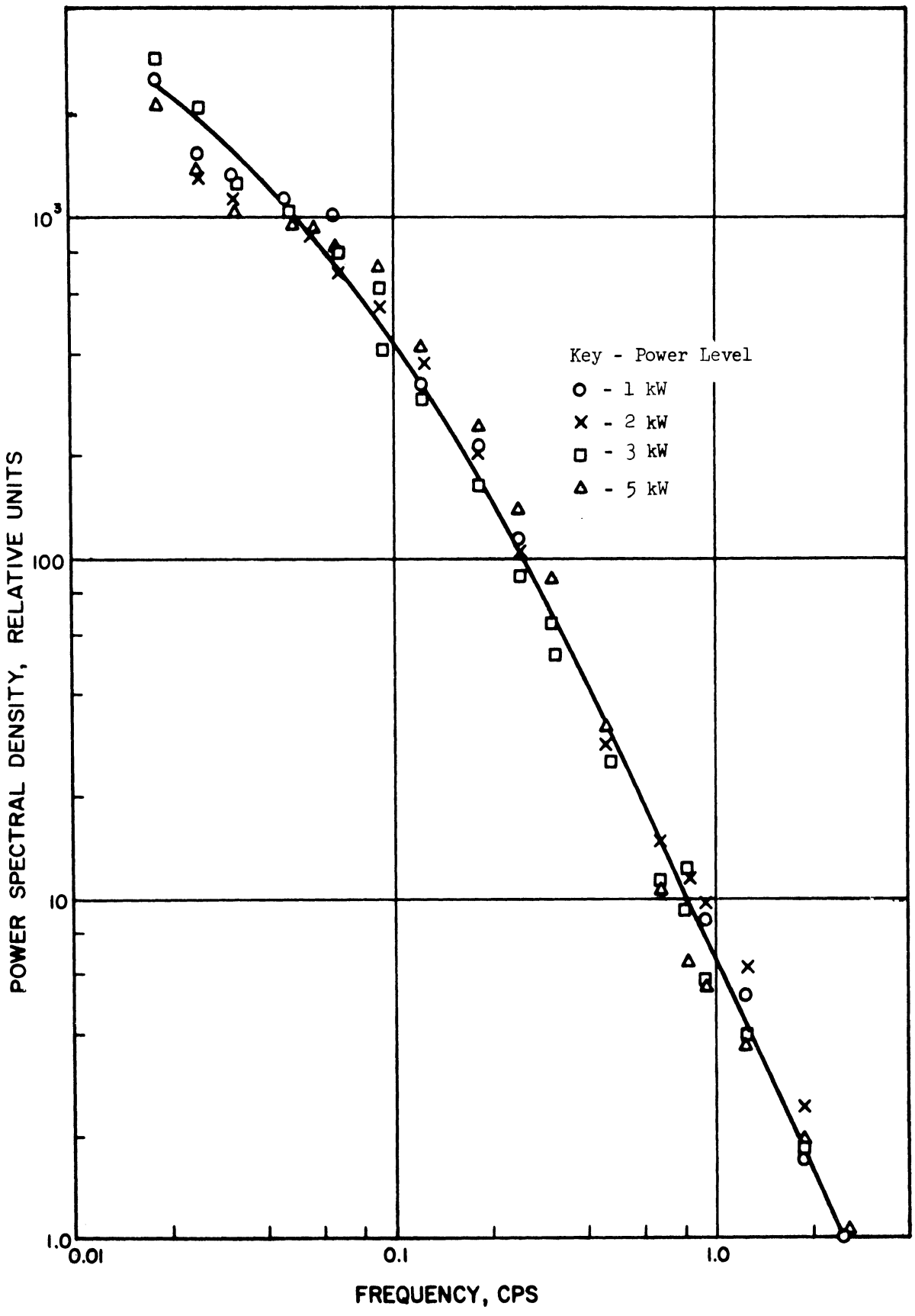


Figure 5-4. Power Spectral Densities of Temperature Fluctuations at Several Power Levels.

The mean values of the low frequency gamma ray PSD's were calculated and Figure 5-5 shows these mean values plotted versus reactor power. The agreement with the reference curve $\phi(w) \propto \rho^2$ is good.

Shown in Figure 5-6 is the measured cross correlation function between the GCD and the thermocouple outputs. The same data records were used for this measurement as were used to compute the PSD's shown in Figure 5-2. It is to be noted that a correlation exists and that a continuity is noted from curve a to b to c . The amplitudes in each curve have no relation to one another as each was obtained from a different record and slightly different equipment settings.

Different records were used because the delay time is governed by the recording speed of the IASC and three such records were used to cover the range from 0 to 5, 0 to 20, and 0 to 163 seconds total delay time. The main feature is that a correlation does exist between the thermocouple output and fluctuations in the power level. The correlation coefficient determined from the average of five trials for the 80 second delay peak was 0.132 ± .009 . The coefficient is defined as

$$\epsilon = \frac{G_{\gamma T}(\tau)}{[C_\gamma(0)\, C_T(0)]^{1/2}}$$

where $G_{\gamma T}(\tau)$ is the measured cross correlation function and $C_\gamma(0)$ and $C_T(0)$ are the values of the auto correlation function of the gamma and thermocouple signals at zero time delay respectively. The coefficient varies between ± 1 depending on the degree of correlation.

All the data presented above were taken on core loading I which was the "dirtiest" of the two.

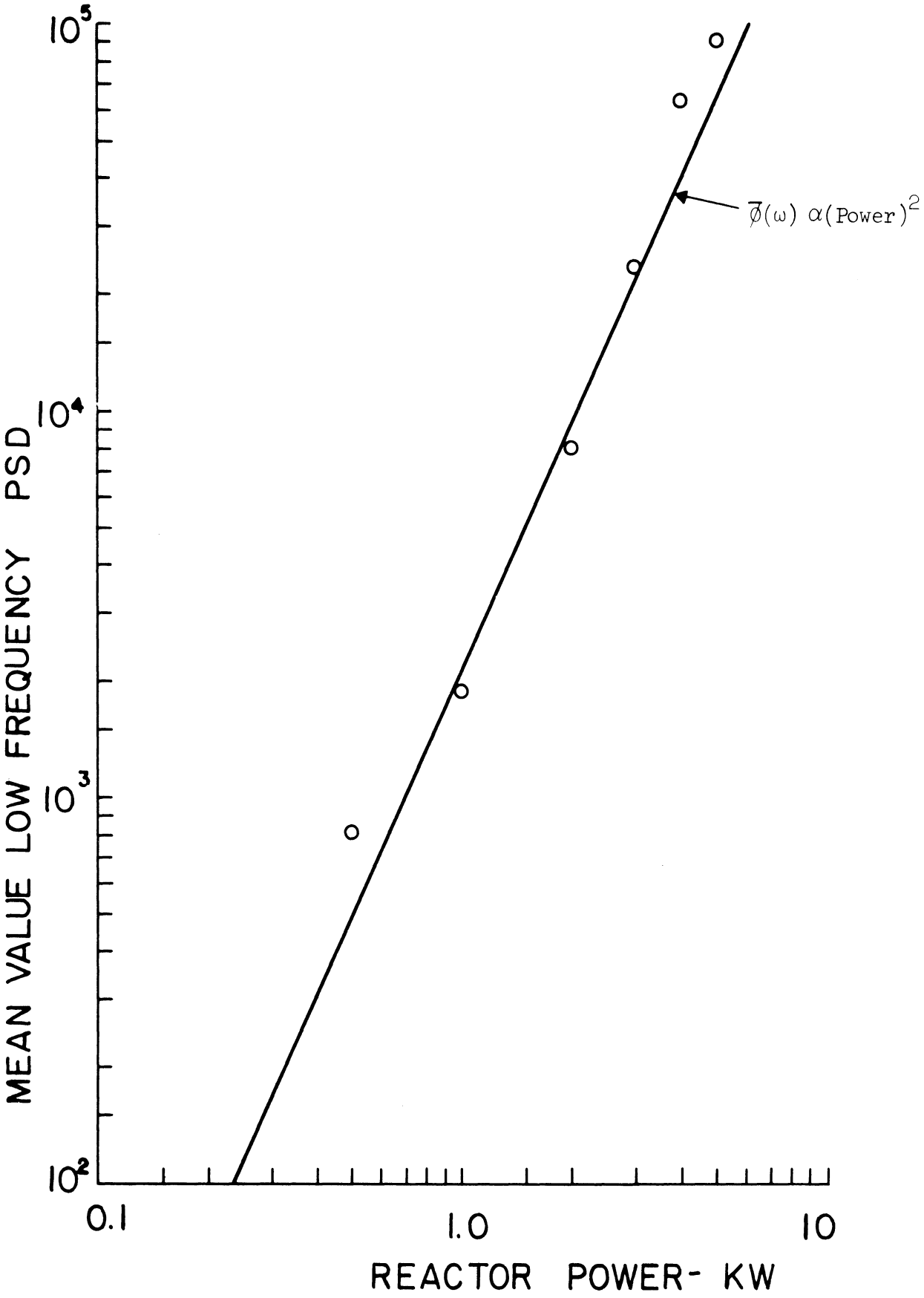


Figure 5-5. Mean Value of the Gamma Ray PSD Versus Reactor Power.

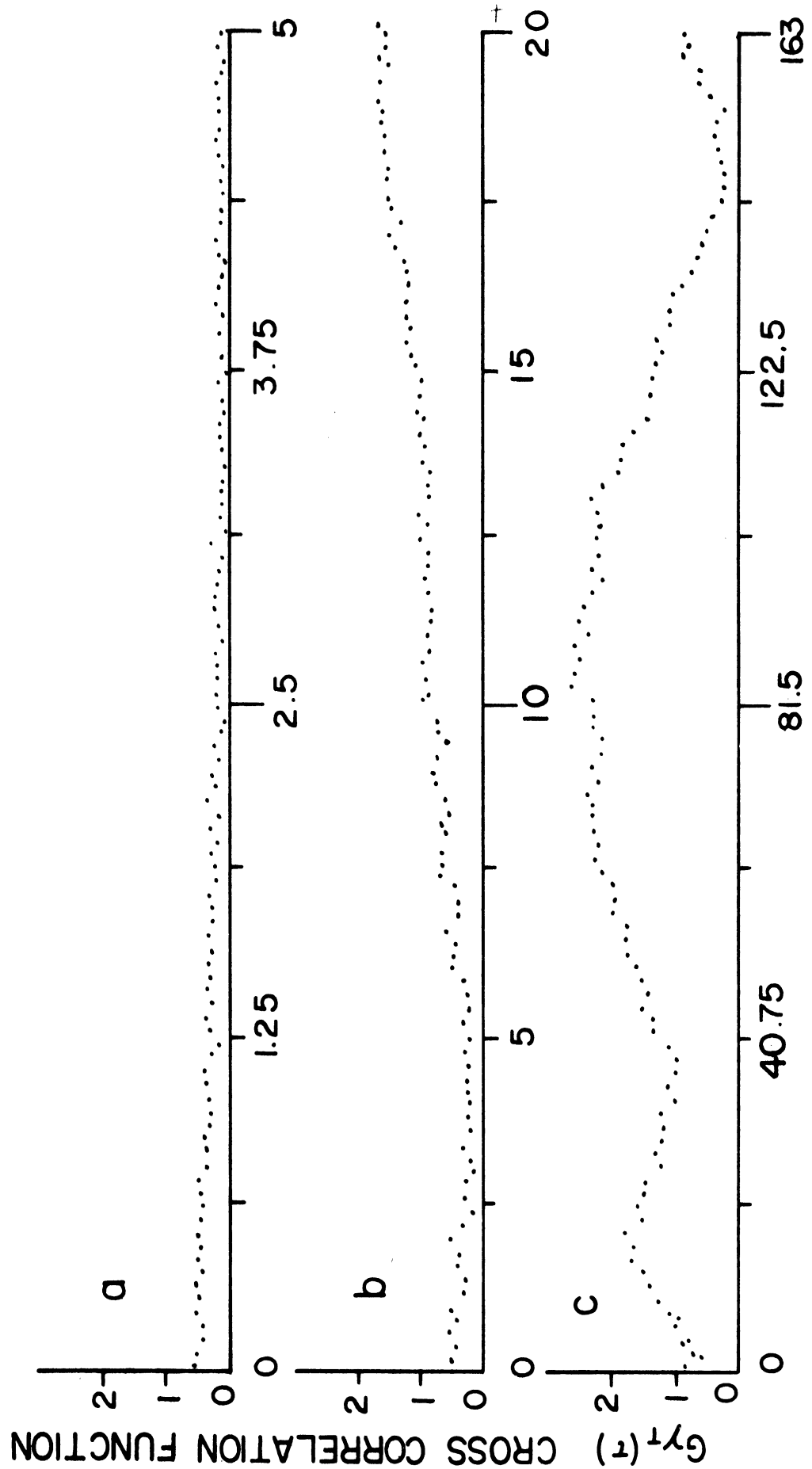


Figure 5-6. Gamma-Temperature Cross Correlation Function.

It was first supposed that the sharp rise in the PSD at low frequencies was due to $N^{16}$ decays and any power level fluctuations were filtered through the $N^{16}$ reaction which would be expected to have a breakpoint in the PSD curve at 0.0149 cps. However a calculation of the 6.13 Mev gamma ray source from $N^{16}$ showed this to be negligible compared to the prompt gamma ray source above 5.0 Mev from fission. See Appendix B

Considering the apparent similarity of the gamma and temperature spectra and the above observations, a more logical explanation of the low frequency behavior is that the power level fluctuations are temperature induced by fission product heating. The heat source is the intense gamma ray flux being absorbed in the fuel and coolant. It has been estimated that the fraction of the reactor operating power generated in the reactor due to fission product decay is approximately $5 \times 10^{-3}$ of full power at two days after shutdown after an operating period of 30 days.(39) Applying this to the FNR which operated at 2 MW during a 25 day cycle, the fission product heat source is approximately 10 kW .

As has been pointed out(51) the amplitudes of the temperature fluctuations are expected to be larger under conditions of free convection than under forced cooling and can have frequencies possibly as high as 10 cps. The amplitudes of the fluctuations can be as large as 1/3 the temperature difference between the fuel plates and the mean pool temperature. The origin of the fluctuations is different in the two cases; under natural convection, the flow rates and flow patterns are induced by the heating of the coolant by conduction from the fuel plates which consequently induces large buoyant forces because of the temperature differences within it. Flow patterns and flow rates are very unstable and

therefore "noisy." With forced convection the temperature fluctuations would be due to variations in pool water temperature which is drawn through the reactor. The above arguments would account for the larger PSD observed with the primary coolant pump off.

The facts that the temperature PSD is independent of reactor power and the gamma ray PSD below 2.5 cps varies as power squared, fix the origin of the fluctuations as not being dependent on reactor operation or power level. While the portion of the PSD which is due to fluctuations in the capture, leakage and fission rates is proportional to reactor power, any portion of the PSD due to fluctuations in reactivity is proportional to the square of the reactor power.[3,4] Since fluctuations in the temperature of the water give rise to reactivity fluctuations through the temperature coefficient of reactivity, these should give rise to contributions to the PSD which vary as the square of the power. Reactivity fluctuations coupled linearly to reactor power result in a component of the PSD which varies as power to the fourth.[3]

The measured value of the correlation coefficient 0.132 is not considered to be a very large value. The fact that it is significantly different from zero suggests a definite correlation exists. Since a single thermocouple measures only local effects and the temperature driving function would be the sum of many local perturbations, the correlation between the temperature fluctuations and power level fluctuations would be expected to be small as measured by only one thermocouple.

The gamma PSD (constant term subtracted) was divided point by point by the temperature PSD. This is shown as the bottom curve in Figure 5-2.

If the observed PSD was due to reactivity fluctuations which were accurately described by the thermocouple output, one would expect the following to hold[3,49]

$$\phi_{oo}(\omega) = \phi_{ii}(\omega) \left| G_p(\omega) \right|^2$$

where $\phi_{oo}(\omega)$ is the output PSD, $\phi_{ii}(\omega)$ is the PSD of the reactivity driving function and $G_p(\omega)$ is the reactor reactivity transfer function.

The transfer function derived in this manner from the experimental data does not agree with the expected zero power transfer function in that the amplitudes at lower frequencies are larger than predicted.

This fact, along with the small value of the correlation coefficient, indicates that the temperature induced reactivity driving function is not adequately described by a measurement at a single point. A local measurement would be accurate only in two extreme cases. The first being when the reactor temperature rises and falls uniformly throughout the whole core and a measurement at one point samples the whole reactor. The second case being when the fluctuations occur in independent "cells"; the reactor being made up of many such cells; each cell having the same frequency dependence. The sampling of one cell would then accurately describe the whole system.

From the above one can tentatively conclude that the reactor constitutes more than one cell, several cells or groups of cells fluctuating in some correlated fashion. Under these conditions one would not expect a local measurement to adequately describe the driving function.

Another possibility for the discrepancy exists in that, fuel temperature fluctuations induce reactivity changes. A thermocouple sampling the coolant temperature may or may not accurately describe the frequency dependence of the fuel temperature oscillations.

To summarize, the low frequency fluctuations in the reactor power level are caused by fission product gamma heating which induce reactivity changes through the temperature coefficient of reactivity. All observations made to date support this contention. While each observation cannot by itself be taken as conclusive proof to support the above statement, the following six observations taken collectively are offered as proof to support the above contention.

1. The spectral shape of the temperature and power level fluctuations show the same general behavior in the low frequency region.

2. The temperature fluctuations are larger in the pump off condition.

3. The temperature fluctuations are independent of reactor power.

4. The power level fluctuations show a power squared dependence, indicative of an external reactivity driving function.

5. A finite correlation coefficient exists between temperature and power level.

6. The CPSD measurements on a "cleaner" FNR core showed lower amplitudes in the low frequency region. These measurements are discussed below in this chapter.

Low frequency PSD measurements under conditions of convective cooling were made by Yamada et al.[52] with very similar results. However, they attributed the measured PSD to control rod vibration, in that the rods were suspended by wires. This effect is discounted in the FNR due to

the more rigid construction of the rod suspension and driving system. However it might become important under forced convection at higher power levels.[4]

C. CPSD Measurements

The results of the two detector CPSD experiments on core loading I are shown in Figure 5-7 while Figure 5-8 shows the results of the experiments on core loading II. The background for core loading II was down a factor of four from core 1. This was reflected in higher signal to noise ratios obtained with core II. Because of the difference in fission product contamination and consequently heating, the amplitudes of the lower frequency components, i.e., temperature induced components, are smaller in the data obtained from core loading II.

Also shown on each graph is the PSD of the outputs of both detectors added. Considerably more structure is evident in the two detector experiments than in the PSD plot. In fact no evidence of a $\beta/\ell$ breakpoint can be inferred from the PSD but is clearly evident in the CPSD measurement. The two detector CPSD measurement is obviously superior in this instance and has resulted in a well defined breakpoint in spite of the presence of the temperature induced spectrum which merges with the regular zero power correlated component. These results clearly demonstrate the advantages of the CPSD method when efficiency is marginal and the correlated to uncorrelated ratio is small. They also appear to contradict the statement by Seifritz et al.[23] that the allowed lower limit to the correlated to uncorrelated ratio is about 0.1.

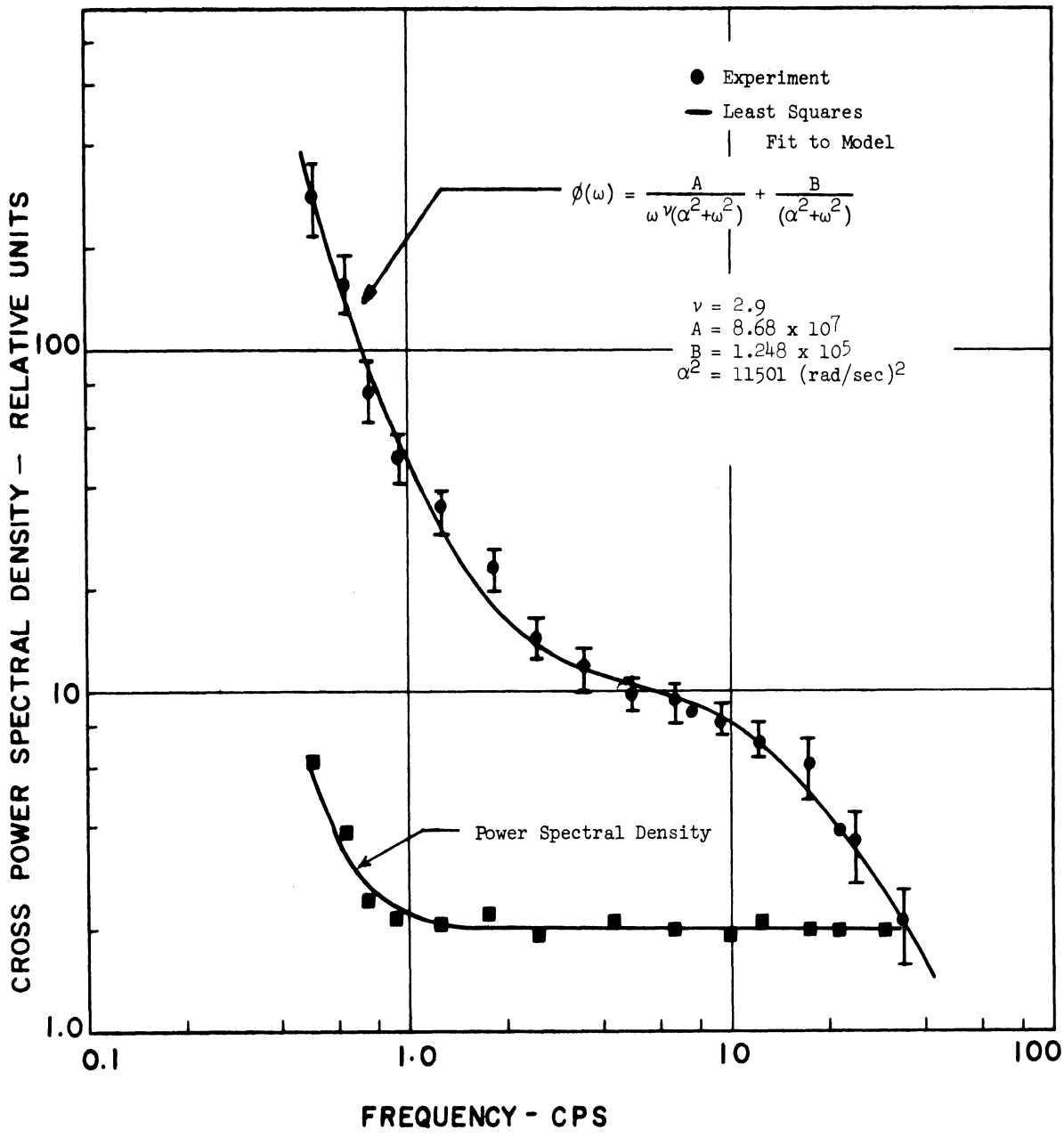


Figure 5-7. Cross Power Spectral Density-Core Loading 1.

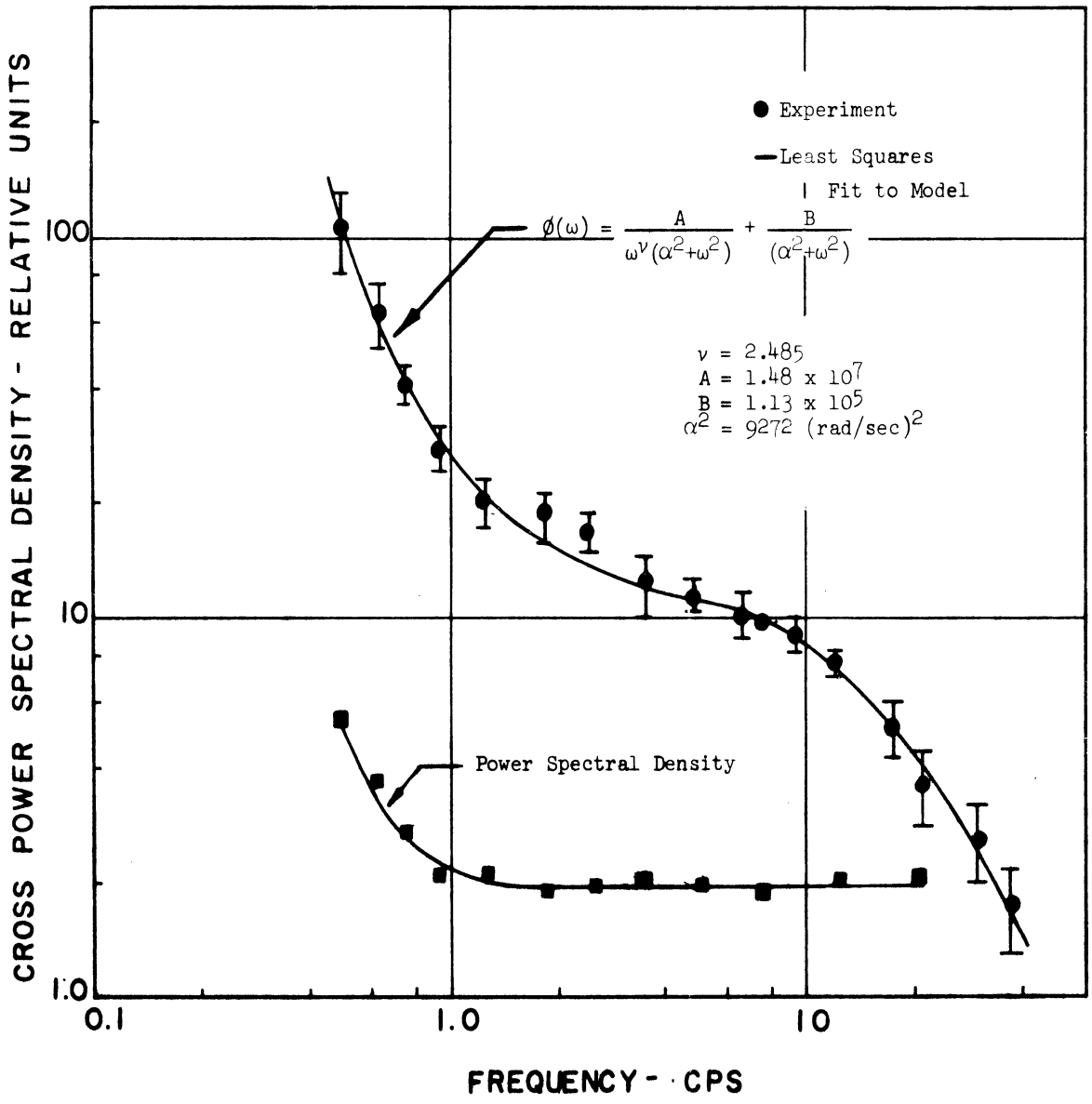


Figure 5-8. Cross Power Spectral Density-Core Loading 2.

The data were fitted to the model depicted by an equation of the form

$$\phi(\omega) = \phi^{T}(\omega)\left|G_{\rho}(\omega)\right|^{2} + \phi^{N}(\omega)\left|G_{s}(\omega)\right|^{2}$$

where $\left|G_{\rho}(\omega)\right|^{2}$ is the square of reactivity transfer function which is of the form $\frac{1}{\alpha^{2}+\omega^{2}}$, and contains a factor proportional to the square of the average power level.

$\left|G_{s}(\omega)\right|^{2}$ is the source transfer function also of the form $\frac{1}{\alpha^{2}+\omega^{2}}$ and is constant with respect to power level.

$\phi^{N}(\omega)$ is the input spectral density of the inherent fluctuations in neutron leakage, absorption and fissions. It is proportional to reactor power and independent of frequency, i.e., a flat spectral distribution.

$\phi^{T}(\omega)$ is the spectral density of the temperature input reactivity fluctuations and is assumed to have a spectral shape that varies as $\frac{1}{\omega^{\gamma}}$ and to be independent of reactor power.

The least squares fitting procedure is discussed in Appendix A.

The fits to the data taken for the different core loadings are;

Loading I $$\phi(\omega) = \frac{8.68\times10^{7}}{\omega^{2.9}(11501+\omega^{2})} + \frac{1.24\times10^{5}}{(11501+\omega^{2})}$$

Loading II $$\phi(\omega) = \frac{1.48\times10^{7}}{\omega^{2.48}(9272+\omega^{2})} + \frac{1.13\times10^{5}}{(9272+\omega^{2})}$$

The variance in the value of $\alpha$ as determined from the six independent experiments on core loading 2 was used with the standard error propagation formulas[37] to yield a value of $78 \pm 15.2$ μsec for the prompt neutron lifetime, based on an effective delayed neutron fraction

of 0.0075. The value of the lifetime obtained from the single measurement on core loading I was 70 μsec, well within the experimental uncertainty. It is not expected that the lifetime of the two different core loadings be very different. The fact that these data on the different core loadings were taken one month apart is an indication of the reproducibility.

Previous measurements of the prompt neutron lifetime in the FNR have yielded the following; Albrecht[20] - 80 ± 10 , Boennighausen[22] - 110 ± 15 and Pluta[21] - 130 ± 20 μseconds, based on the same effective delay fraction above. The best agreement is with Albrecht's result, however, because of the wide discrepancy in the previous results only a qualitative comparison is possible. The prior measurements were also made on small clean, graphite reflected cores while the cores here were larger and water reflected.

Ricker[9] has measured neutron lifetimes of 68 μsec in the Pool Critical Facility at Oak Ridge on cores made up of similar type fuel elements as used in the FNR.

Another aspect of the cores used in these experiments make a quantitative comparison impossible. They are the large fission product gamma ray source and the $D_2O$ tank on the north face of the present core. Because of these the photoneutron source is very large and as a result the effective delayed neutron fraction is increased. No attempt has been made to take this into account here.

The results obtained are indicative of neutron lifetimes expected in the FNR and show that useful noise measurements are possible observing the gamma distribution.

# CHAPTER VI

# CONCLUSIONS AND RECOMMENDATIONS

## A. Conclusions

The overall conclusion of this work is that parameter measurements can be done on reactor systems by observing the gamma distribution by use of the detection concept conceived here. In addition, the predictions of Gelinas and Osborn have been verified in that a successful measurement of $\beta/\ell$ by gamma observation has been done on the FNR. Equally important is the fact that the experiments were done on a reactor core which had surface gamma dose rates comparable to those found in power reactors. The $\beta/\ell$ value measured here is in agreement with rough estimates as calculated by simple diffusion theory and is in qualitative agreement with previous experiments on similar core configurations.

The temperature noise source uncovered in this investigation will play a very important role in fluctuation experiments on reactors with large fission product inventories. Types of experiments in which the effect will be important are in shutdown margin measurements and $\beta/\ell$ measurements, particularly in reactors which have $\beta/\ell$ values such that the breakpoint is at frequencies where the temperature effects are still important. The temperature induced reactivity oscillations preclude the possibility of directly observing delayed neutron effects in "dirty" reactors.

It is possible that in other reactor types with smaller temperature coefficients the fluctuations observed here might not be as important. At low reactor power these effects are smaller and so it should be possible

to minimize them by conducting the experiments at reduced power levels. This, however, would require a redesign of the present detector to achieve lower backgrounds and consequently higher signal to noise ratios at the lower power levels.

A detector based on the GCD concept could be used as a multi-decade power level monitor. The advantages of simplicity of construction, freedom from radiation damage, and virtually instant response are obvious. A properly designed detector could, in principle, monitor reactor power from the source range to full power with level changes made through photo-tube voltage control. In certain situations the detector could prove superior to existing reactor instruments. For instance, in systems where fast response is required, the Cerenkov concept based on light transmission would have a much smaller response time (several nanoseconds) than an ion chamber whose response is governed by ion collection times, which are typically several microseconds.

Freedom from radiation damage is exemplified by the fact that the detector portion near the reactor does not require any radiation damage susceptible material such as insulators. Burnup problems as evidenced with other detectors are not present. The radiator gas can be easily replaced.

The two detector noise measurements done here appear to be a most powerful technique for extracting useful information from low level signals. In fact, the results reported above appear to extend the lower limit of the correlated to uncorrelated ratio, at which CPSD measurements may be done successfully, below the previously estimated minimum of 0.1. The method does not give any more information than a PSD measurement, but

it might be the only way to obtain the information due to small values of the C/U ratio.

B. Recommendations

The most obvious thing to do in the opinion of the author is to strive to reduce the size and background and increase the efficiency of the present device. For only then can the full potential of the detection concept be realized. The efficiency can be increased by putting the detector in core or in closer proximity to the fuel. This requires a smaller size device. The reduced size results in restricted electron path lengths, and as a result, reduced photon production. This reduced photon production can be more than offset by increasing the radiator pressure. For instance, the author has calculated that a 2.5 inch OD in core, $CO_2$ Cerenkov detector, operating at $\sim$ 400 psia would be approximately 8 to 10 times more efficient than the present model and still produce sufficient numbers of Cerenkov photons. As shown in Chapter II, the effect of lowering the threshold by increased pressure does not result in any sizeable contribution to the net output from delayed gammas. Along with work to improve efficiency and light production, efforts should be made to reduce the background. This can be accomplished by either making the vertical or horizontal sections longer (in smaller diameter version) or by incorporating one or more 90° bends to reduce the scattered gamma flux on the pressure vessel endwindow and phototube envelope. In certain applications (pulse operation) the background can be significantly reduced by coincidence counting techniques. To accomplish the above recommentdations on efficiency improvement, the following should be considered.

A search for a more suitable radiator gas with the following properties should be instituted:

1. Must not scintillate.

2. Must transmit in the wavelength region covered by the response of the photomultiplier.

3. Must be stable in a radiation field and any reaction products should readily recombine without interacting with structural materials and mirror surfaces.

4. Should have high refractive index at low pressures without heating.

A further study of phototubes should be undertaken to select a reasonably priced tube that has low noise, high quantum efficiency, and a wide range of spectral sensitivity.

Optical and light collection systems could be possibly improved by considering focusing mirrors and/or lenses, thinner pressure vessel end windows and improved reflecting surfaces.

Gamma to electron conversion schemes should be studied. Since the conversion is dependent on surface area, a large surface to volume ratio is desirable. A method of increasing surface area is to rule the surface with very closely spaced grooves. Materials with higher intrinsic efficiencies could also be used to line the pressure vessel as could a gas with a large macroscopic cross section for electron conversion.

With an improved detector, efforts should be made to do other reactor experiments and to test the device as a power level monitor from its lower limit to full power. A monitoring channel based on this concept is entirely feasible.

Other experiments one might do are PSD and CPSD with varying values of the correlated to uncorrelated ratio. The idea being to establish a lower limit of the ratio using practical record lengths. Along with this a more thorough theoretical and experimental study of the effects of this and other detectors should be made.

Along with the above, a series of experiments designed to measure shutdown margins might be conducted. The problem is especially important in "dirty" reactors which multiply a large source due to the photoneutrons caused indirectly by the fission product gammas. In these systems the critical state is next to impossible to determine.

A further study, both theoretical and experimental, of the temperature fluctuations is recommended. Things which warrant investigation are both the amplitude and frequency dependence of this noise source and their effect on the regular zero power spectrum.

Finally, it might be very desirable to undertake a further study to calculate detection efficiencies for a device of this type. At the present time this calculation is very difficult. For instance, little is known about the energy and angular distribution of electrons ejected by higher energy gamma rays from a surface. The efficiency and response of the detector could be studied experimentally by using various energy gamma ray sources. To cover the range from 2 Mev to 6 Mev (no long lived gamma sources exist in this energy range) a solution containing a suitable isotope could be passed through the reactor in a closed loop to form the active gamma emitter.

Also, since the shape of the count rate versus pressure has been established from a plausible theoretical model, the possibility exists of developing suitable spectrum stripping techniques to enable the device to be used as a high energy gamma ray spectrometer.

# APPENDIX A

## MULTIPLE LINEAR REGRESSION TECHNIQUE

The equation to which the CPSD data is to be fit is

$$\phi(\omega) = \frac{A}{\omega^{\nu}(\alpha^2+\omega^2)} + \frac{B}{(\alpha^2+\omega^2)} \qquad \text{(A-1)}$$

It is required that the best fit to the data be obtained by adjusting A, B, $\nu$ and $\alpha$.

Since the normal equations for this problem are nonlinear and a linearization by a suitable transformation is impossible, we procede by expanding Equation (A-1) in a Taylor series about some suitable point on the contour defined by A, B and $\alpha$. $\nu$ was not included as a parameter to be fit by the regression analysis. It was instead determined by finding the best fit to the data with $\nu$ fixed. The residues between the values predicted by the regression equation and the data points were calculated and totaled. $\nu$ was then varied systematically to yield a minimum value of the sum of the residues. This value which yielded the minimum was then used in the final regression equation.

A Taylor's expansion gives

$$\phi(\omega) = \frac{A'}{\omega^{\nu}(\alpha'^2+\omega^2)} + \frac{B'}{(\alpha'^2+\omega^2)}$$

$$+ E_1 \left.\frac{\partial\phi}{\partial A}\right|_{A=A'} + E_2 \left.\frac{\partial\phi}{\partial B}\right|_{B=B'} + E_3 \left.\frac{\partial\phi}{\partial\alpha^2}\right|_{\alpha=\alpha'} + \cdots\cdots \qquad \text{(A-2)}$$

where the E's denote suitable deviations of the respective parameters from their true values.

Supposing we can guess $A'$, $B'$, and $\alpha'^2$ quite accurately, we are justified in neglecting the higher order terms, as $(E_1)^2$, $(E_2)^2$, and $(E_3)^2$ will be small.

The Equation (A-2) is then linear in the E's and the standard techniques of multiple linear regression analysis can be applied to determine them. These are then used to correct the original estimates and the procedure is repeated to a desired precision.(54)

This problem has been programmed in the Basic Language for solution on the Ford Computer in Dearborn, access being through the Time Sharing Terminal in the Nuclear Engineering Computer Laboratory.

## APPENDIX B

## $N^{16}$ SOURCE CALCULATION

The $N^{16}$ source is due to the $O^{16}(n,p)N^{16}$ reaction in the coolant water. The reaction threshold is approximately 10 Mev. The number of $N^{16}$ atoms formed per fission is proportional to the ratio of absorption cross section of $O^{16}$ and the scattering cross section of hydrogen, which is the most important reaction at high energies. The effect of neglecting the other competing reactions is negligible.

The number of neutrons per fission is obtained from the Watt spectrum

$$N(E) = .484 \sinh \sqrt{2E}\, e^{-E}\, dE \qquad \text{(B-1)}$$

The number of $N^{16}$ atoms formed per fission is

$$N^{16} = \int_{E_0}^{\infty} N(E) \frac{\sigma_a}{\sigma_s(E)}\, dE$$

where $\sigma_a = 1.9 \times 10^{-5}$ barns[39] and $\sigma_s = \frac{10.97}{E+1.66}$ barns.[39] Evaluating we get $N^{16} = 3.5 \times 10^{-6}$ Nitrogen atoms/fission.

This number is insignificant compared to 0.047, the number of prompt gammas per fission above 5 Mev. On this basis the observed low frequency PSD cannot be attributed to the filtering effect of the $O^{16}(n,p)N^{16}$ reaction.

REFERENCES


1. de Hoffman, F. et al. La-183 Los Alamos Scientific Laboratory or AECD-3051 U. S. Atomic Energy Commission (1944).

2. Moore, M. N. "The Determination of Reactor Parameters from Measurements at Steady Operation." Nuc. Sci. and Eng., 3, 387 (1958).

3. Thie, J. Reactor Noise. Rowman and Littlefield Inc., New York, 1963.

4. Stephenson, S., Roux, D. P. and Fry, D. N. "Neutron Fluctuation Spectra in the Oak Ridge Research Reactor." ORNL-TM-1401, Oak Ridge National Laboratory, 1966.

5. Uhrig, R. (ed.). Noise Analysis in Nuclear Systems. TID 7679 USAEC, 1964.

6. Griffin, C. W. and Randall, R. L. "At-Power, Low Frequency, Reactor-Power Spectrum Measurements and Comparison with Oscillation Measurements." Nuc. Sci. and Eng., 15, 131 (1963).

7. Cohn, C. E. "Determination of Reactor Kinetic Parameters by Pile Noise Analysis." Nuc. Sci. and Eng., 5, 331 (1959).

8. Rajagopal, V. "Determination of Reactor Transfer Functions by Statistical Correlation Methods." Nuc. Sci. and Eng., 12, 218 (1966).

9. Ricker, C. W. Measurement of Reactor Fluctuation Spectra and Subcritical Reactivity. Ph.D. Thesis University of Michigan, 1965.

10. Kryter, R. C., Fry, D. N. and Roux, D. P. "Two Detector Shutdown Margin Measurements in Gamma Fluxes." Trans. Amer. Nuc. Soc., 10, 283 (1967).

11. Stegeman, D. "Die Analyse des Neutronenrauschens in Reaktoren." INR-4/66-1, Kernforschungszentrum Karlsruhe, 1966.

12. Nomura, T. "Improvement in S/N Ratio of Reactor Noise Spectral Density." J. Nucl. Sci. Tech., 2, 76 (1965).

13. Nomura, T. et al. In Neutron Noise, Waves and Pulse Propagation. R. Uhrig, Coor., CONF 660206, p. 217 (1967).

14. Shultz, M. In Neutron Noise, Waves, and Pulse Propagation. R. Uhrig, Coor., CONF 660206, p. 413 (1967).

15. Roux, D. P. "Optimization of Reactor Shutdown Margin Measurements in High Gamma Fluxes." Nuc. Appl., 3, 575 (1967).

16. Hanauer, S. H., Trimko, J. R. Jr., Buhl, A. R. and Roux, D. P. "Subcritical Reactivity Measurement Using Fluctuations from a Pulse Type Detector." Trans. Amer. Nuc. Soc., 9, 523 (1966).

17. Gelinas, R. and Osborn, R. "Reactor Noise Analysis by Photon Observation." Nuc. Sci. and Eng., 24, 184 (1966).

18. Kenney, E. In Neutron Noise, Waves and Pulse Propagation. R. Uhrig, Coor., CONF 660206, p. 399 (1962).

19. Velez, C. Autocorrelation Functions of the Counting Rate in Nuclear Reactors and Their Application to the Design of Reactor Control Instrumentation. Ph.D. Thesis, University of Michigan, 1959.

20. Albrecht, R. W. The Measurement of Dynamic Reactor Parameters by Methods of Stochastic Processes. Ph.D. Thesis, University of Michigan, 1961.

21. Pluta, P. R. An Analysis of Nuclear Reactor Fluctuations by Methods of Stochastic Processes. Ph.D. Thesis, University of Michigan, 1962.

22. Boennighausen, T. On the Direct Measurement of Power Spectral Density. Master's Thesis, University of Michigan, 1963.

23. Seifretz, W., Stegeman, D. and Vath, W. In Neutron Noise, Waves, and Pulse Propagation. CONF-660206, R. Uhrig, Coor., USAEC, p. 195 (1966).

24. Vovenko, A. S. "Gas Filled Cerenkov Counters." Soviet Physics Uspekhi, 6, 794 (May-June, 1964).

25. Atkinson, J. H., and Perez-Mendez, V. "Gas Cerenkov Counters." Rev. Sci. Instr., 30, 864 (1959).

26. Swanson, R. J., and Masek, F. E. "Large Gas Cerenkov Counters." Rev. Sci. Instr., 30, 864 (1959).

27. Boley, F. I. "Atmospheric Cerenkov Radiation from Cosmic Ray Showers." Revs. Mod. Phys., 36, 792 (1964).

28. Jelley, J. V. Cerenkov Radiation and Its Applications. Pergamon Press, London, 1958.

29. Jennings, R. E. and Kalmus, P. I. P. "A Gas Cerenkov Counter for the Accurate Determination of Electron Beam Energy." Nuc. Instr. and Meth., 6, 209 (1960).

30. Doyle, J. E. and Dickinson, W. C. "The Cerenkov Response of Lucite and Quartz to Gamma and Fast Neutron Radiation." UCRL 7032, Lawrence Radiation Laboratory, 1962.

31. Rippon, S. E. "Cerenkov Detectors for the Measurement of Reactor Power." Nucl. Instr. and Meth., 21, 192 (1963).

32. Strindehag, O. "A Fast Fission Product Monitor." Nucl. Instr. and Meth., 33, 314 (1965).

33. Weiss, H. "Power Measurement and Automatic Reactor Control by Gamma or Cerenkov Radiation." Proc. of the Conf. on Nuc. Electronics and Instrumentation, Bombay, Nov. 1965, IAEA, Vienna (1967).

34. Sarram, M. Design of a Cerenkov Power Monitor for FNR. Master's Thesis, University of Michigan, 1967.

35. Freeman, D. D. An Investigation of the Blue Glow Radiation for the FNR. Master's Thesis, University of Michigan, 1963.

36. Price, W. J. Nuclear Radiation Detection. 2nd Edition, McGraw-Hill, New York, 1964.

37. Evans, R. D. The Atomic Nucleus. McGraw-Hill, New York, 1955.

38. Hayes, E. R. et al. "Index and Dispersion of Some Cerenkov Counter Gases." ANL 6916, Argonne National Library, 1964.

39. Reactor Physics Constants, 2nd Ed., ANL 5800, Argonne National Laboratory, 1963.

40. Glasstone, S. and Sesonske, A. Nuclear Reactor Engineering. Van Nostrand, New York, 1963.

41. Dr. A. Gordus, private communication.

42. Birks, J. The Theory and Practice of Scintillation Counting. Macmillan, New York, 1964.

43. Osborn, R. K. and Nieto, J. M. "Detector Effects on the Statistics of Neutron Fluctuations." Nuc. Sci. and Eng., 26, 511 (1966).

44. Akcasu, Z. and Osborn, R. K. "Application of Langevin's Technique to Space and Energy-Dependent Noise Analysis." Nuc. Sci. and Eng., 26, 13 (1966).

45. Natelson, M. An Analysis of Space and Energy Effects in Reactor Fluctuation Experiments. Ph.D. Thesis, University of Michigan, 1965.

46. Keepin, G. R. Physics of Nuclear Kinetics. Addison-Wesley Publishing Co., Reading, Mass., 1965.

47. Cohn, C. E. "A Simplified Theory of Pile Noise." Nuc. Sci. and Eng., 7, 472 (1960).

48. Dr. C. W. Ricker, private communication.

49. Papoulis, A. Probability, Random Variables, and Stochastic Processes. McGraw-Hill, New York, 1965.

50. Bendat, J. and Piersol, A. Measurement and Analysis of Random Data. J. Wiley and Sons Inc., New York, 1966.

51. Dr. R. Cheeswright, private communication.

52. Yamada, S. and Kage, H. "Reactor Noise Caused by Coolant Flow Fluctuation." In Neutron Noise, Waves, and Pulse Propagation, R. Uhrig, Coor., CONF-660206, USAEC (1966).

53. Krall, H. R. "Evaluation of New Photomultiplier for Scintillation Counting." IEEE Trans. on Nuc. Sci., 12, 39 (1965).

54. Wylie, C. R. Jr. Advanced Engineering Mathematics. McGraw-Hill Book Co. Inc., New York (1951).